

## **Supplementary Information**

# **Total Degradation of Extracellular Amyloids by Miniature Artificial Proteases**

**Tanmay Mondal and Bhubaneswar Mandal\***

Department of Chemistry, Indian Institute of Technology Guwahati, Assam-781039, India

## Methods

**DFT Calculation.** The most stable conformation of mAPs and the intermediate were obtained after performing density functional theory (DFT) based methods using B3LYP as energy function and 6-31G as the basis set through Gaussian 5.0.9 program.

**Molecular Docking.** Molecular docking study was performed by AutoDock Vina version 1.1.2 software.

**A $\beta$  sample preparation.** A $\beta_{1-40}$  was purchased from GL Biochem Shanghai, China. The required amount of A $\beta_{1-40}$  was dissolved in 20  $\mu$ L of TFA which was further evaporated by purging nitrogen gas. To remove TFA completely, HFIP was added and evaporated to complete dryness using nitrogen gas to get disaggregated A $\beta_{1-40}$  peptide. This process was repeated twice. PBS (50 mM, pH 7.4) was added into the disaggregated peptide, followed by sonication and vortex to obtain a transparent stock solution.

**Sample preparation for MALDI Mass analyses.** Purified and lyophilized peptide samples were dissolved in PBS (50 mM, pH 7.4) to obtain stock solutions, while mA $\beta$  was pretreated with TFA and HFIP before adding PBS. Peptide samples were co-incubated in different molar ratio at physiological pH and temperature on a water bath. mA $\beta$  or A $\beta$  alone and each of the mAPs was incubated separately at the same condition as control. Aliquots were tested by a MALDI-TOF mass spectrometer in a time-dependent manner. MALDI-TOF mass of the peptide samples was analyzed using CHCA matrix on BRUKER autoflex speed instrument which consists of a MALDI ionization source for samples in the solid state and a TOF/TOF mass analyzer, equipped with Bruker daltonics flex analysis software. To prepare CHCA matrix, 1.0 mg of CHCA was dissolved in 100  $\mu$ L of CH<sub>3</sub>CN/H<sub>2</sub>O (1:1) containing 0.1% TFA.

### Ultra Violet-Visible (UV-Vis) Spectroscopy:

Purified solid peptide sample and p-nitrophenyl acetate were dissolved in PBS (50 mM, pH 7.0) with 2 vol % of ethanol to obtain a stock solution of 1 mM. To perform the UV-VIS study, the stock solution of the peptide was diluted as required and mixed with p-nitrophenyl acetate and incubated at 25 °C on a water bath. The kinetics was performed at 275 nm and 400 nm respectively. 2 mL of the sample was taken in a cuvette with a path length of 1 cm.

For UV-Vis absorption study Spectra were recorded from 200 nm to 700 nm on Perkin Elmer (lambda 35). The text files were plotted using OriginPro 8 software.

**Thioflavin T (ThT) Fluorescence Assay.** The fluorescent dye Thioflavin T (ThT) is used to monitor amyloid fibril formation *in vitro* because of the large enhancement of its fluorescence emission (at around 485 nm when excited at 445 nm) upon binding to amyloid fibrils, and a linear correlation was reported between the ThT fluorescent intensity with amyloid concentration over a wide range of ThT concentrations. ThT was purchased from Sigma Aldrich. To perform ThT assay, stock solutions were prepared and co-incubated as described earlier, and the fibrils were sonicated and vortexed to make the most number of accessible ThT binding sites on the amyloid. At different time intervals, 40  $\mu\text{L}$  of peptide samples from the stock were mixed with 200  $\mu\text{L}$  of ThT solution (50  $\mu\text{M}$ ) and 160  $\mu\text{L}$  of PBS (50 mM, pH 7.4). Fluorescence was measured ( $\lambda_{\text{ex}} = 445 \text{ nm}$ ,  $\lambda_{\text{em}} = 485 \text{ nm}$ , and slit 5 nm) and normalized spectra were plotted as the average of the three replicate solutions with observed standard deviation.

**Circular Dichroism (CD).** To perform the CD studies, the stock solutions (prepared as described earlier) were diluted with respective buffer solutions to obtain the final concentration of 100  $\mu\text{M}$  (50  $\mu\text{M}$  for  $\text{A}\beta_{1-40}$ ). 400  $\mu\text{L}$  of the sample was taken in a cuvette (Model SPC-001) having a bandwidth of 1 mm. Spectra were recorded from 190 nm to 260 nm as the average of three scans on a JASCO (Model J-1500) instrument. Observed ellipticity (mDeg) [obtained from Data Dump in Spectra Manager] was converted to mean residue molar ellipticity using the following equation:

$$[\theta] \text{ (deg. cm}^2 \cdot \text{dmol}^{-1}\text{)} = \text{Ellipticity (mdeg). } 10^6 / \text{Pathlength (mm). [Protein] } (\mu\text{M}). \text{N}$$

**Fourier Transformation Infra Red (FTIR).** For FTIR analysis, 20  $\mu\text{L}$  of the sample from each stock solution was taken out separately, mixed with KBr and pellets were prepared after complete dryness, which was analyzed with background subtraction to obtain the final spectra. OriginPro 8 software was used to plot the graph from text files.

**Transmission Electron Microscopy (TEM).** From the stock peptide solution, 10  $\mu\text{L}$  aliquot was taken out and drop-casted over the carbon-coated copper grid and allowed to float for 1 min. Then for negative staining, 2% uranyl acetate solution (5  $\mu\text{L}$ ) was added on the same grid and allowed to float for another 1 min. Excess solution was removed by using blotting

paper. The sample was air-dried at room temperature and kept in desiccators. TEM analyses were performed on a JEOL instrument (Model: JEM 2100) at 200 kV.

**Atomic Force Microscopy (AFM).** To perform AFM analysis, the stock solution was diluted with Milli-Q water to obtain the final concentration of 5  $\mu\text{M}$  (1  $\mu\text{M}$  for  $\text{A}\beta_{1-40}$ ). 20  $\mu\text{L}$  aliquot from the diluted peptide solution was added over the coverslips, washed with Milli-Q water and dried at room temperature and analyzed on Agilent STM 5500 instrument.

**Congo-Red Stained Birefringence.** Commercially available Congo red was dissolved in 80 % aqueous ethanol to prepare a saturated solution. Then saturated sodium chloride solution was added into the saturated Congo red solution and used for analysis after filtration. 20  $\mu\text{L}$  aliquot of peptide stock solution was drop-casted over a glass slide followed by 40  $\mu\text{L}$  of the saturated Congo red solution. Excess solution was removed by blotting paper. The sample was dried at room temperature and kept in desiccators. Birefringence analyses were performed on a Leica ICC50 HD polarizable microscope.

**Dynamic Light Scattering (DLS).** The size distributions of  $\text{A}\beta_{1-40}$  aggregates and mAP3 were analyzed using Zetasizer Nano-ZS90 (Malvern Instruments). To perform DLS analysis, stock solutions were diluted with Milli-Q water to obtain the final concentration of 100  $\mu\text{M}$  (50  $\mu\text{M}$  for  $\text{A}\beta_{1-40}$ ). All the DLS results were reported as the average of three measurements.

**Large unilamellar vesicles (LUVs).** Dye leakage studies were performed using carboxyfluorescein dye entrapped LUVs to check the toxicity of the peptide fragments generated from  $\text{A}\beta_{1-40}$  after proteolysis by mAPs. Details are described in the supplementary information.

**Table S1. Screening of peptide sequences.**

Sl. no.	Name of the peptide	Peptide sequence
1	Peptide 1	DHS-NH <sub>2</sub>
2	Peptide 2	ADAHASA-NH <sub>2</sub>
3	Peptide 3	GDAHASG-NH <sub>2</sub>
4	Peptide 4	GDGHGSG-NH <sub>2</sub>

**Table S2. Peptide sequences and their roles in the current study.**

Sl. no.	Short name of the peptides	Peptide sequence (one-letter code)	Role of the peptide
1	mAP1	Ac-GDAHASAVFFAG-NH <sub>2</sub>	Proteolysis
2	mAP2	Ac-GDGHGSGVFFAG-NH <sub>2</sub>	Proteolysis
3	mAP3	Ac-GDGHGSGGVFFAG-NH <sub>2</sub>	Proteolysis
4	mA $\beta$	Ac-GGAV <sub>12</sub> HHQKLVFFA <sub>21</sub> G-NH <sub>2</sub>	Prototype of A $\beta$
5	A $\beta$ <sub>1-40</sub>	D <sub>1</sub> AEFRHDSGYEVHHQKLVFFAEDVGSNKG AIIGLMVGGVV <sub>40</sub> -NH <sub>2</sub>	Target peptide
6	DTP28	GS <sub>505</sub> SDSIGVLGYQKTV DHTKVN SKLSLF <sub>530</sub> G -NH <sub>2</sub>	Control

**Chemical Structure of the peptides:**

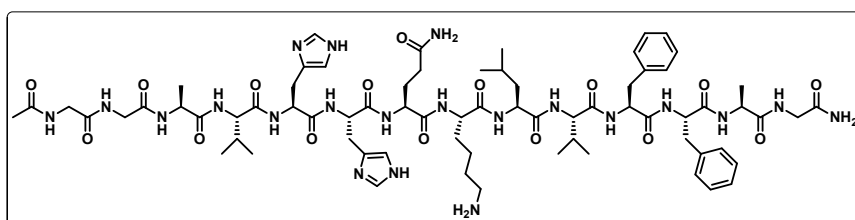


**Fig. S1. Chemical structure of the mA $\beta$  peptide.**

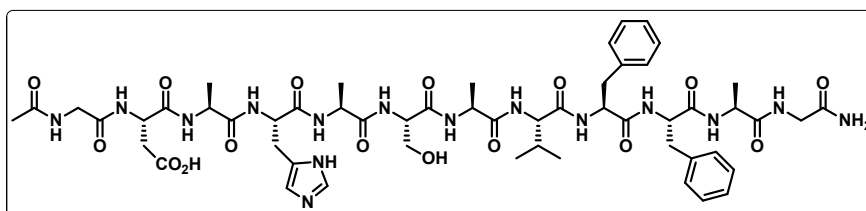


**Fig. S2. Chemical structure of the mAP1.**

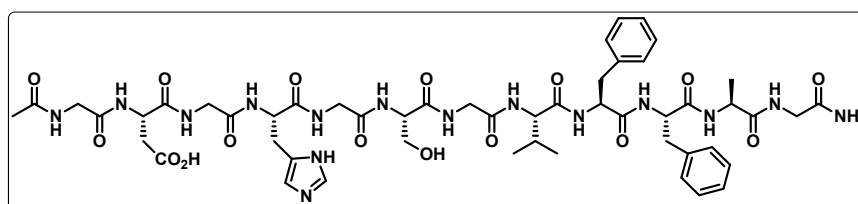


**Fig. S3. Chemical structure of the mAP2.**

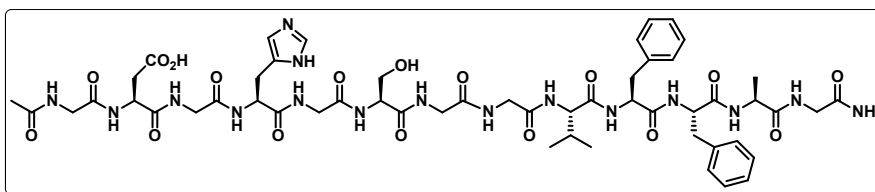


Fig. S4. Chemical structure of the mAP3.

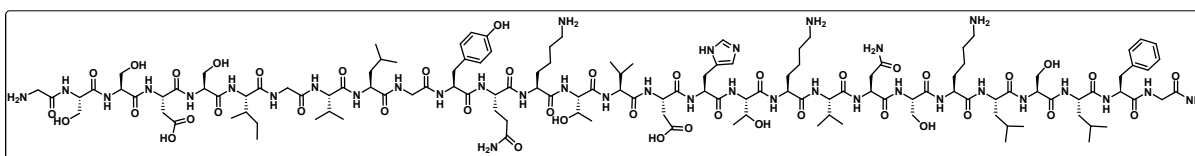


Fig. S5. Chemical structure of the DTP28.

**DFT Calculation of mAPs:**

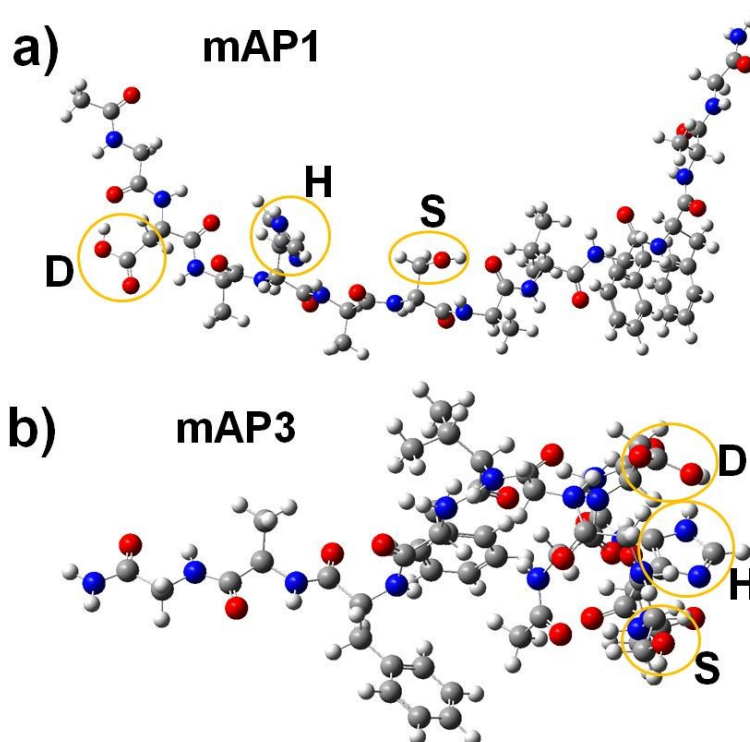


Fig. S6. The most stable conformation of (a) mAP1 and (b) mAP3 [image generated by Gaussian 09W] obtained from DFT calculation [Calculation Method: B3LYP, Basis Set: 6-31G]. Total Energy - 4126.84361306 a.u. for mAP1, and -4216.85942003 a.u. for mAP3. Nitrogen & Oxygen atoms are represented in blue & red, respectively.

Table S3. List of fluorescence labeled model Amyloid  $\beta$  (FmA $\beta$ ).

Sl. no.	Name	Peptide sequence	Role of the Peptide
1	FmA $\beta$ 1	Ac-GGAVHHQKLVFFAG-W-NH <sub>2</sub>	FRET donor
2	FmA $\beta$ 2	Dansyl-GGAVHHQKLVFFAG-NH <sub>2</sub>	FRET acceptor
3	FmA $\beta$ 3	Dansyl-GGAVHHQKLVFFAG-W-NH <sub>2</sub>	FRET donor-acceptor

## Inhibition of amyloid accumulation of A $\beta$ <sub>1-40</sub> by mAPs:

### ThT fluorescence assay of A $\beta$ <sub>1-40</sub>:<sup>1</sup>

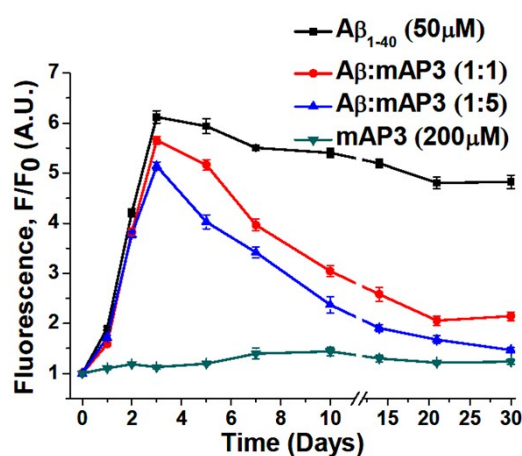


Fig. S7. Normalized profiles of dose-dependent ThT fluorescence assay. Spectra of A $\beta$ <sub>1-40</sub> in the absence (black), presence of one-fold mAP3 (red), five-fold mAP3 (blue), and mAP3 alone (dark cyan). Error bars represent standard deviations of at least three independent measurements. All the peptide solutions were incubated in PBS pH 7.4 (50 mM) at 37 °C in parallel.

### CD experiments of A $\beta$ <sub>1-40</sub>:<sup>3</sup>

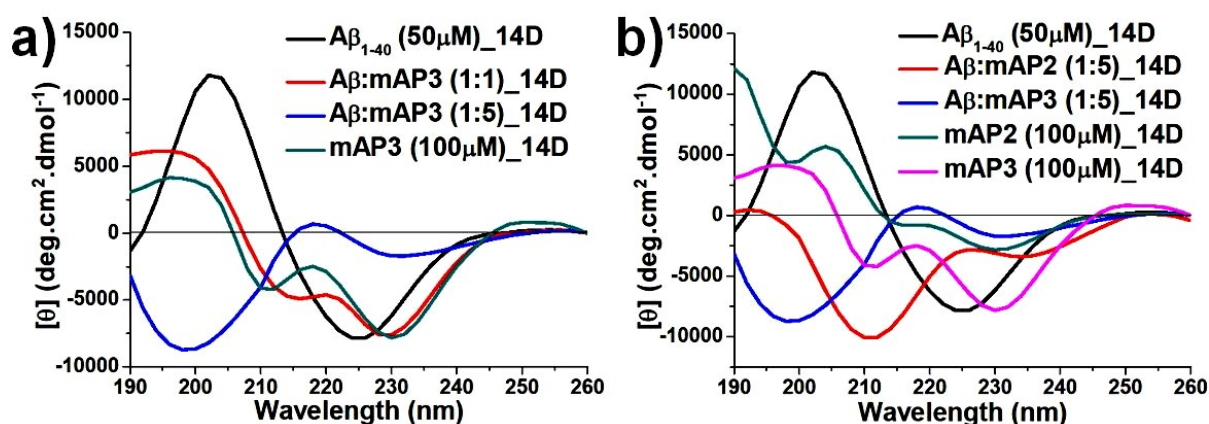


Fig. S8. CD spectra of A $\beta$ <sub>1-40</sub> in absence and presence of mAPs after 14 days of incubation. (a) Spectra of A $\beta$ <sub>1-40</sub> in the absence (black), presence of one-fold mAP3 (red), five-fold mAP3 (blue), and mAP3 alone (dark cyan). (b) CD Spectra of A $\beta$ <sub>1-40</sub> in the absence (black), presence of five-fold mAP2 (red), five-fold

mAP3 (blue), mAP2 alone (dark cyan), and mAP3 alone (magenta). The peptide solutions were incubated in PBS pH 7.4 (50 mM) at 37 °C.

### FTIR spectra of A $\beta$ <sub>1-40</sub>:<sup>3</sup>

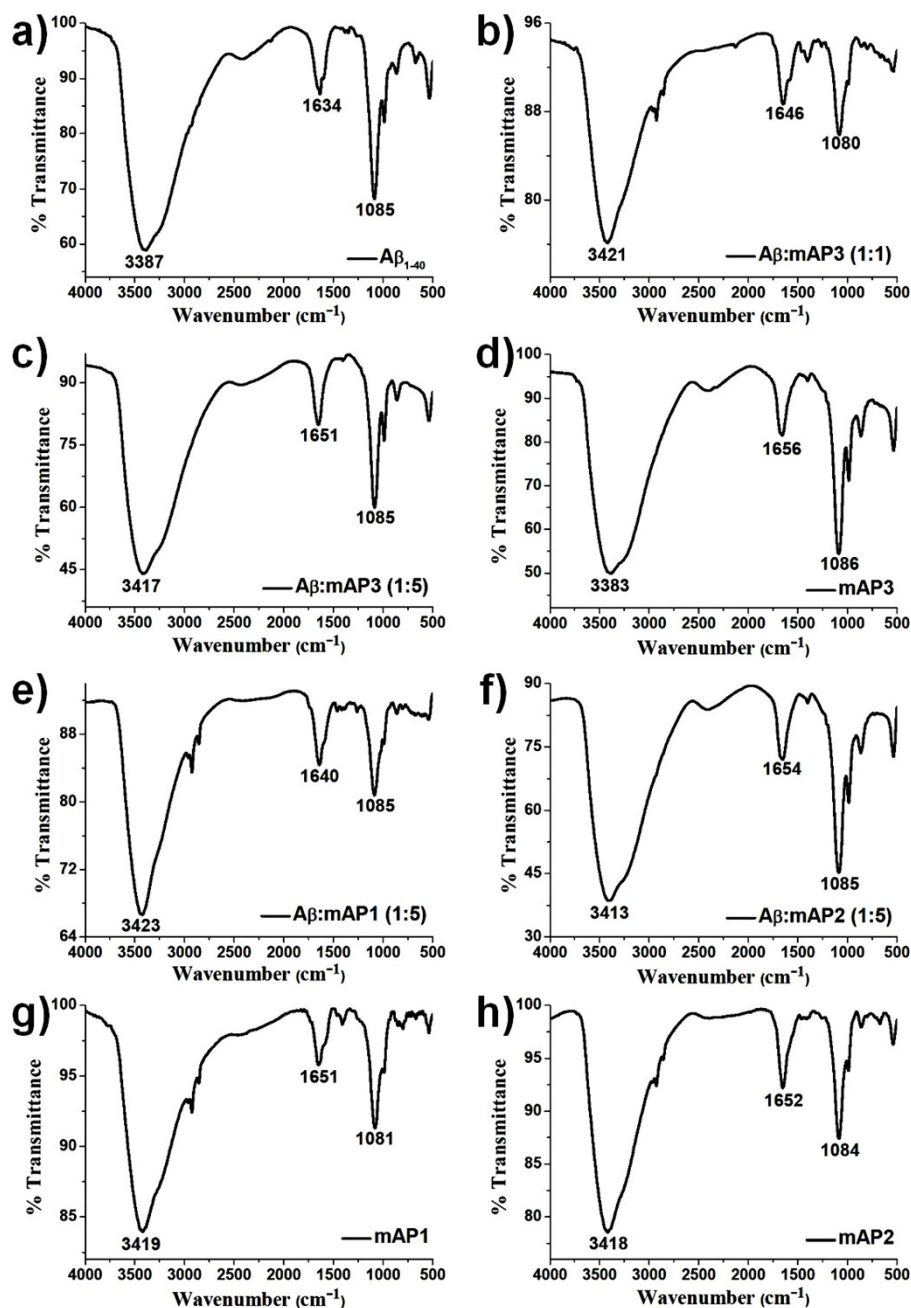


Fig. S9. FTIR spectra of A $\beta$ <sub>1-40</sub> in the absence and presence of mAPs after fourteen days of incubation. FTIR Spectra of A $\beta$ <sub>1-40</sub> (a) in absence, presence of (b) one-fold mAP3, (c) five-fold mAP3, and (d) mAP3 alone. FTIR Spectra of A $\beta$ <sub>1-40</sub> in the presence of (e) five-fold mAP1, (f) five-fold mAP2, (g) mAP1 alone, and (h) mAP2 alone. All the peptide solutions were incubated in PBS pH 7.4 (50 mM) at 37 °C.

TEM images, Congo red stained birefringence images, and AFM images of amyloid fibrils formed by  $A\beta_{1-40}$ :<sup>3</sup>

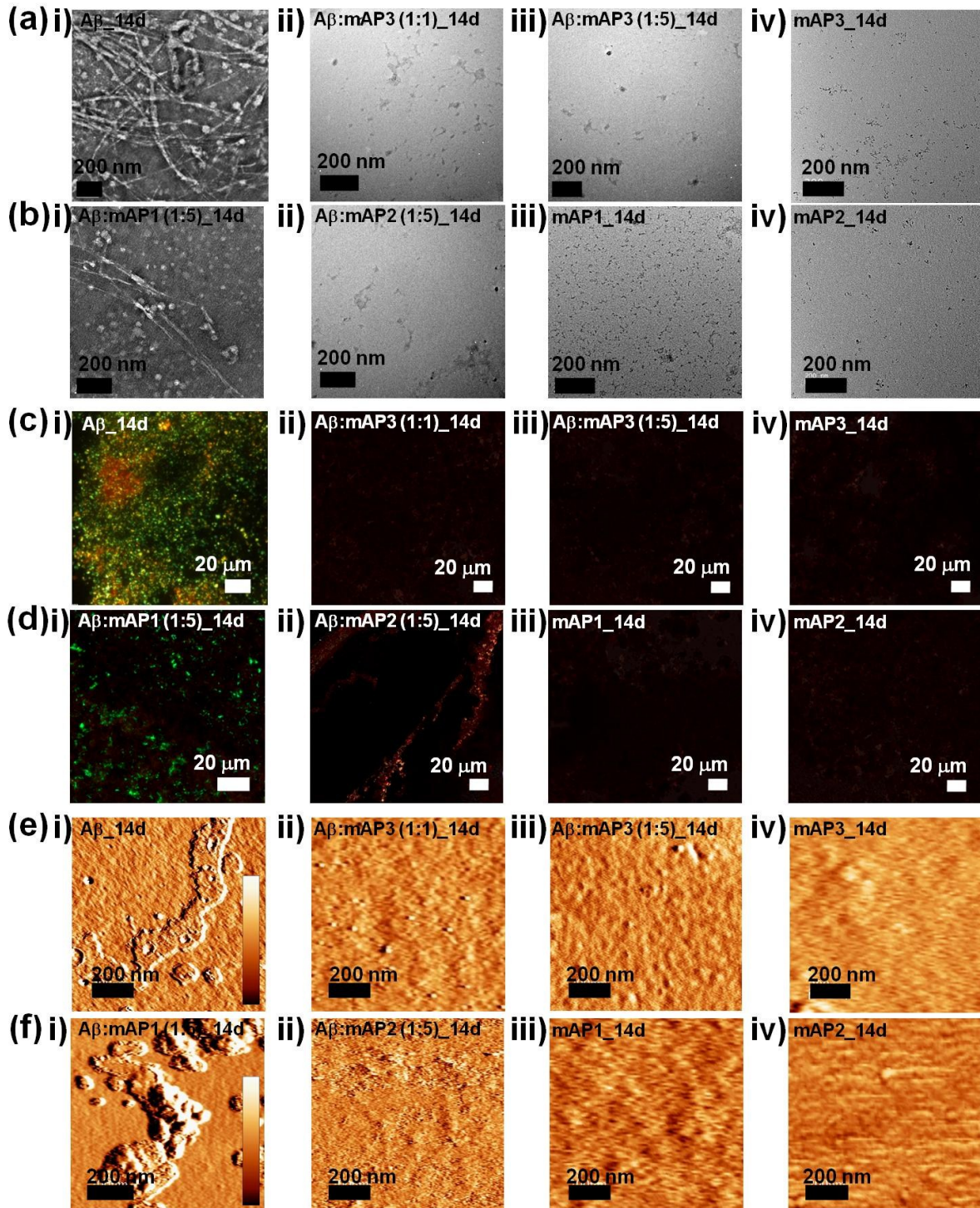


Fig. S10. (a-b) TEM images, (c-d) Congo red stained birefringence images, and (e-f) AFM images of  $A\beta_{1-40}$  (i) in the absence, and presence of (ii) one-fold mAP3, (iii) five-fold mAP3, and (iv) mAP3 alone. (b) TEM images, (d) Congo red stained birefringence images, and (f) AFM images of  $A\beta_{1-40}$  in the presence of (i) five-fold mAP1, (ii) five-fold mAP2, (iii) mAP1 alone, and (iv) mAP2 alone. Scale bars are indicated as 200 nm for TEM and AFM images [height data (inset), scan size 1  $\mu\text{m}$ , Z range 90nm for c-i & f-i, and 20 nm for (c, f)-(ii-iv)], and 20  $\mu\text{m}$  for birefringence images. All the images were captured after fourteen days of incubation.

## Disruption of amyloid accumulation of $A\beta_{1-40}$ by mAPs:

ThT fluorescence assay of  $A\beta_{1-40}$ :<sup>3</sup>

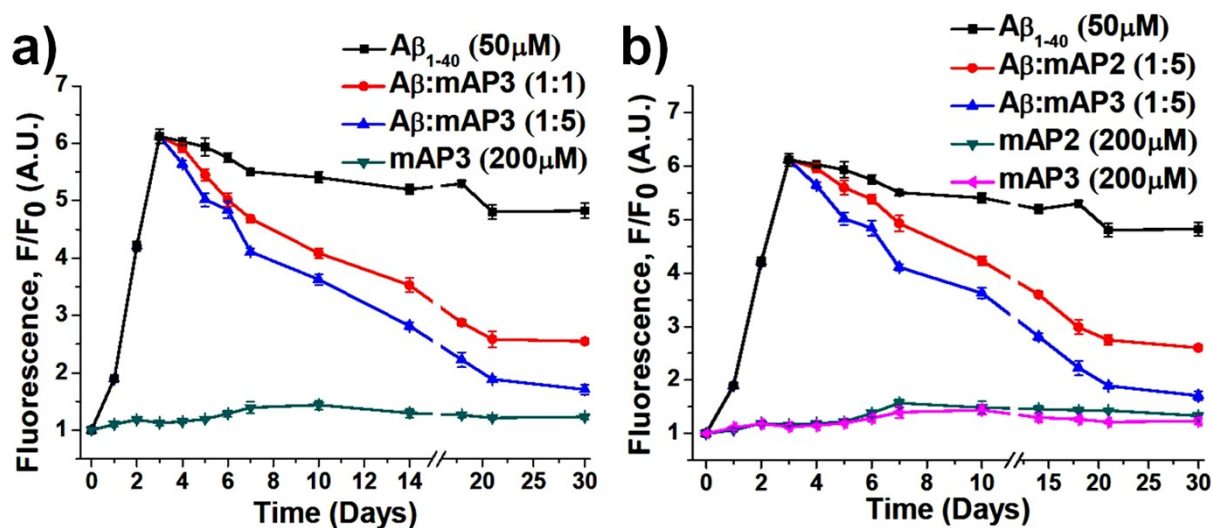


Fig. S11. Normalized profiles of (a) dose-dependent, and (b) time-dependent ThT fluorescence assay where mAPs were added after three days to the preformed fibril of  $A\beta_{1-40}$ . (a) Spectra of  $A\beta_{1-40}$  in the absence (black), presence of one-fold mAP3 (red), five-fold mAP3 (blue), and mAP3 alone (dark cyan). (b) Spectra of  $A\beta_{1-40}$  in absence (black), presence of five-fold mAP2 (red), five-fold mAP3 (blue), mAP2 alone (dark cyan), and mAP3 alone (magenta). Error bars represent standard deviations of at least three independent measurements. All the peptide solutions were incubated in PBS pH 7.4 (50 mM) at 37 °C in parallel.

CD experiments of  $A\beta_{1-40}$ :<sup>3</sup>

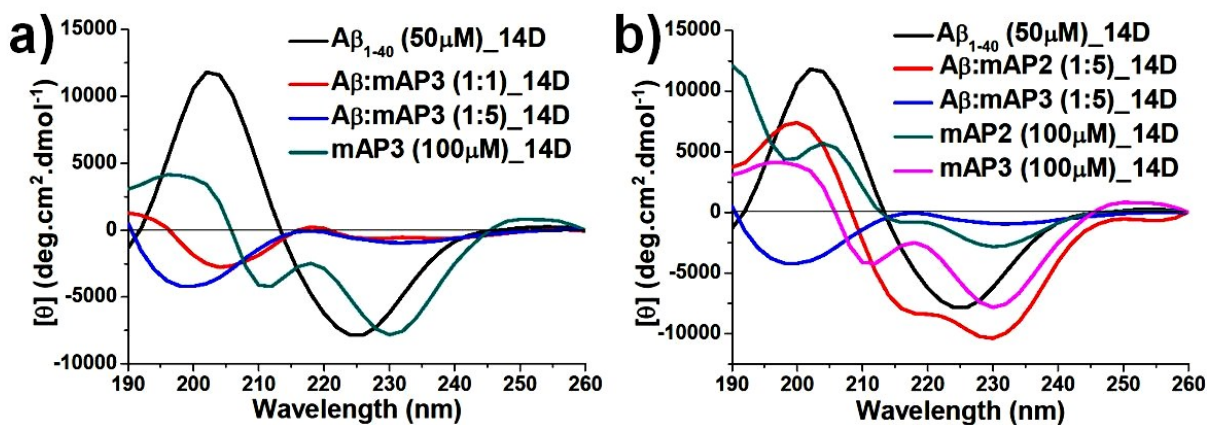


Fig. S12. CD spectra of  $A\beta_{1-40}$  in absence and presence of mAPs after fourteen days of incubation. (a) Spectra of  $A\beta_{1-40}$  in the absence (black), presence of one-fold mAP3 (red), five-fold mAP3 (blue), and mAP3 alone (dark cyan). (b) CD Spectra of  $A\beta_{1-40}$  in the absence (black), presence of five-fold mAP2 (red), five-fold mAP3 (blue), mAP2 alone (dark cyan), and mAP3 alone (magenta). The peptide solutions were incubated in PBS pH 7.4 (50 mM) at 37 °C.

FTIR spectra of  $A\beta_{1-40}$ :<sup>3</sup>

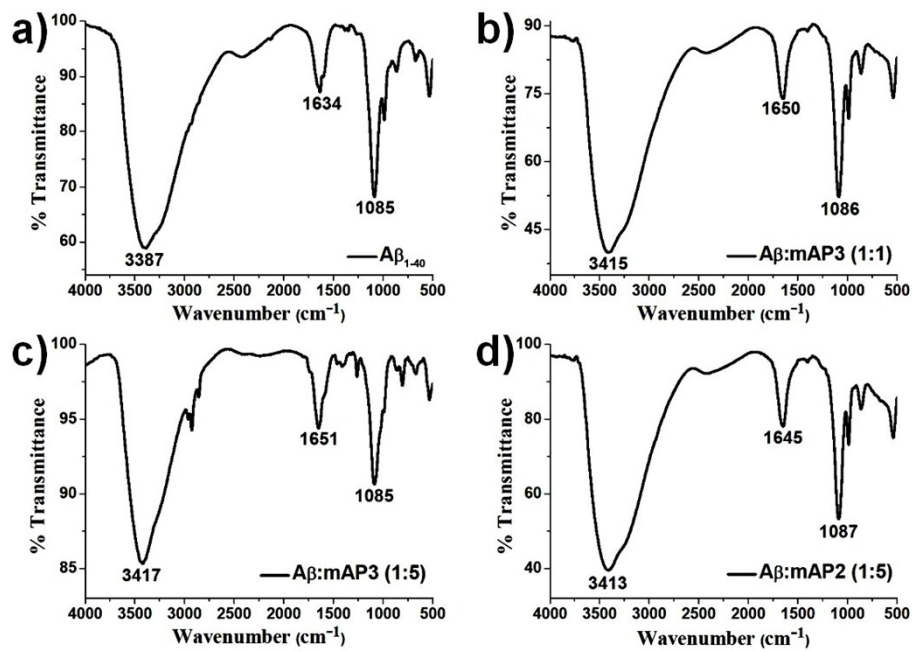


Fig. S13. FTIR spectra of  $A\beta_{1-40}$  in the absence and presence of mAPs after fourteen days of incubation. FTIR Spectra of  $A\beta_{1-40}$  (a) in the absence, presence of (b) one-fold mAP3, (c) five-fold mAP3, and (d) five-fold mAP2.

TEM images, Congo red stained birefringence images, and AFM images of amyloid fibrils formed by  $A\beta_{1-40}$ :<sup>3</sup>

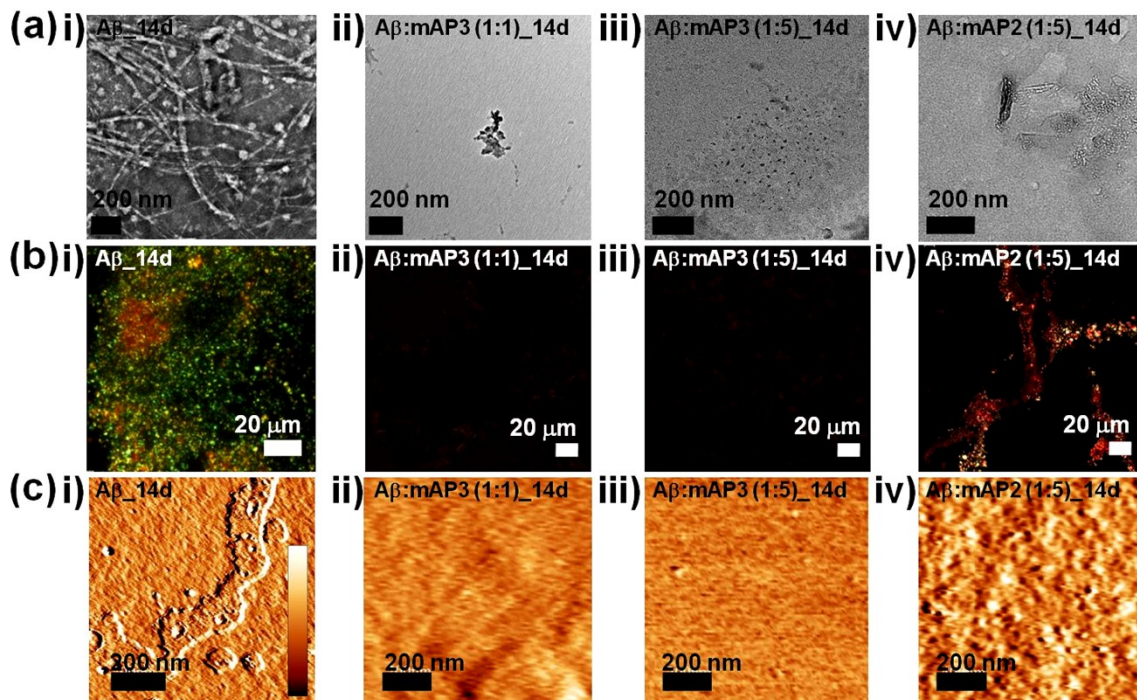


Fig. S14. (a) TEM images, (b) Congo red stained birefringence images, and (c) AFM images of  $A\beta_{1-40}$  (i) in the absence, and presence of (ii) one-fold mAP3, (iii) five-fold mAP3, and (iv) five-fold mAP2. Scale bars are indicated as 200 nm for TEM and AFM images [height data (inset), scan size 1  $\mu\text{m}$ , Z range 90nm for c-i, and 20 nm for c-(ii-iv)], and 20  $\mu\text{m}$  for birefringence images. All the peptide solutions were incubated in PBS pH 7.4 (50 mM) at 37  $^{\circ}\text{C}$  in parallel. All the images were captured after fourteen days of incubation.

### DLS analysis of inhibiting $A\beta_{1-40}$ fibril formation by mAP3:<sup>2</sup>

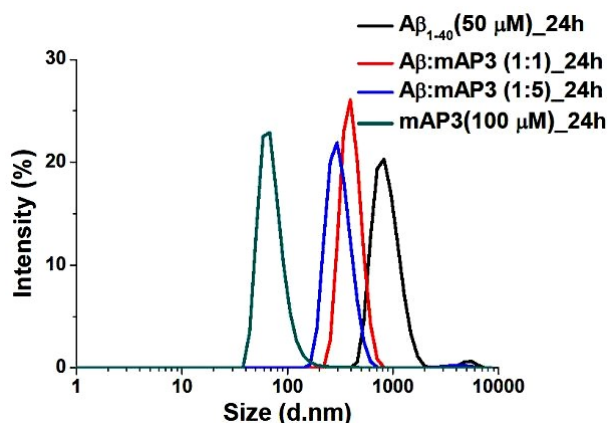


Fig. S15. The overlay of DLS profiles of  $A\beta_{1-40}$  after 24 h of incubation in the absence (black), and presence of one-fold molar excess of mAP3 (red), five-fold molar excess of mAP3 (blue); and mAP3 alone (dark cyan).

### Vesicle leakage study:

Three different lipids; DPPC, Cholesterol, and GM1 were mixed with 68:30:2 molar ratios to prepare large unilamellar vesicles (LUVs). To perform vesicle leakage studies, four sets of peptide solutions (three replicates for each set of solutions) were prepared along with untreated LUVs: (A)  $A\beta_{1-40}$  (incubated for 24 h), (B)  $A\beta_{1-40}$  (incubated for 10 days), (C)  $A\beta_{1-40}$  : mAP2 (1:5, mAP2 was added to the preformed fibrillar aggregates of  $A\beta_{1-40}$  after 72 h and incubated up to 10 days), (D)  $A\beta_{1-40}$  : mAP3 (1:5, mAP3 was added to the preformed fibrillar aggregates of  $A\beta_{1-40}$  after 72 h and incubated up to 10 days). The leakage study was performed as described in the article.<sup>2</sup>

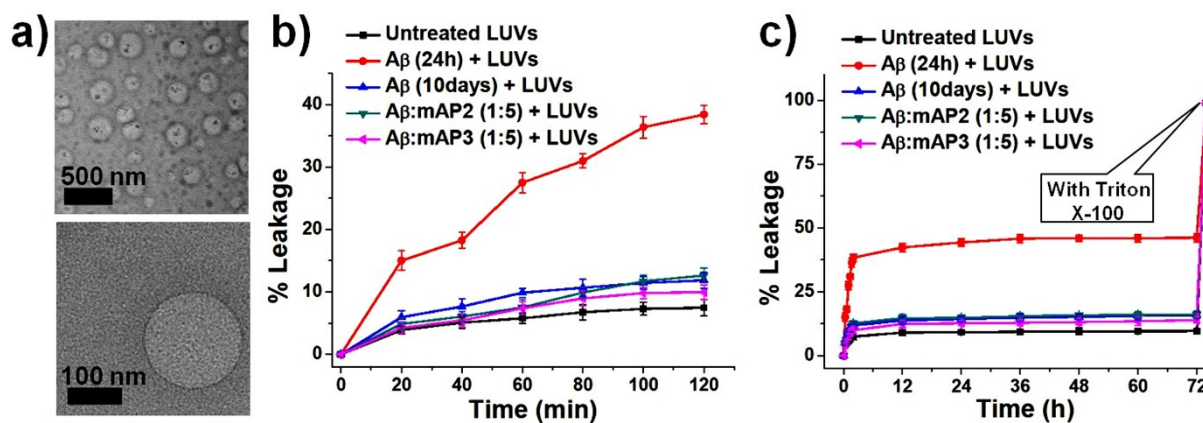


Fig. S16. (a) TEM images of negatively stained LUVs. The concentration of the sample was 100  $\mu$ M. Scale bars are indicated as 500 nm (for upper one) and 100 nm (for lower one). % dye (carboxyfluorescein) leakage from LUVs (b) up to 120 min, and (c) up to 72 h. % of dye leakage by untreated LUVs (black), LUVs treated with A $\beta$ <sub>24 h</sub> (red), LUVs treated with A $\beta$ <sub>10 d</sub> (blue), LUVs treated with A $\beta$ :mAP2(1:5)<sub>10 d</sub> (dark cyan), and LUVs treated with A $\beta$ :mAP3(1:5)<sub>10 d</sub> (magenta) [mAPs were added after 3 days to the preformed fibril of A $\beta$ <sub>1-40</sub>]. Error bars represent standard deviations of at least three independent measurements.

### Examination of the proteolytic activity of the mAPs on mA $\beta$ :

#### Self-degradation of mA $\beta$ :

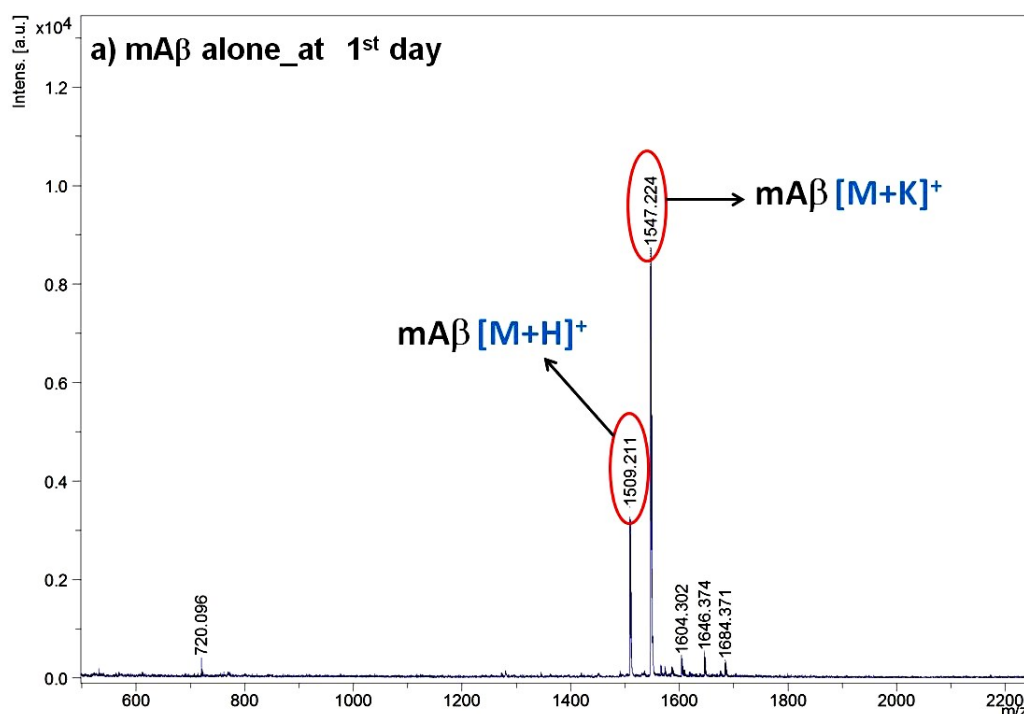
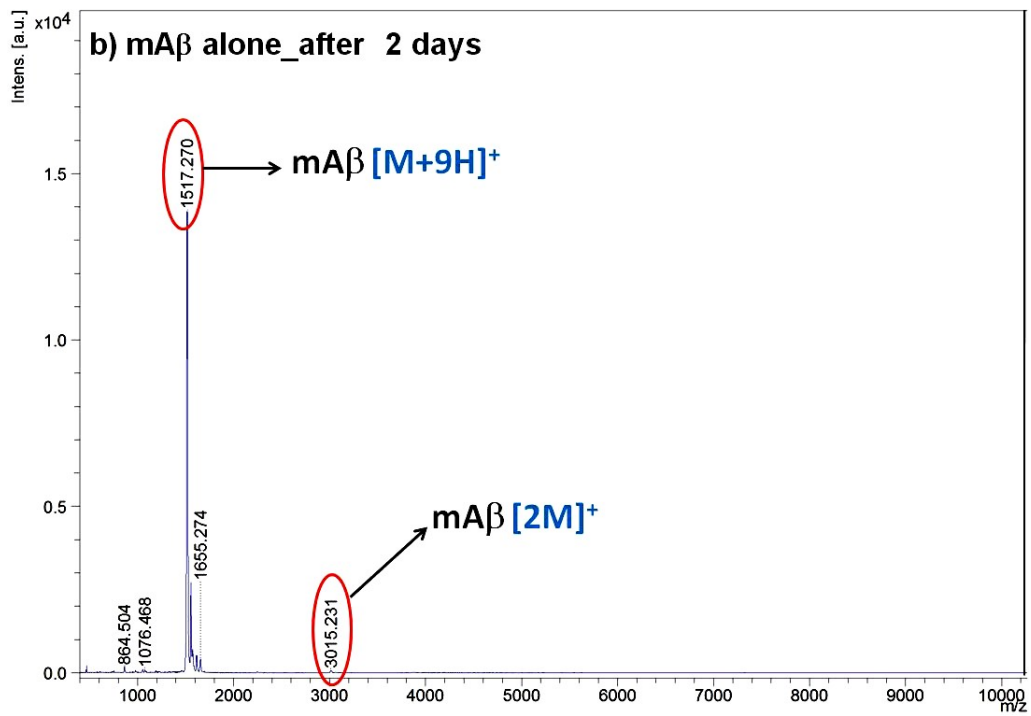
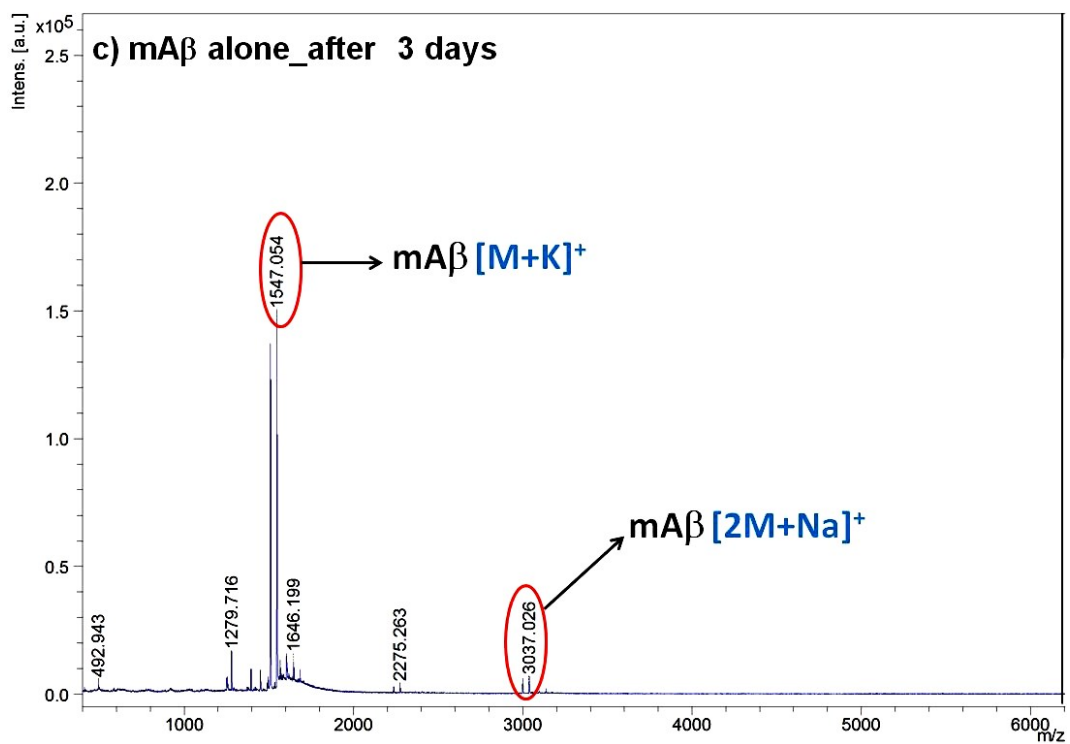


Fig. S17. MALDI-TOF mass spectrum of mA $\beta$  on the first day of incubation in PBS pH 7.4 at 37  $^{\circ}$ C. Here different singly-charged ionized species of mA $\beta$  were obtained.



**Fig. S18.** MALDI-TOF mass spectrum of mAb $\beta$  after two days of incubation in PBS. Here multiply-charged ionized species of mAb $\beta$  was obtained along with its singly-charged dimer.



**Fig. S19.** MALDI-TOF mass spectrum of mAb $\beta$  after three days of incubation in PBS.

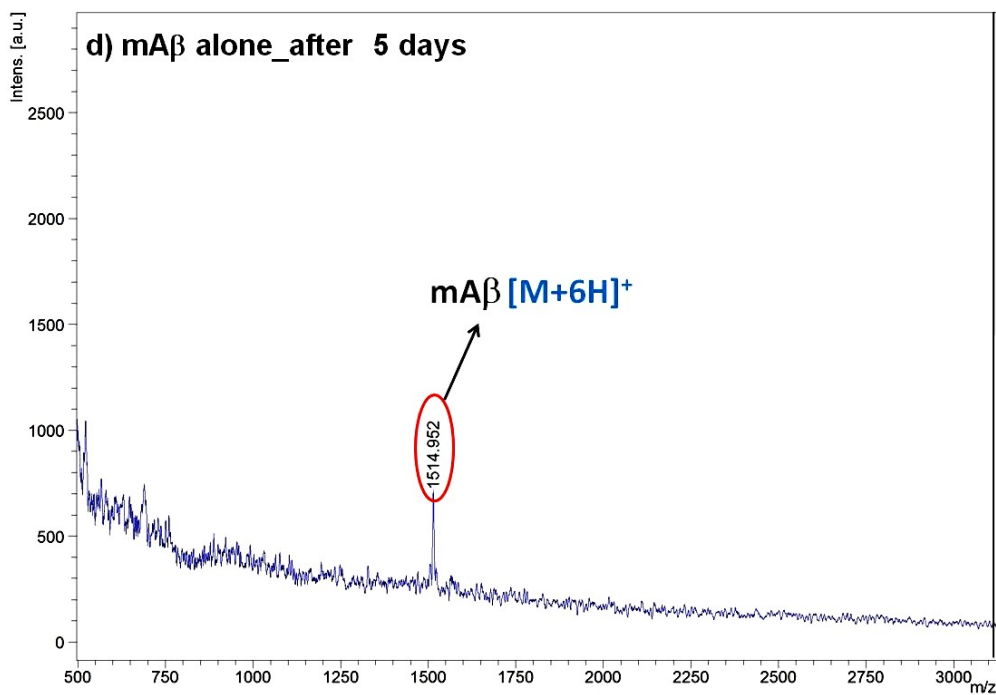


**Fig. S20.** MALDI-TOF mass spectrum of mAb $\beta$  after five days of incubation in PBS. Here multiply-charged ionized species of mAb $\beta$  was obtained.

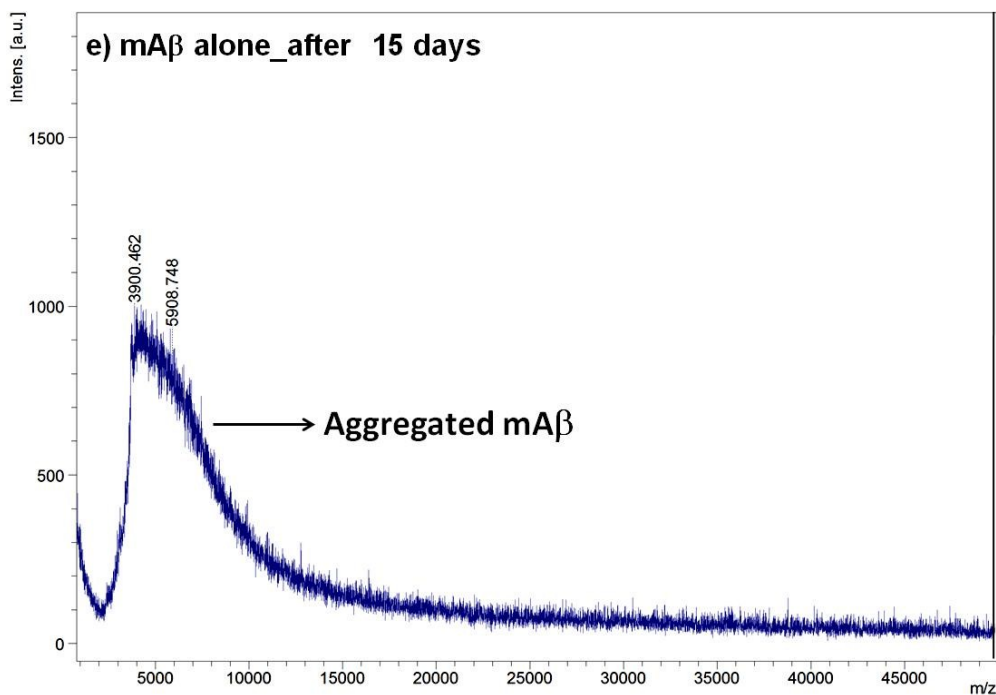


**Fig. S21.** MALDI-TOF mass spectrum of mAb $\beta$  (aggregated) after fifteen days of incubation in PBS.

## Self-degradation of mAP3:

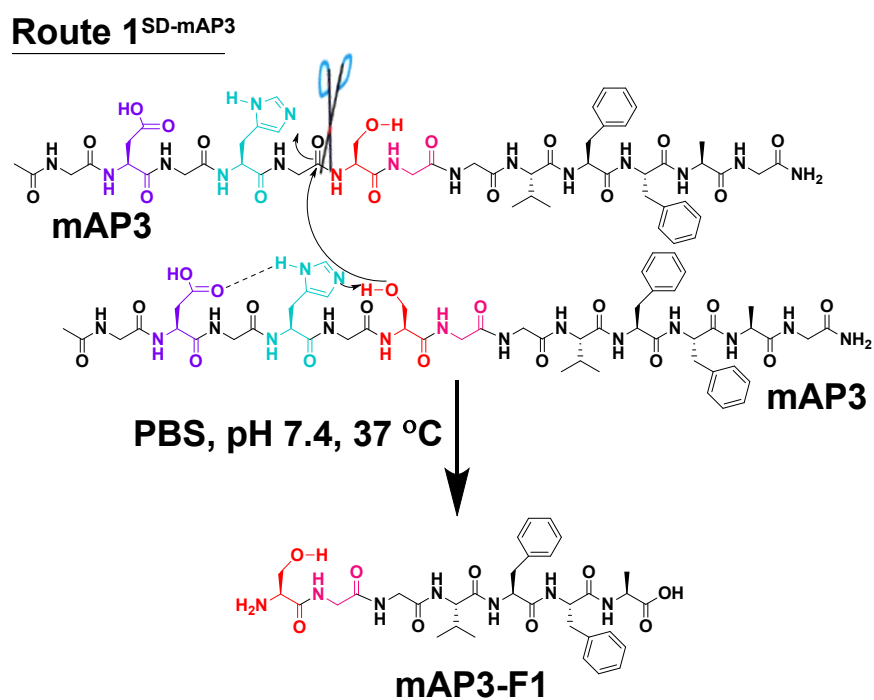


Fig. S22. Plausible route of the self-degradation of mAP3 into mAP3-F1 fragment (Route 1<sup>SD-mAP3</sup>). The nucleophilicity of Serine increases by cooperative interactions (intra-molecular hydrogen bonding) in-between the side chain of Asp-His-Ser residue resulting in Serine protease-like hydrolytic activity.

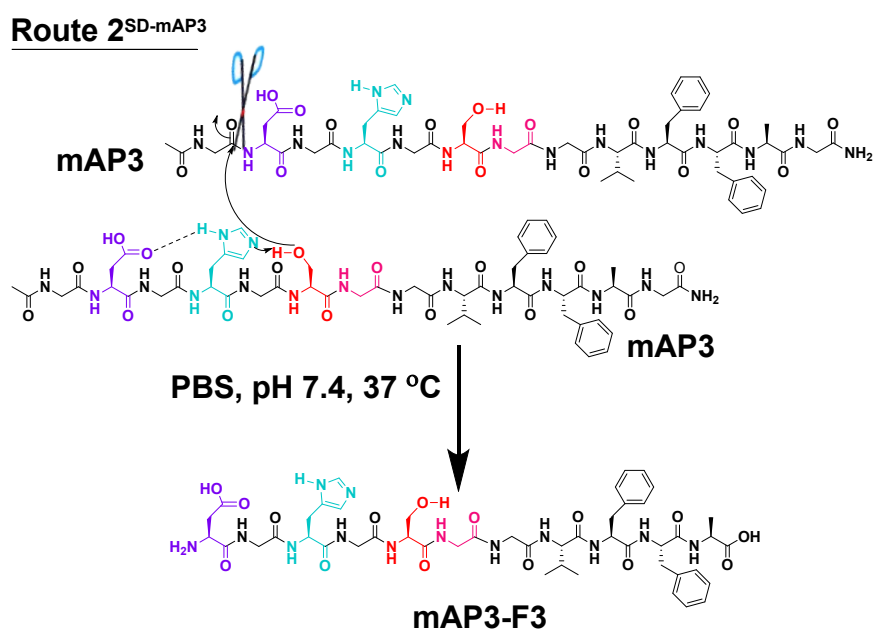


Fig. S23. Plausible route of the self-degradation of mAP3 into mAP3-F3 fragment (Route 2<sup>SD-mAP3</sup>).

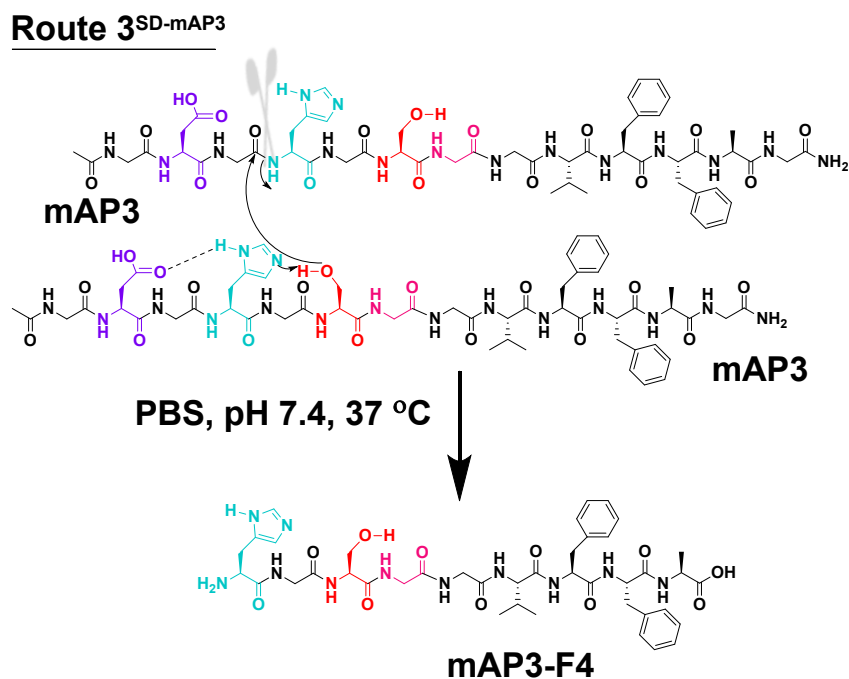


Fig. S24. Plausible route of the self-degradation of mAP3 into mAP3-F4 fragment (Route 3<sup>SD-mAP3</sup>).

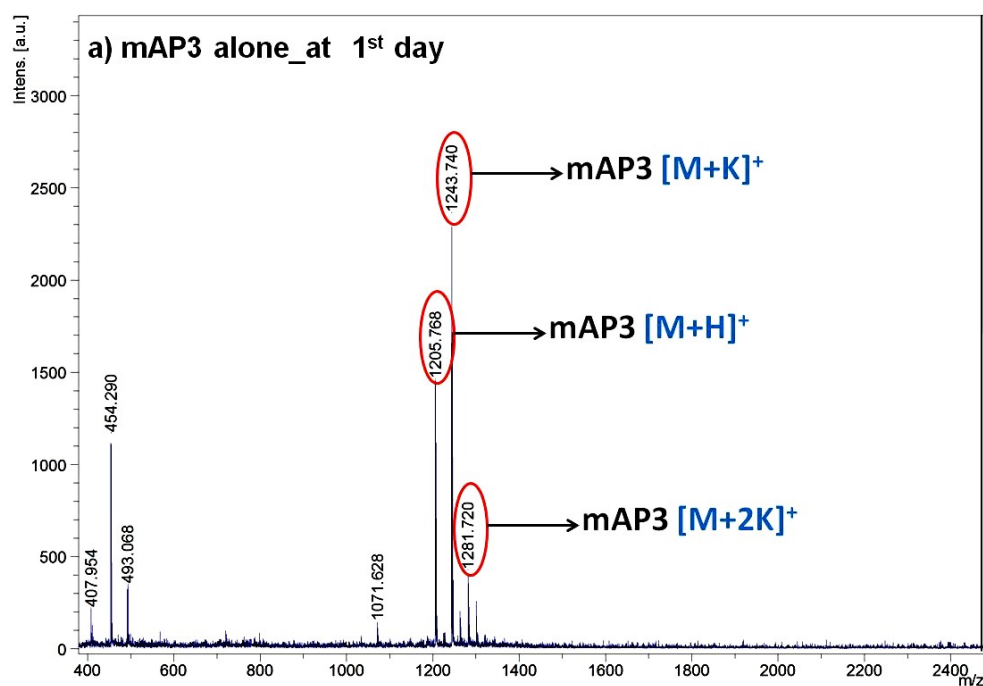


Fig. S25. MALDI-TOF mass spectrum of mAP3 on the first day of incubation in PBS pH 7.4 at 37 °C. Here different multiply-charged ionized species of mAP3 was obtained along with its singly-charged ions.

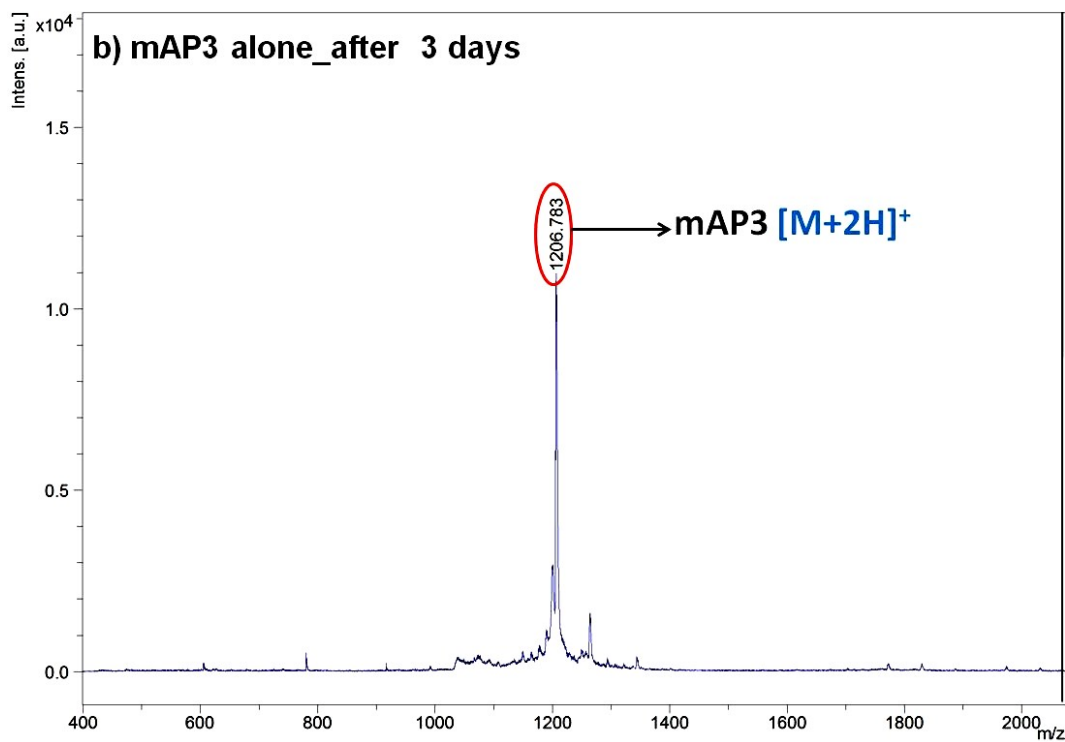


Figure S26. MALDI-TOF mass spectrum of mAP3 after three days of incubation in PBS. Here multiply-charged ionized species of mAP3 was obtained.

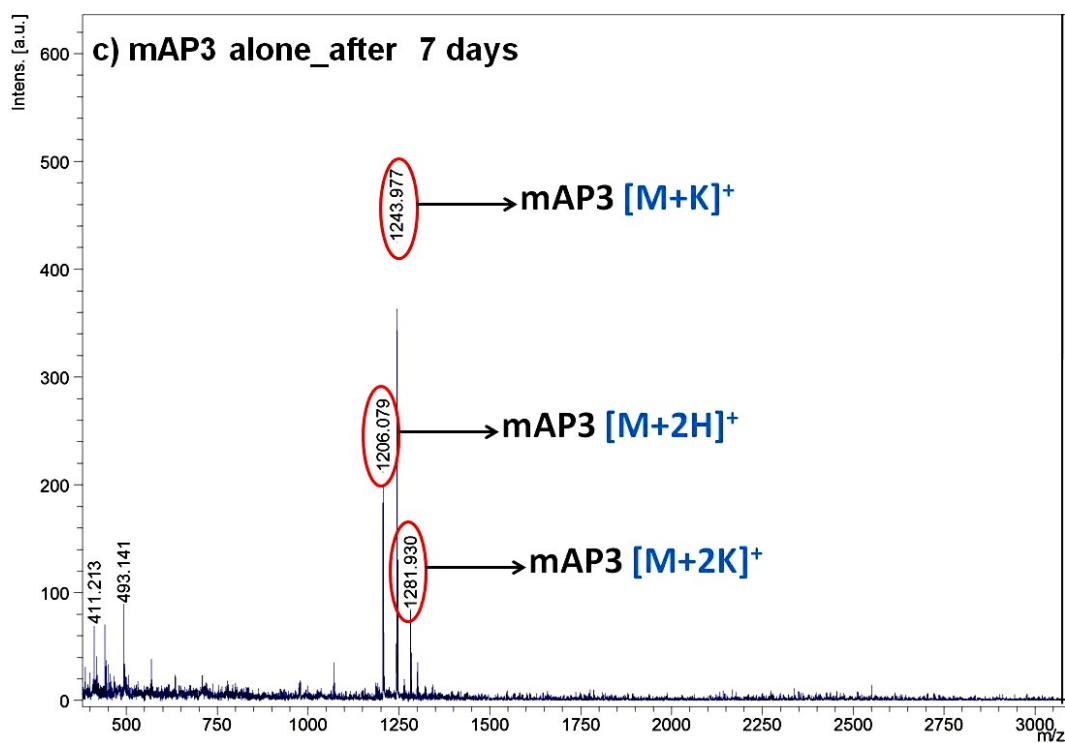
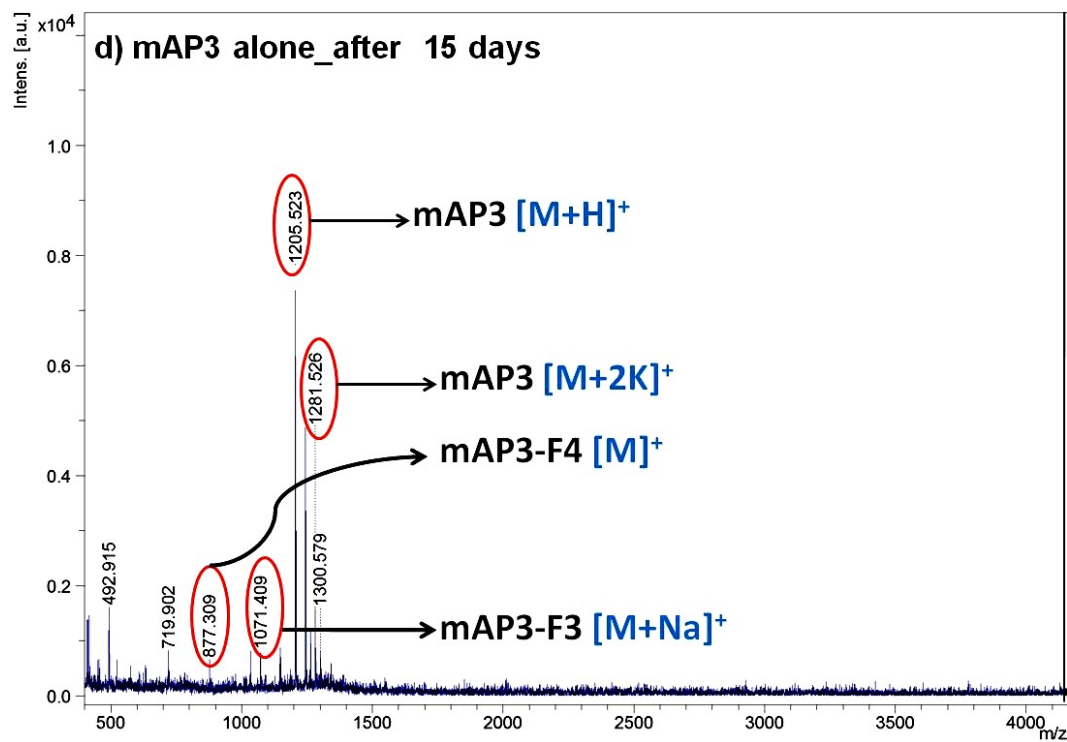


Fig. S27. MALDI-TOF mass spectrum of mAP3 after seven days of incubation in PBS. Here different multiply-charged ionized species of mAP3 were obtained along with its singly-charged ion.



**Fig. S28.** MALDI-TOF mass spectrum of mAP3 after fifteen days of incubation in PBS. Here different multiply-charged ionized species of mAP3 was obtained along with the singly-charged mAP3-F3 and mAP3-F4.

Plausible routes of the proteolytic cleavage of mA $\beta$  by mAP3:

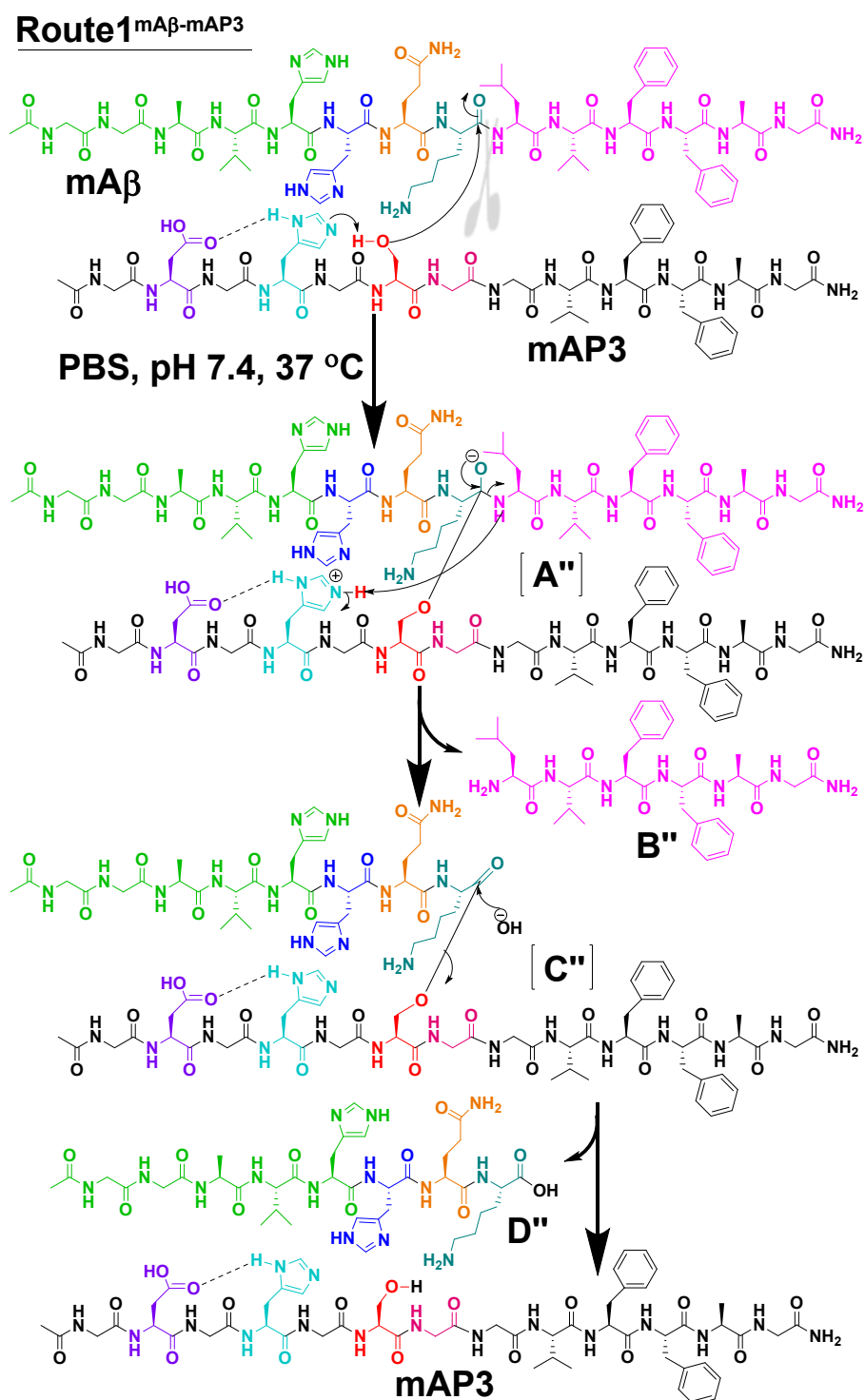


Fig. S29. Plausible route for the proteolysis of mA $\beta$  by mAP3 into B'' and D'' fragments (Route 1<sup>mA $\beta$ -mAP3</sup>). The fragments within the third brackets were not observed. The nucleophilicity of Serine increases by cooperative interactions (intra-molecular hydrogen bonding) in-between the side chain of Asp-His-Ser residue resulting in Serine protease-like hydrolytic activity.

### Route2<sup>mAβ-mAP3</sup>

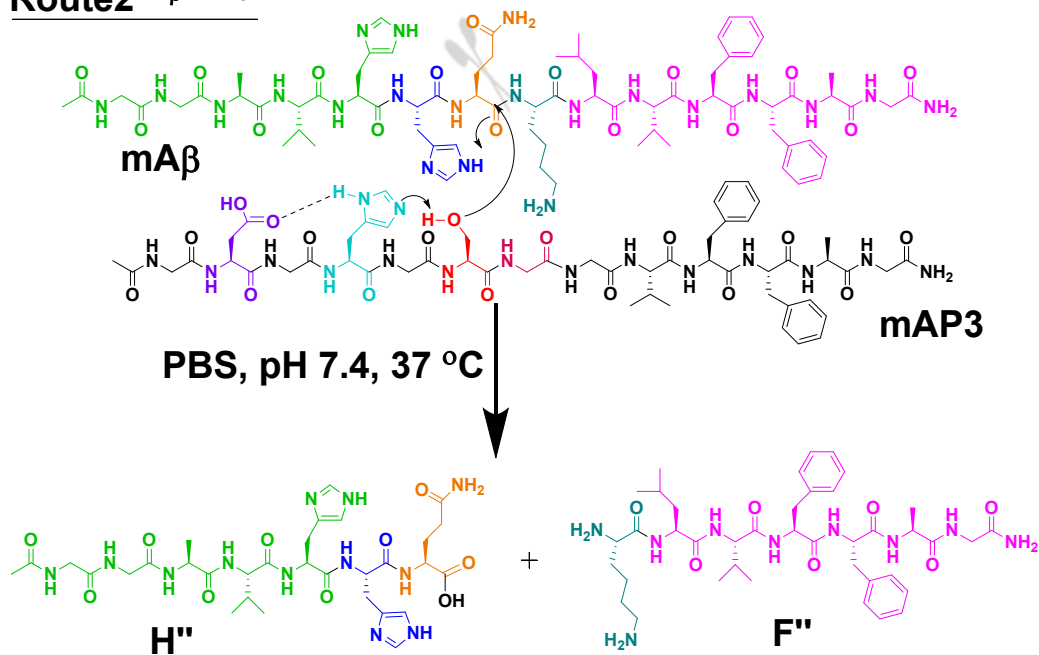


Fig. S30. Plausible route for the proteolysis of mAβ by mAP3 into F'' and H'' fragments (Route 2<sup>mAβ-mAP3</sup>).

### Route3<sup>mAβ-mAP3</sup>

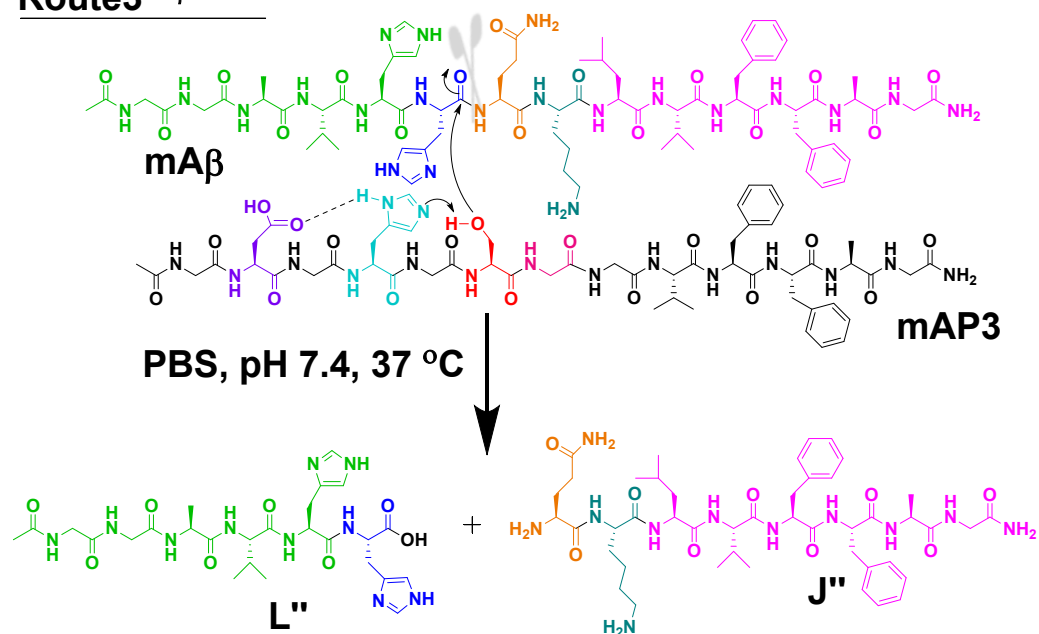


Fig. S31. Plausible route for the proteolysis of mAβ by mAP3 into J'' and L'' fragments (Route 3<sup>mAβ-mAP3</sup>).

### Route4<sup>mAβ-mAP3</sup>

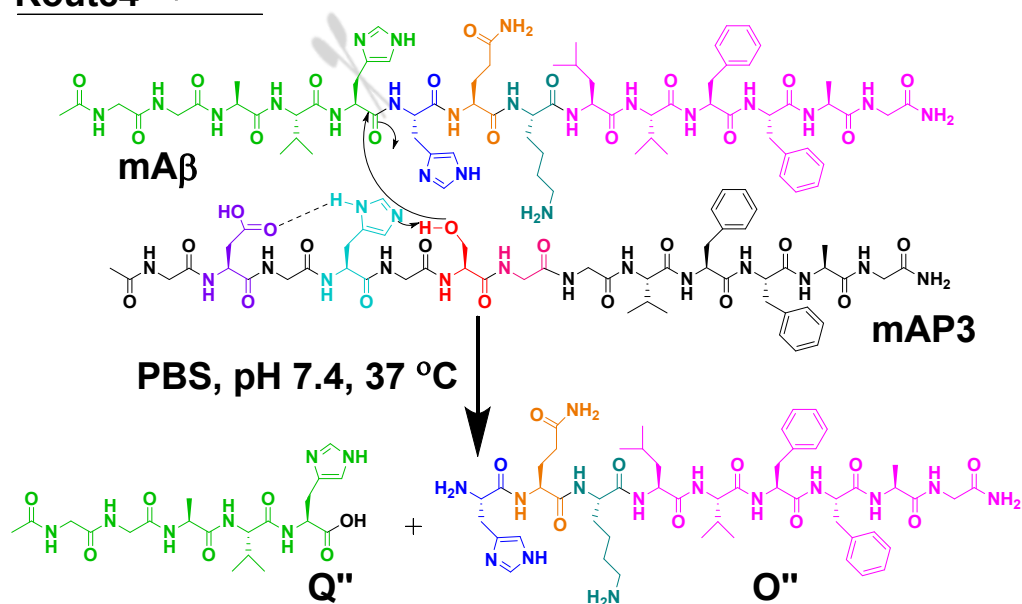


Fig. S32. Plausible route for the proteolysis of mAβ by mAP3 into O'' and Q'' fragments (Route 4<sup>mAβ-mAP3</sup>).

### Route5<sup>mAβ-mAP3</sup>

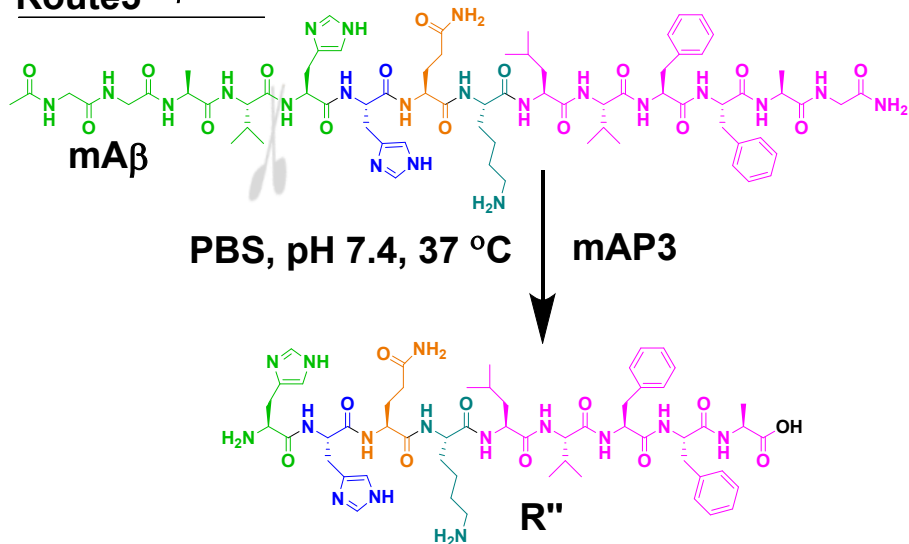


Fig. S33. Plausible route for the proteolysis of mAβ by mAP3 into R'' fragment (Route 5<sup>mAβ-mAP3</sup>).

### Route6<sup>mAβ-mAP3</sup>

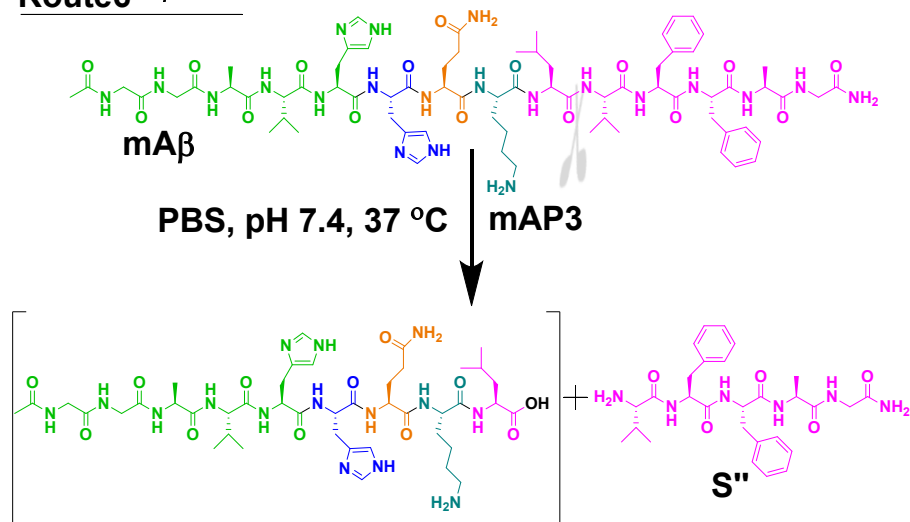


Fig. S34. Plausible route for the proteolysis of mAβ by mAP3 into S'' fragment (Route 6<sup>mAβ-mAP3</sup>). The fragment within the third bracket was not found.

### Route7<sup>mAβ-mAP3</sup>

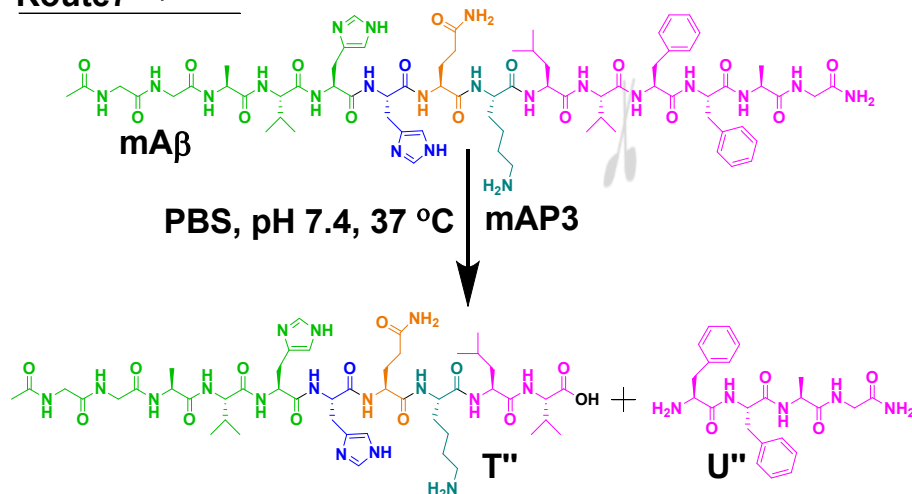


Fig. S35. Plausible route for the proteolysis of mAβ by mAP3 into U'' and T'' fragments (Route 7<sup>mAβ-mAP3</sup>).

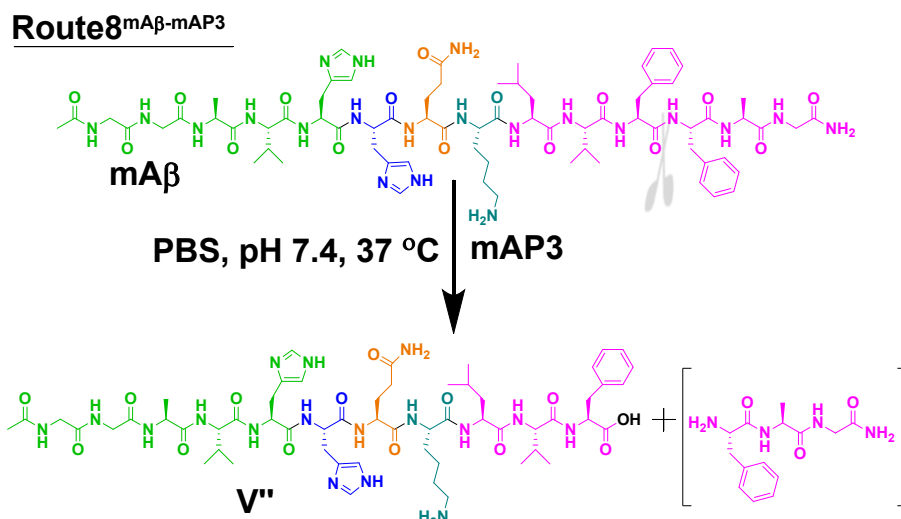


Fig. S36. Plausible route for proteolysis of mAβ by mAP3 into V'' fragment (Route 8<sup>mAβ-mAP3</sup>). The fragment within the third bracket was not found.

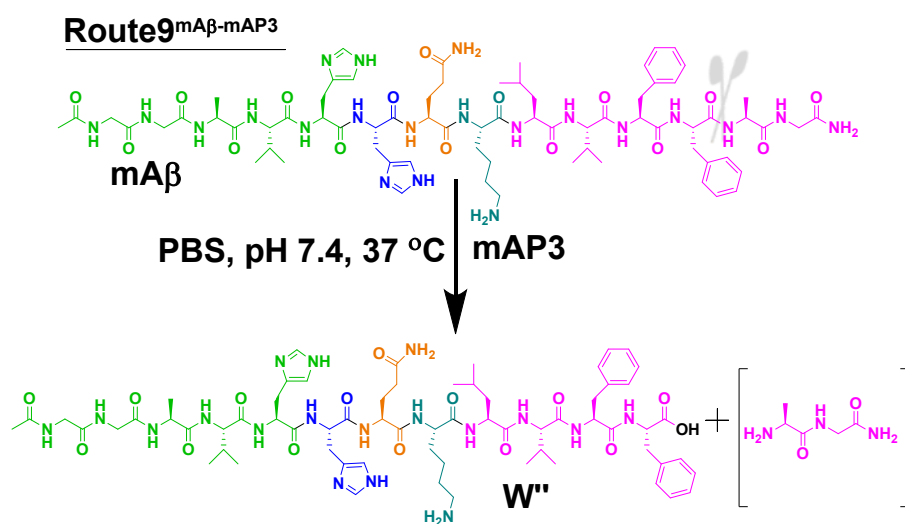


Fig. S37. Plausible route for proteolysis of mAβ by mAP3 into W'' fragment (Route 9<sup>mAβ-mAP3</sup>). The fragment within the third bracket was not found.

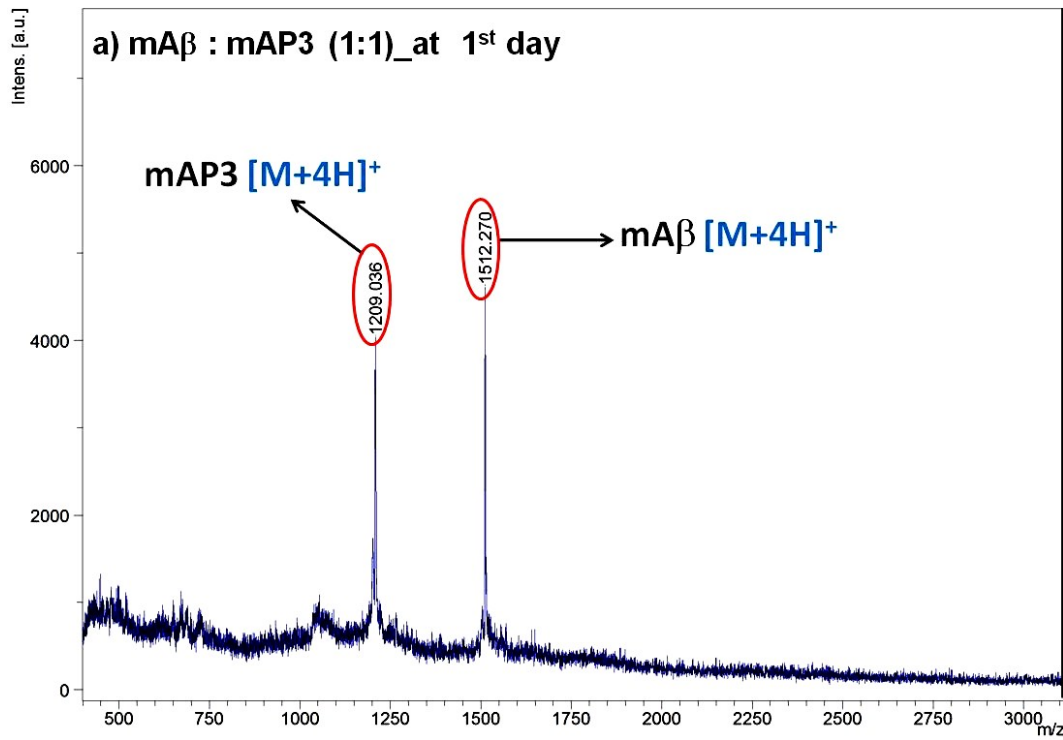


Fig. S38. MALDI-TOF mass spectrum of mAbeta in the presence of mAP3 (1:1) on the first day of incubation in PBS pH 7.4 at 37 °C. Here multiply-charged ionized species of mAbeta and mAP3 were obtained.

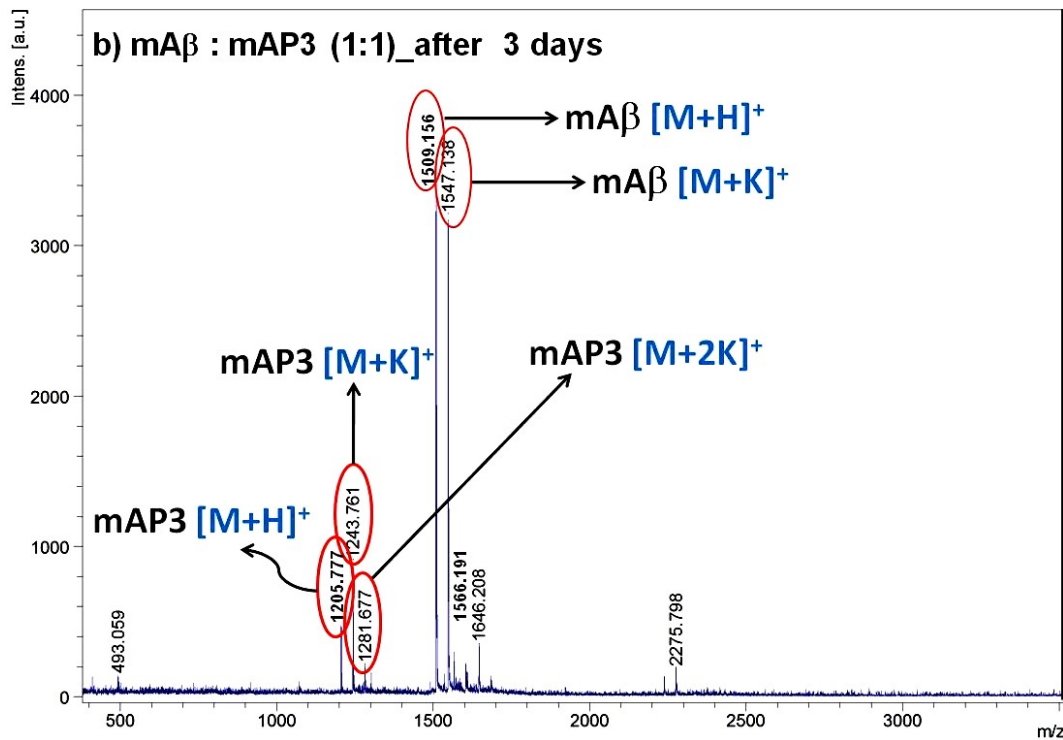


Fig. S39. MALDI-TOF mass spectrum of mAbeta in the presence of mAP3 (1:1) after three days of incubation in PBS. Here different multiply-charged ionized species of mAbeta and mAP3 were obtained.

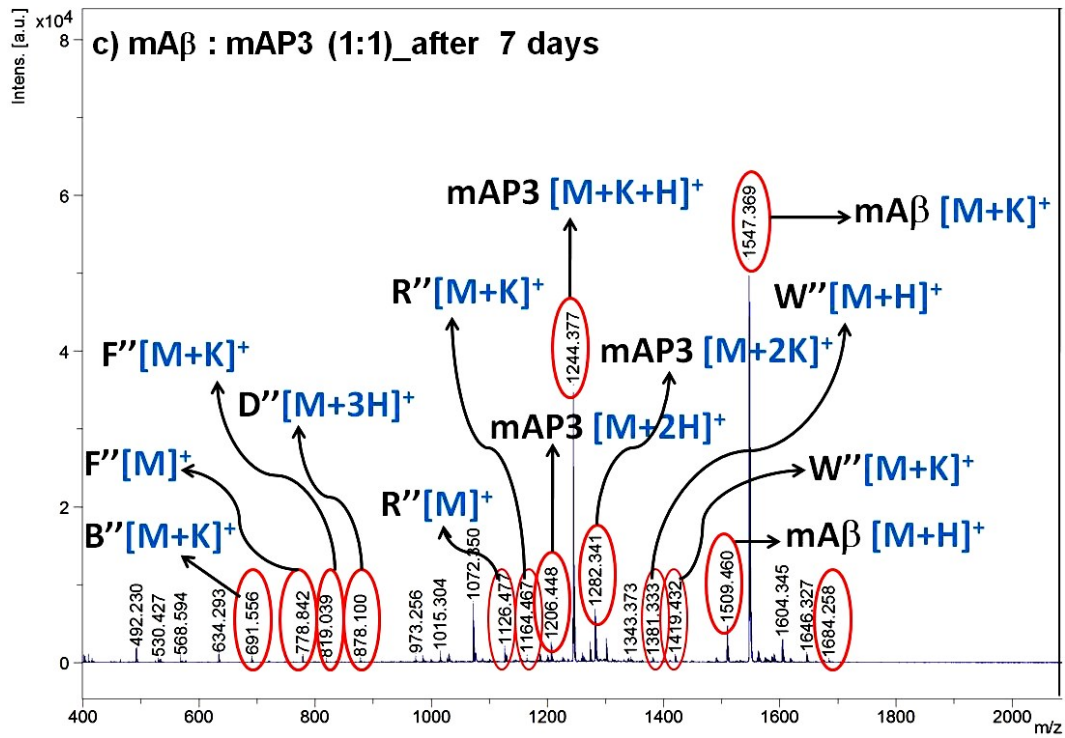


Fig. S40. MALDI-TOF mass spectrum of mAb in the presence of mAP3 (1:1) after seven days of incubation in PBS. Here different multiply-charged ionized species of mAP3 and D'' were obtained along with singly charged mAb, B'', F'', P'', R'' and W''.

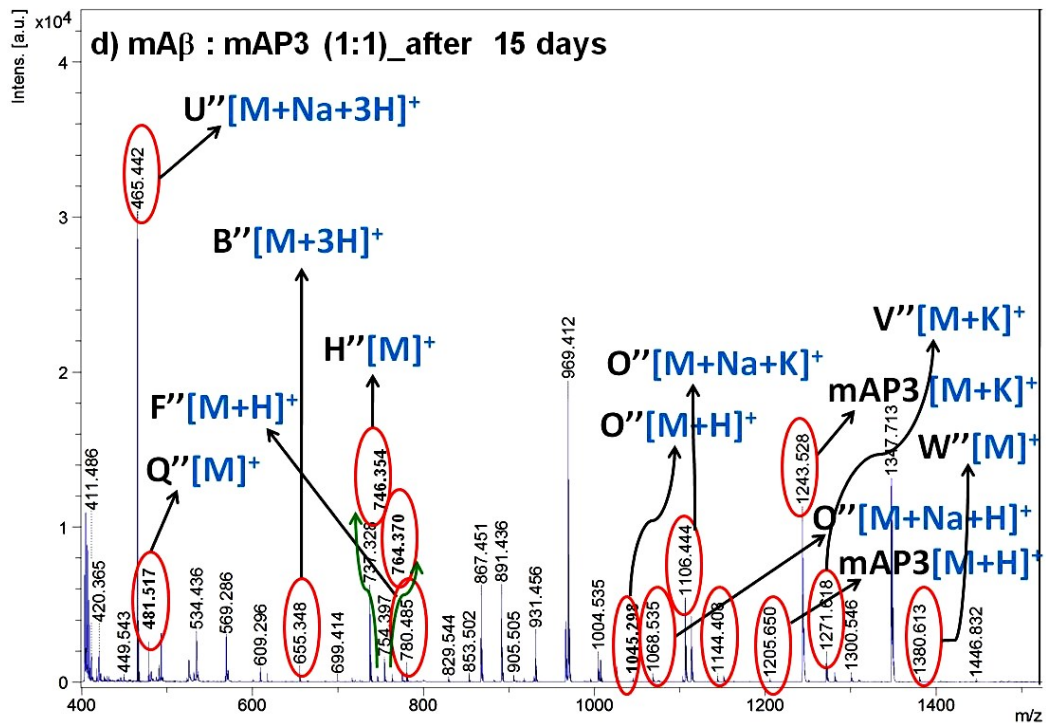
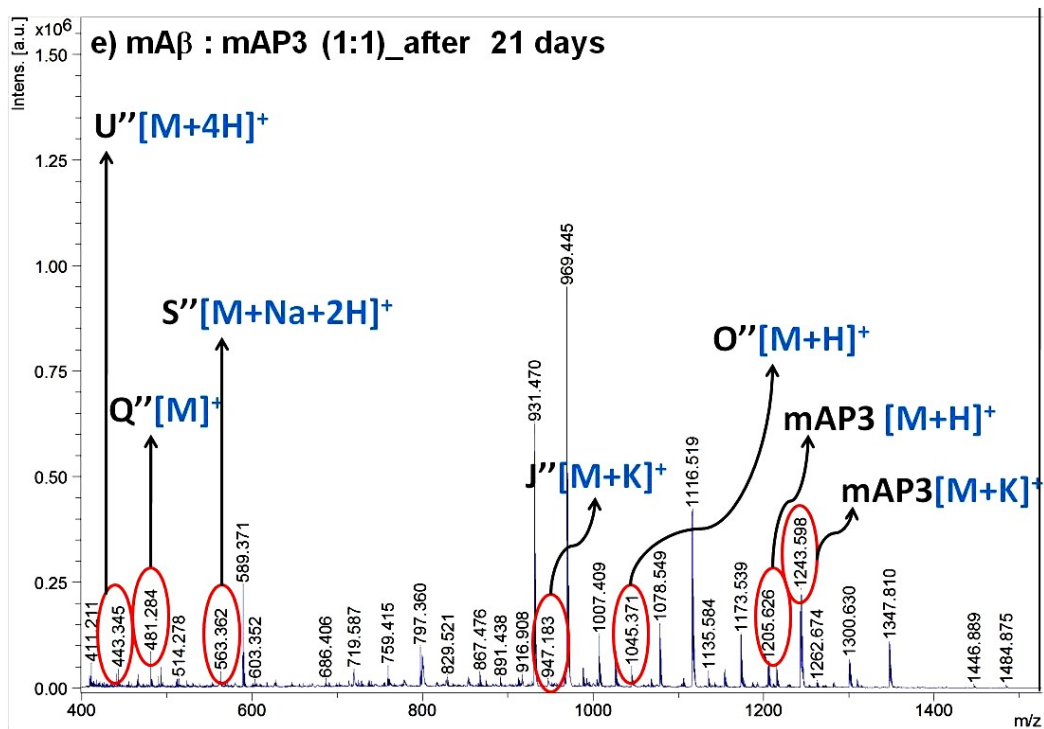


Fig. S41. MALDI-TOF mass spectrum of mAb in the presence of mAP3 (1:1) after fifteen days of incubation in PBS. Here different multiply-charged ionized species of B'', L'', O'' and U'' were obtained along with singly charged mAP3, F'', H'', Q'', V'' and W''.



**Fig. S42.** MALDI-TOF mass spectrum of mAP3 in the presence of mAP3 (1:1) after twenty-one days of incubation in PBS. Here different multiply-charged ionized species of mAP3, O'', S'' and U'' were obtained along with singly charged J'' and Q''.



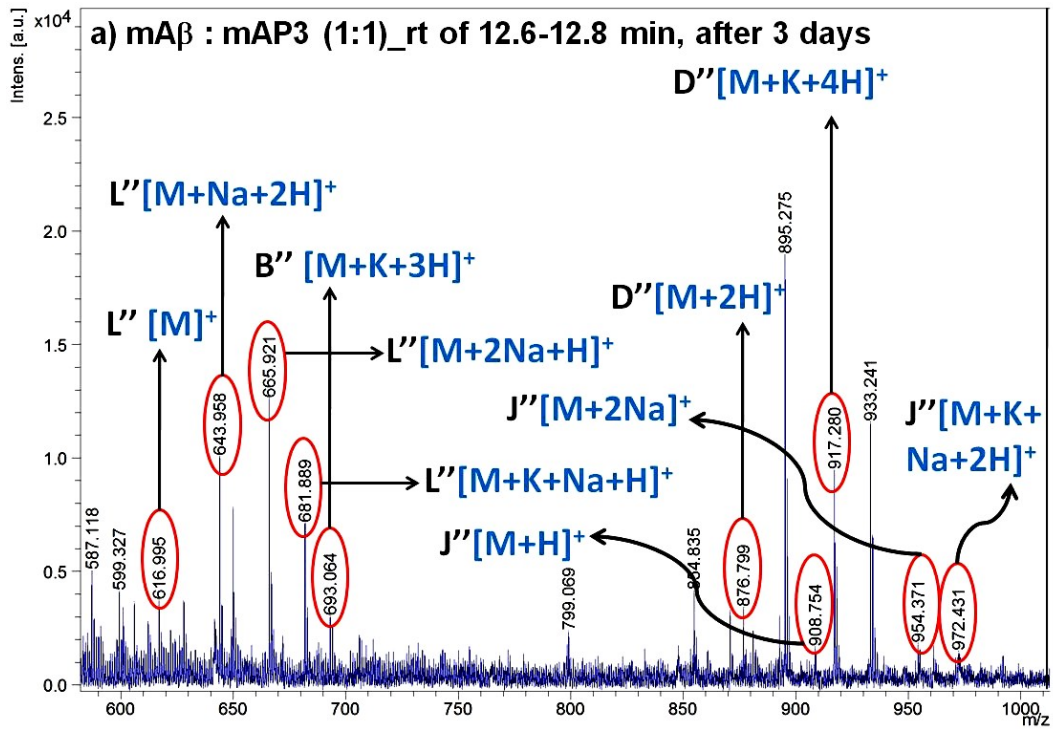


Fig. S45. MALDI-TOF mass spectrum of the HPLC fragments corresponding to retention time of 12.6-12.8 min from the solution of mAb in the presence of mAP3 (1:1) after three days of incubation in PBS. Here different multiply-charged ionized species were obtained.

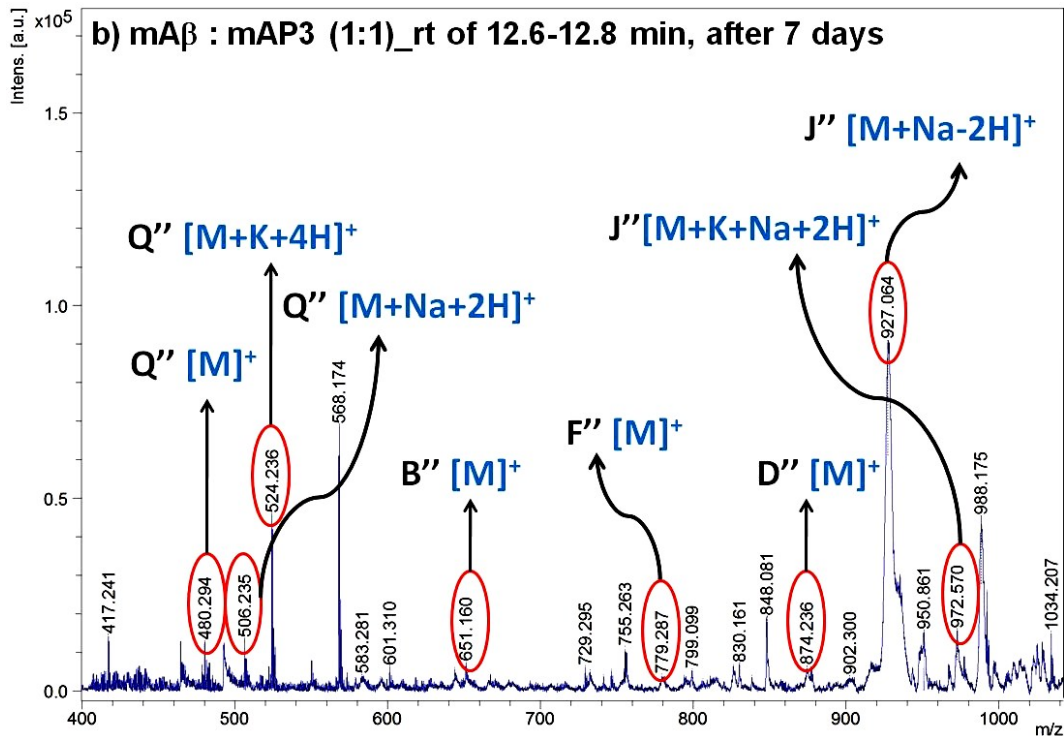
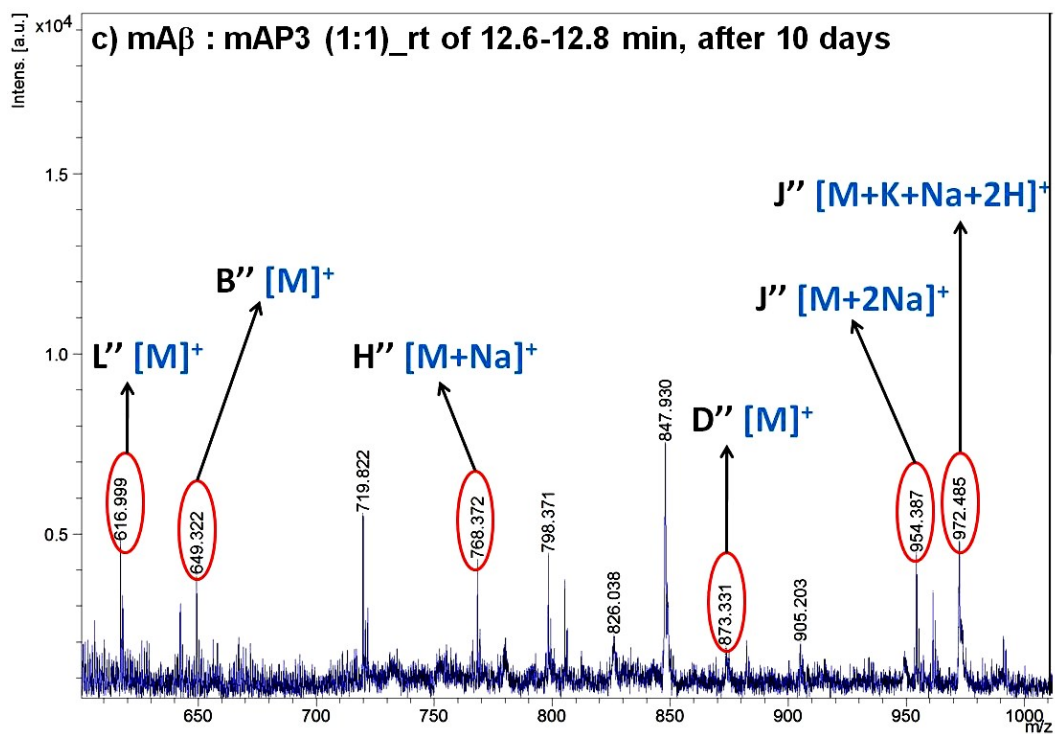
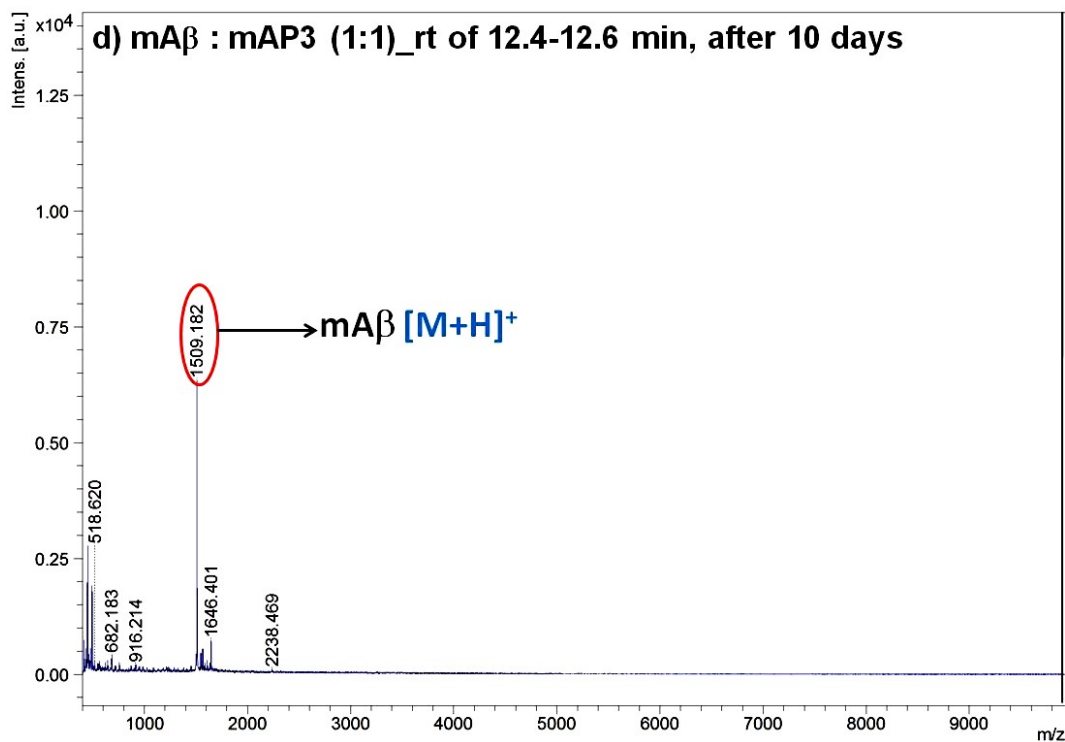


Fig. S46. MALDI-TOF mass spectrum of the HPLC fragments corresponding to retention time of 12.6-12.8 min from the solution of mAb in the presence of mAP3 (1:1) after seven days of incubation in PBS. Here different multiply-charged ionized species were obtained along with singly charged B'' and D''.



**Fig. S47.** MALDI-TOF mass spectrum of the HPLC fragments corresponding to retention time of 12.6-12.8 min from the solution of mA $\beta$  in the presence of mAP3 (1:1) after ten days of incubation in PBS. Here multiply-charged ionized species of J'' was obtained along with singly charged B'', D'', H'' and L''.



**Fig. S48.** MALDI-TOF mass spectrum of the HPLC fragments corresponding to retention time of 12.4-12.6 min from the solution of mA $\beta$  in the presence of mAP3 (1:1) after ten days of incubation in PBS. Here multiply-charged ionized species of mA $\beta$  was obtained.

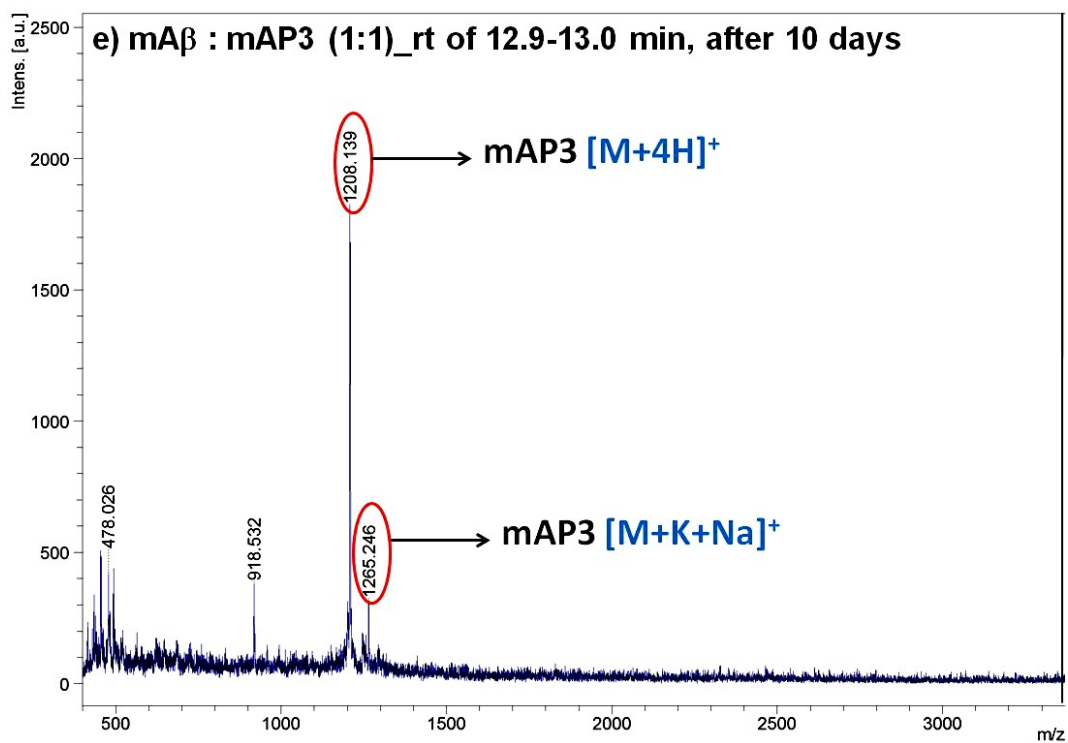


**Fig. S49.** MALDI-TOF mass spectrum of the HPLC fragments corresponding to retention time of 12.9-13.0 min from the solution of mA $\beta$  in the presence of mAP3 (1:1) after ten days of incubation in PBS. Here different multiply-charged ionized species of mAP3 were obtained.

Overlap of emission and absorbance spectrum of FmAβ1 and FmAβ2:

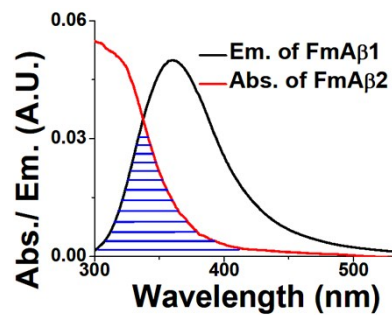


Fig. S50. Overlap of the emission spectrum of donor-peptide FmAβ1 (black) and the absorbance spectrum of acceptor-peptide FmAβ2 (red).

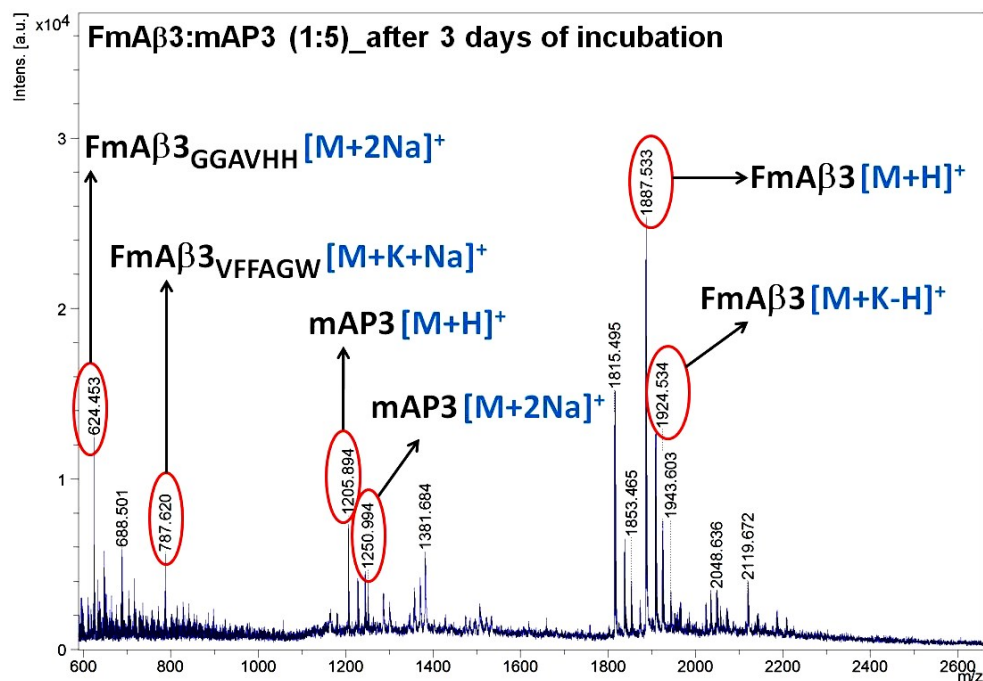


Fig. S51. MALDI-TOF mass spectrum of FmAβ3 in the presence of five-fold mAP3 after three days of incubation in PBS pH 7.4 at 37 °C. mAP3 cleave FmAβ3 in-between Leu<sub>17</sub>-Val<sub>18</sub> to produce FmAβ3<sub>VFFAGW</sub>. mAP3 also cleave FmAβ3 in-between His<sub>14</sub>-Gln<sub>15</sub> to produce FmAβ3<sub>GGAVHH</sub>.

## Examination of the proteolytic activity of mAPs on $A\beta_{1-40}$ :

**Self-degradation of  $A\beta_{1-40}$ :** The time-dependent MALDI-MS spectra of self-degradation of  $A\beta_{1-40}$  were found to be the same as reported earlier.<sup>2</sup>

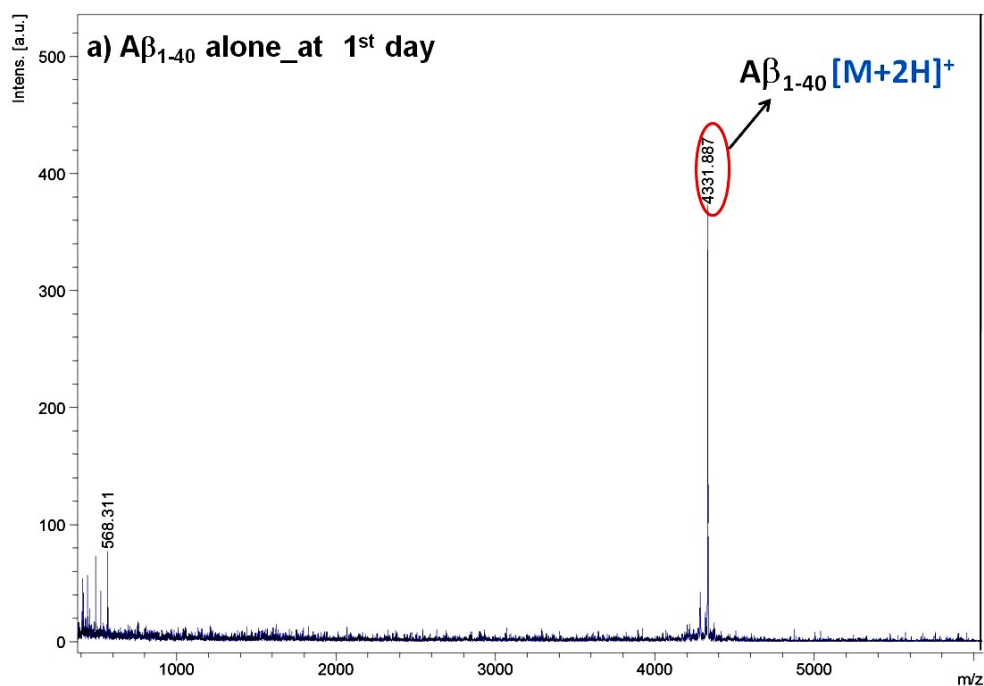


Fig. S52. MALDI-TOF mass spectrum of  $A\beta_{1-40}$  at the 1<sup>st</sup> day of incubation in PBS pH 7.4 at 37 °C.

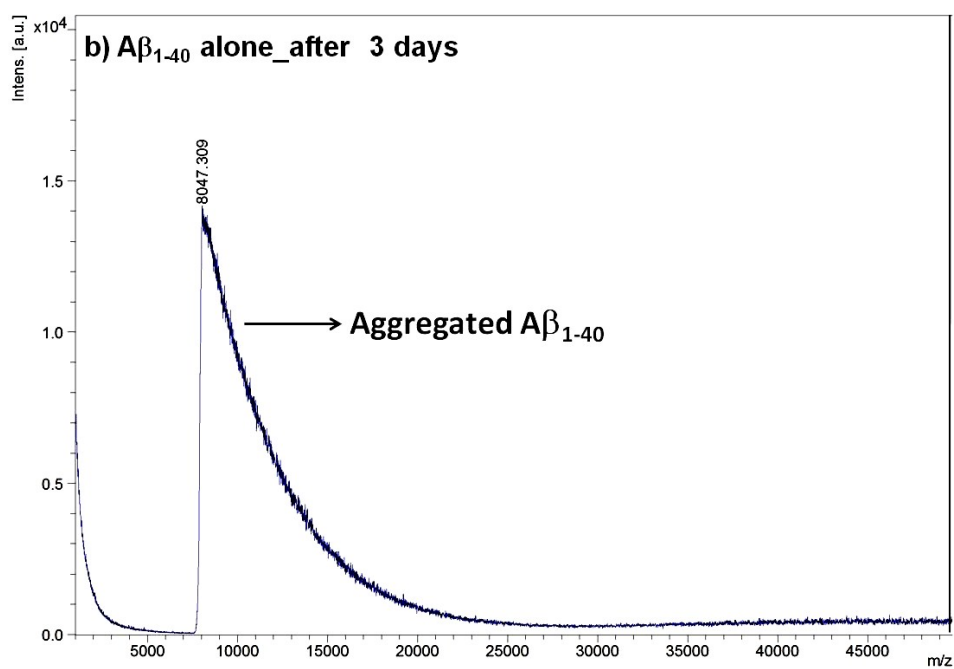


Fig. S53. MALDI-TOF mass spectrum of  $A\beta_{1-40}$  after three days of incubation in PBS.

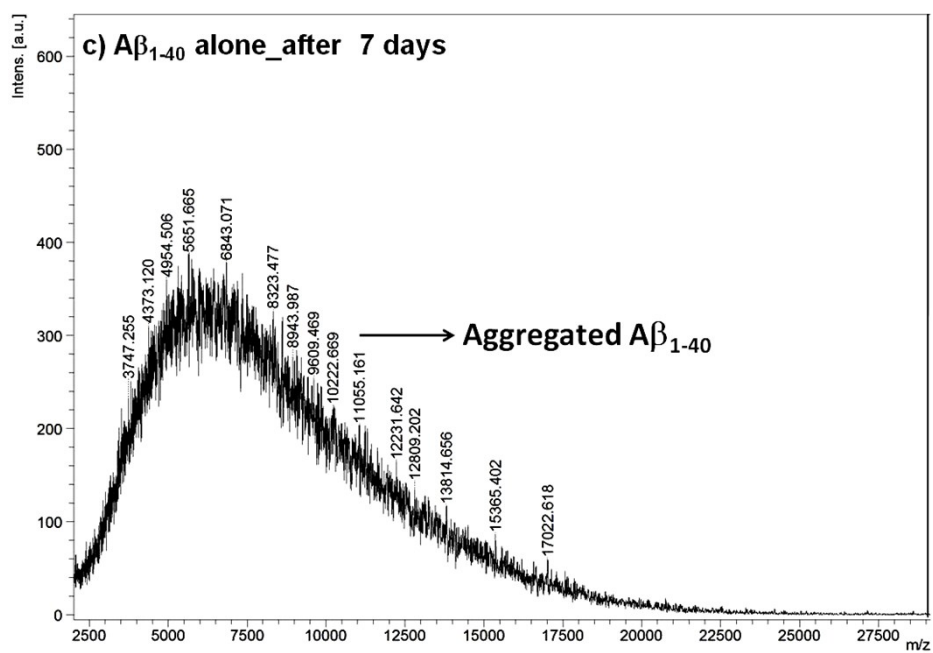


Fig. S54. MALDI-TOF mass spectrum of  $A\beta_{1-40}$  after seven days of incubation in PBS.

Plausible routes of the proteolytic cleavage of  $A\beta_{1-40}$  by mAP2 and mAP3:

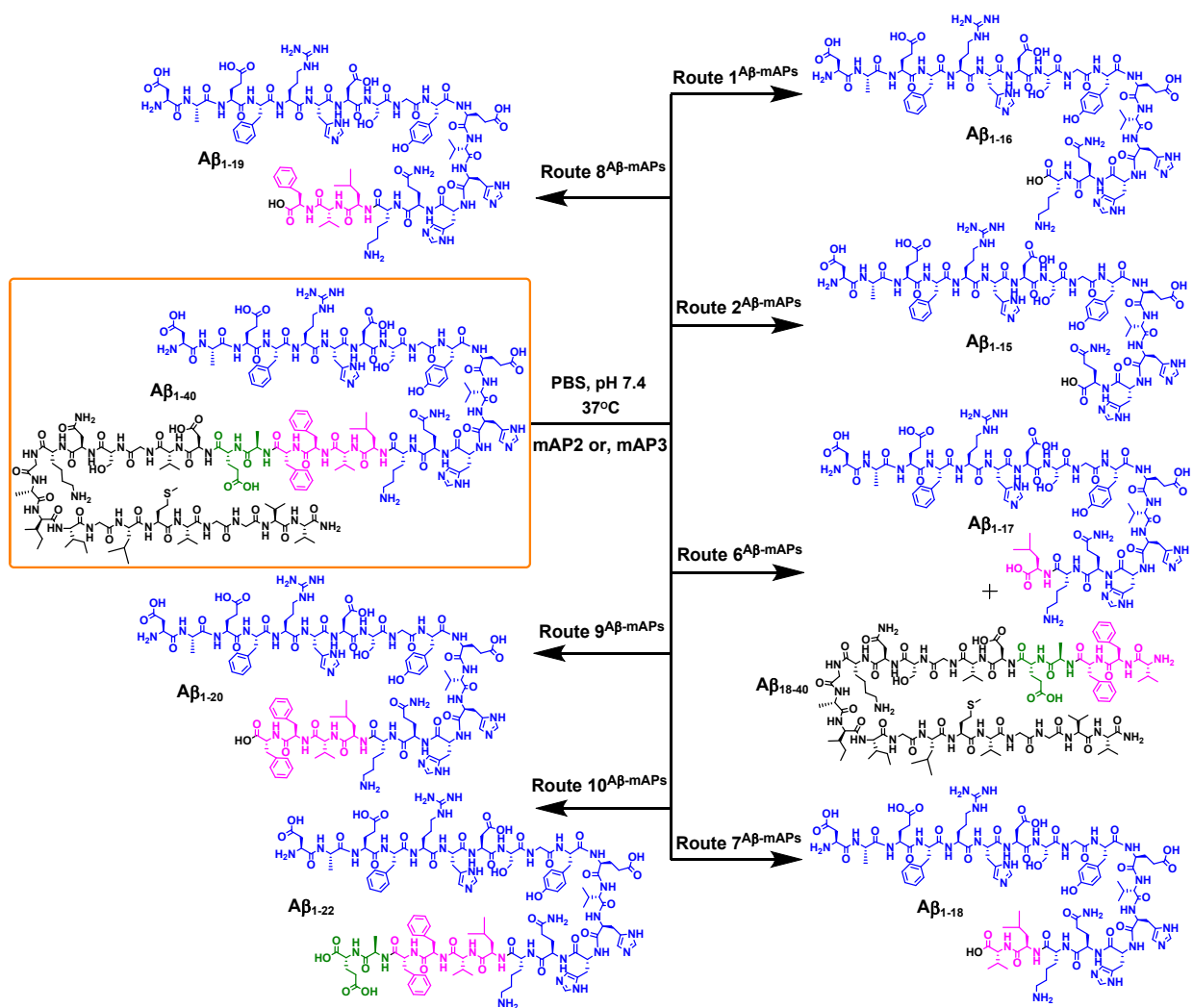


Fig. S55. Plausible routes of the proteolysis of  $A\beta_{1-40}$  into various fragments ( $A\beta_{1-15}$ ,  $A\beta_{1-16}$ ,  $A\beta_{1-17}$ ,  $A\beta_{1-18}$ ,  $A\beta_{1-19}$ ,  $A\beta_{1-20}$ ,  $A\beta_{1-22}$ , and  $A\beta_{18-40}$ ) by mAPs (Route 1<sup>m</sup> $A\beta$ -mAP<sub>2/3</sub>, Route 2<sup>m</sup> $A\beta$ -mAP<sub>2/3</sub>, Route 6<sup>m</sup> $A\beta$ -mAP<sub>2/3</sub>- Route 10<sup>m</sup> $A\beta$ -mAP<sub>2/3</sub>).

### Proteolytic activity of mAP3 on A $\beta$ <sub>1-40</sub>:

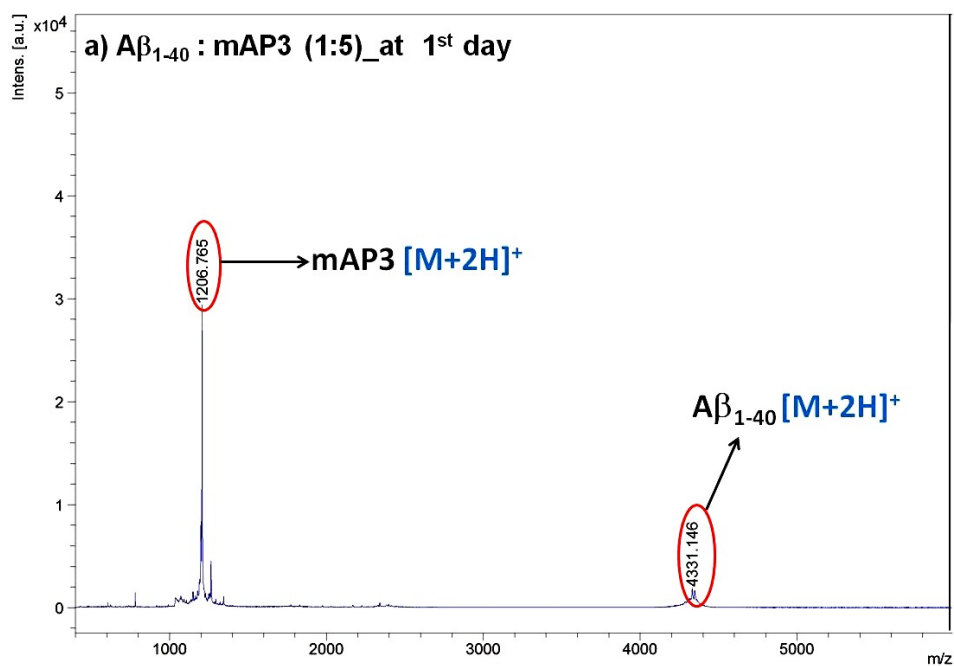


Fig. S56. MALDI-TOF mass spectrum of A $\beta$ <sub>1-40</sub> in the presence of mAP3 (1:5) on the first day of incubation in PBS pH 7.4 at 37 °C. Here multiply-charged ionized species of mAP3 and A $\beta$ <sub>1-40</sub> were obtained.

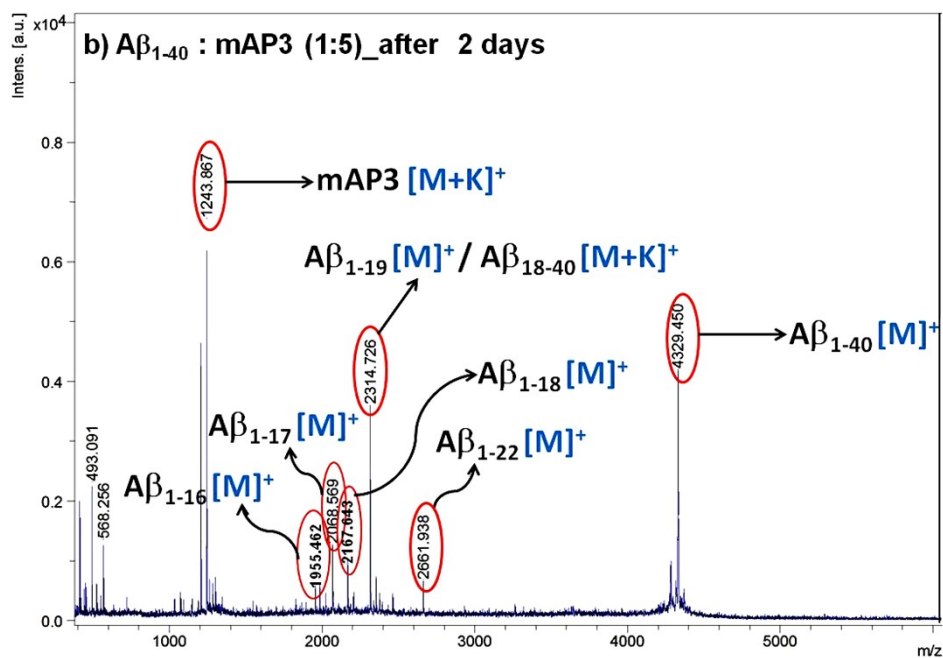


Fig. S57. MALDI-TOF mass spectrum of A $\beta$ <sub>1-40</sub> in the presence of mAP3 (1:5) after two days of incubation in PBS. Here singly-charged ionized species were obtained.

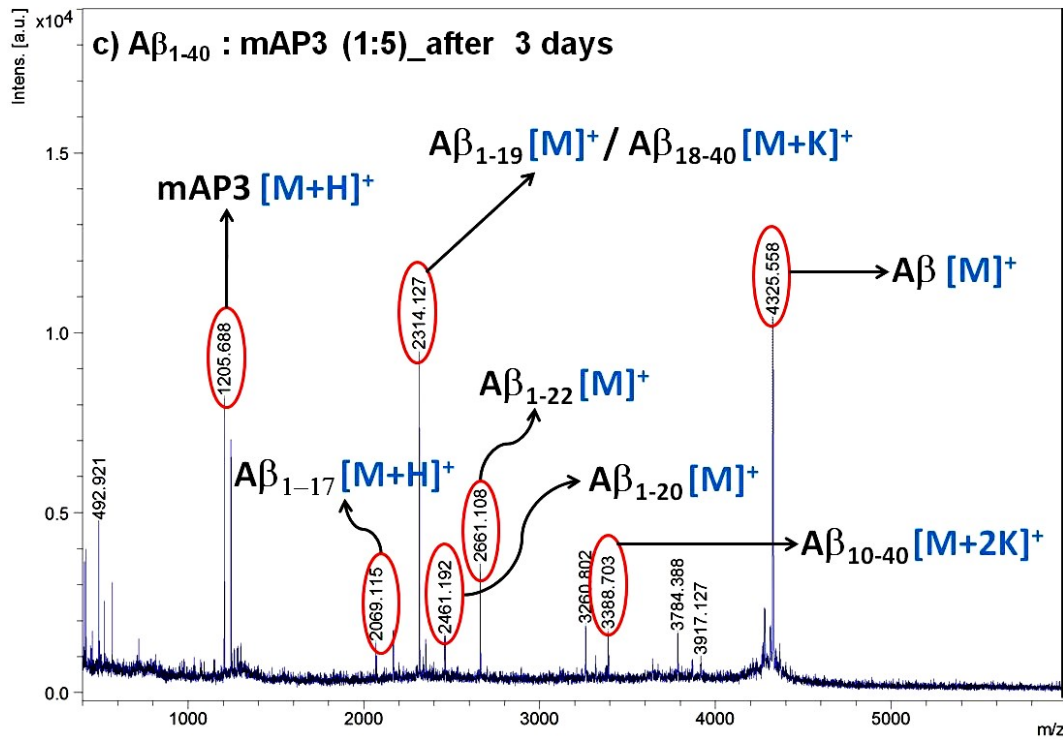


Fig. S58. MALDI-TOF mass spectrum of A $\beta$ <sub>1-40</sub> in the presence of mAP3 (1:5) after three days of incubation in PBS. Here multiply-charged ionized species of A $\beta$ <sub>10-40</sub> were obtained along with singly-charged mAP3, A $\beta$ <sub>1-40</sub>, A $\beta$ <sub>1-17</sub>, A $\beta$ <sub>1-19</sub>, A $\beta$ <sub>1-20</sub>, A $\beta$ <sub>1-22</sub>, A $\beta$ <sub>10-40</sub>, and A $\beta$ <sub>18-40</sub> ions.

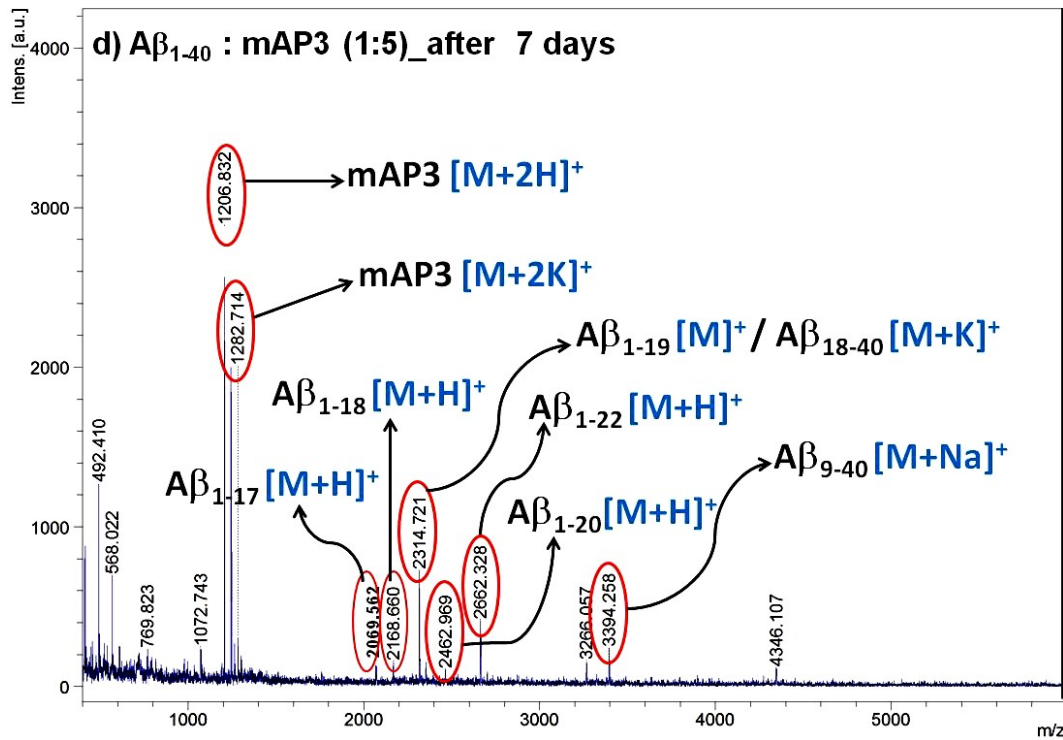
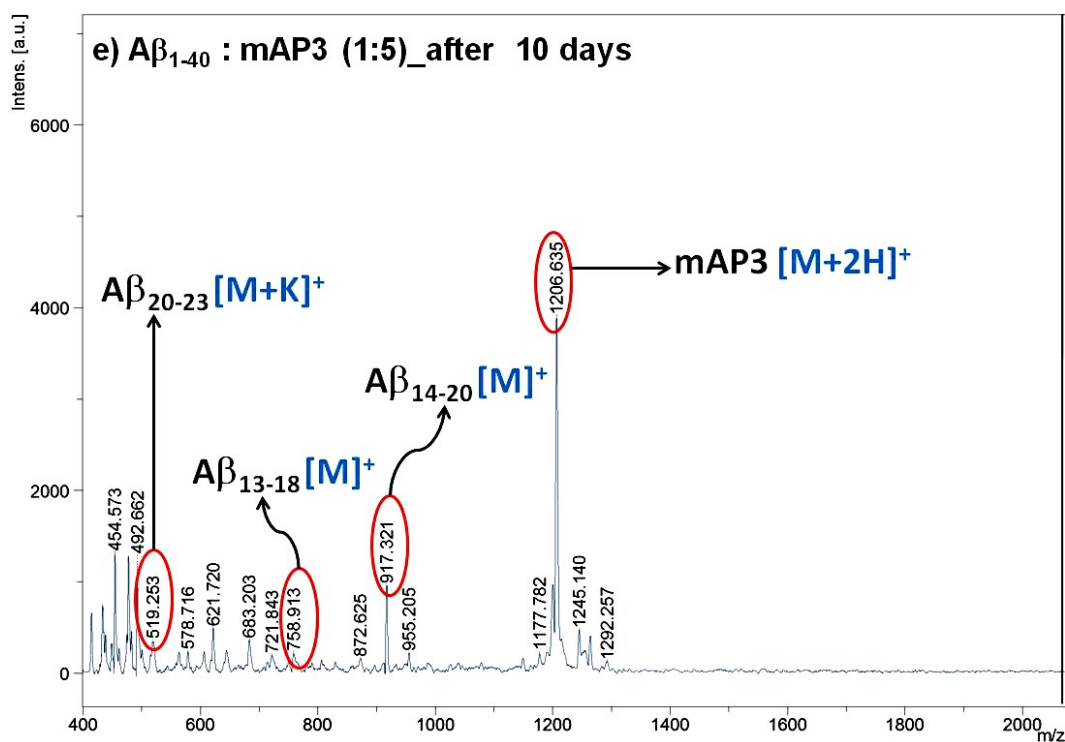
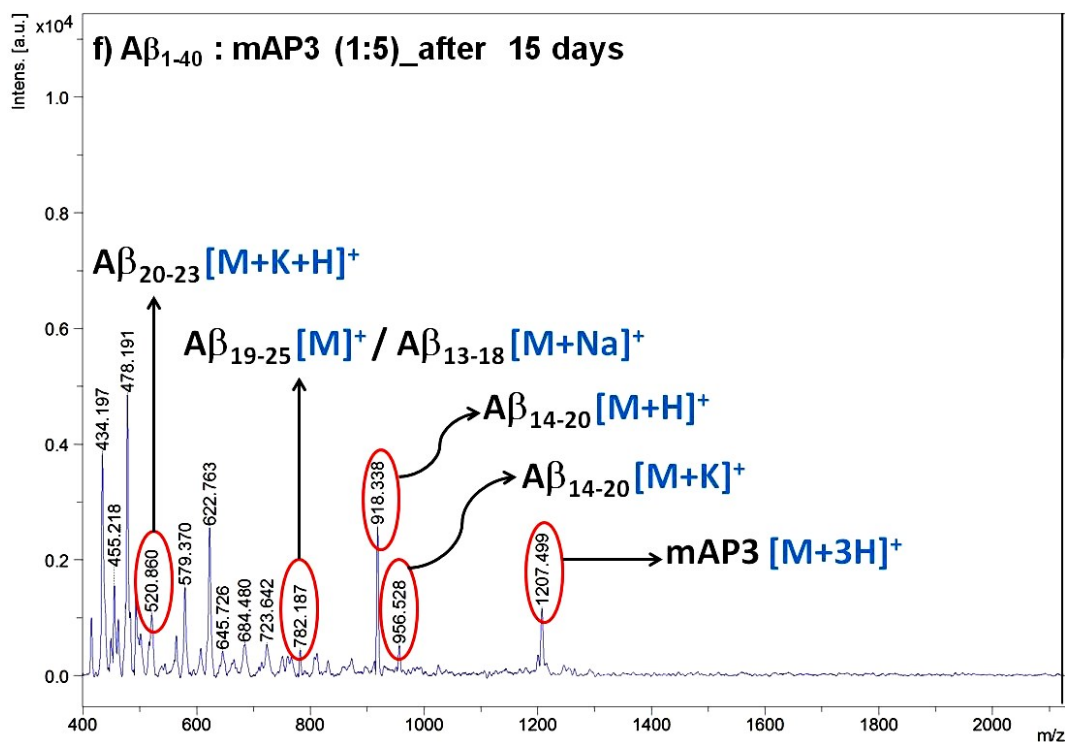


Fig. S59. MALDI-TOF mass spectrum of A $\beta$ <sub>1-40</sub> in the presence of mAP3 (1:5) after seven days of incubation in PBS. Here different multiply-charged ionized species of mAP3 were obtained along with singly-charged A $\beta$ <sub>1-40</sub>, A $\beta$ <sub>1-17</sub>, A $\beta$ <sub>1-18</sub>, A $\beta$ <sub>1-19</sub>, A $\beta$ <sub>1-20</sub>, A $\beta$ <sub>1-22</sub>, A $\beta$ <sub>9-40</sub> and A $\beta$ <sub>18-40</sub> ions.



**Fig. S60.** MALDI-TOF mass spectrum of  $A\beta_{1-40}$  in the presence of mAP3 (1:5) after ten days of incubation in PBS. Here multiply-charged ionized species of mAP3 was obtained along with singly-charged  $A\beta_{13-18}$ ,  $A\beta_{14-20}$ ,  $A\beta_{1-22}$  and  $A\beta_{20-23}$  ions.



**Fig. S61.** MALDI-TOF mass spectrum of  $A\beta_{1-40}$  in the presence of mAP3 (1:5) after fifteen days of incubation in PBS. Here multiply-charged ionized species of mAP3 was obtained along with singly-charged  $A\beta_{13-18}$ ,  $A\beta_{14-20}$ ,  $A\beta_{20-23}$  and  $A\beta_{19-25}$  ions.

### Time-dependent existence map of various fragments of $A\beta_{1-40}$ :

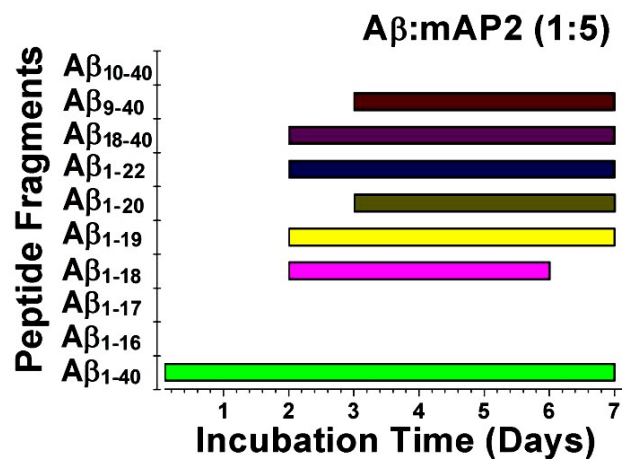


Fig. S62. The time-dependent persistence map of various fragments of  $A\beta_{1-40}$  in the presence of mAP2.

### Inhibitory ability of KLVFF on $A\beta_{1-40}$ :

MALDI-TOF mass spectra of  $A\beta_{1-40}$  in the presence of KLVFF were analysed in a time-dependent manner (up to 15 days). However, mAPs mediated no such degradation product was observed in MALDI-TOF mass spectra, a few self-degraded peptide fragments were appeared due to the inhibition of  $A\beta_{1-40}$  by KLVFF.

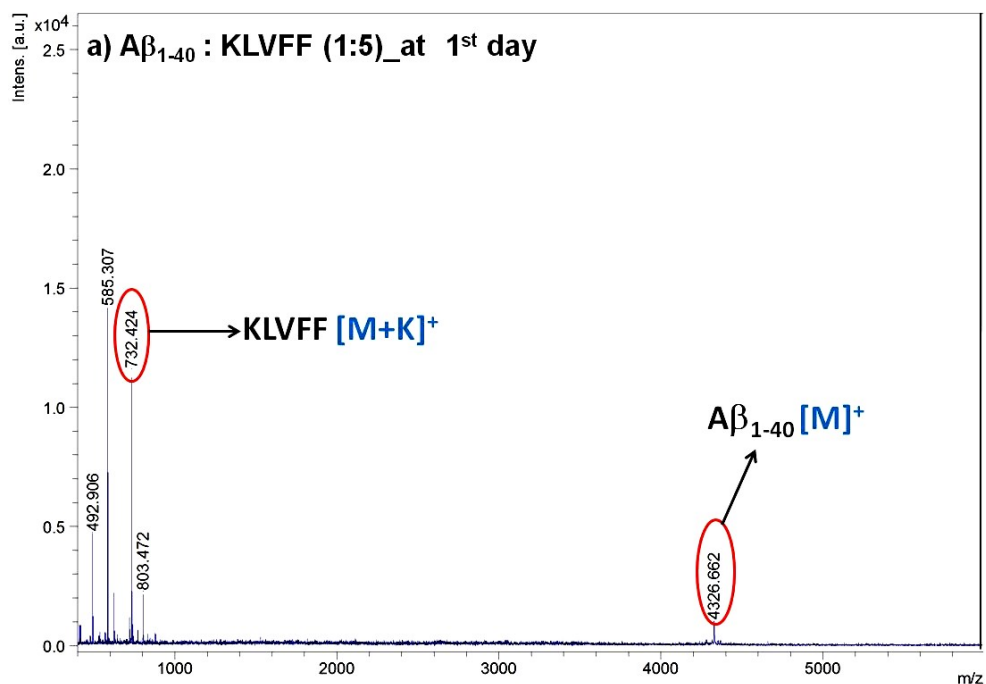


Fig. S63. MALDI-TOF mass spectrum of  $A\beta_{1-40}$  in the presence of KLVFF (1:5) on the first day of incubation in PBS pH 7.4 at 37 °C.

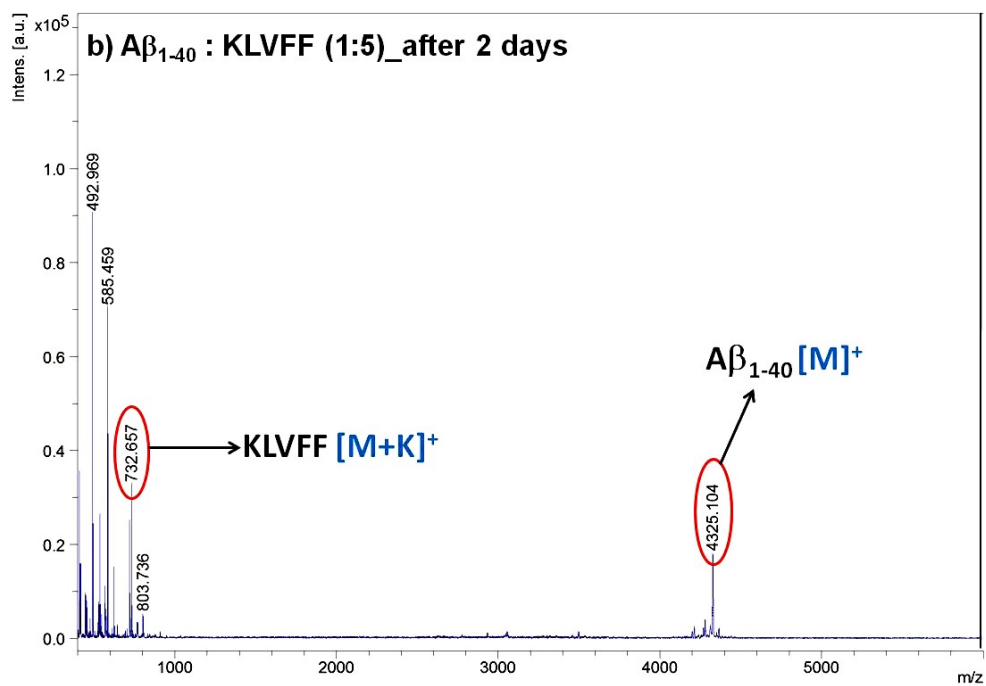


Fig. S64. MALDI-TOF mass spectrum of A $\beta$ <sub>1-40</sub> in the presence of KLVFF (1:5) after two days of incubation in PBS.

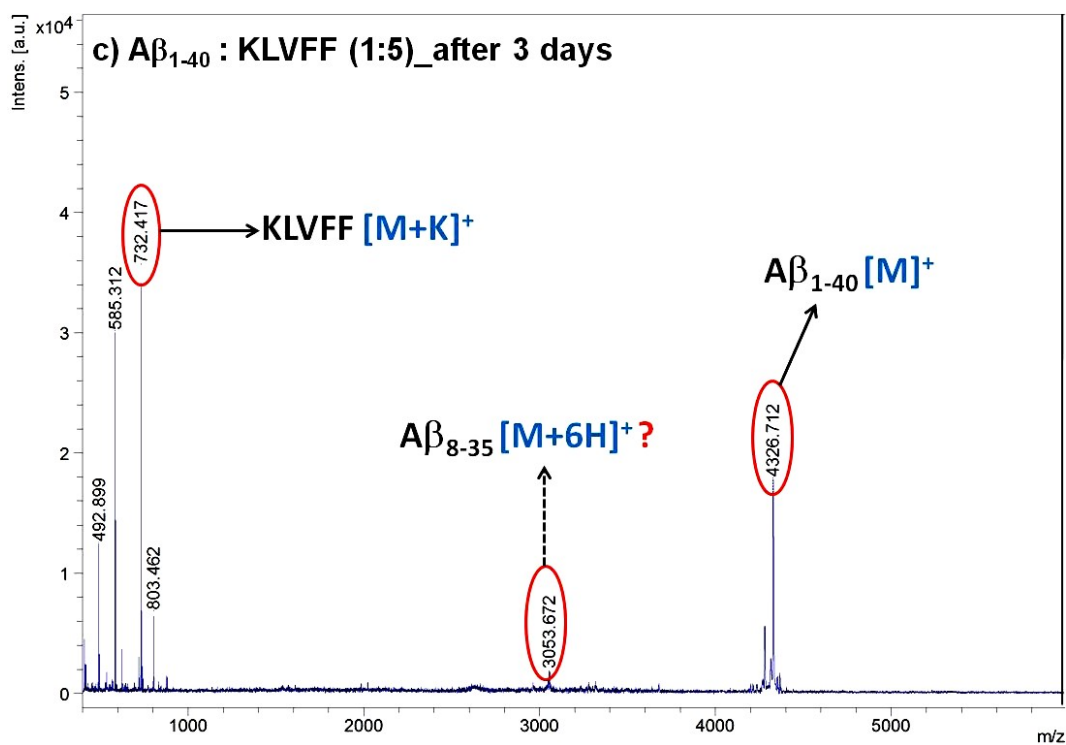


Fig. S65. MALDI-TOF mass spectrum of A $\beta$ <sub>1-40</sub> in the presence of KLVFF (1:5) after three days of incubation in PBS due to Ser-mediated proteolysis.

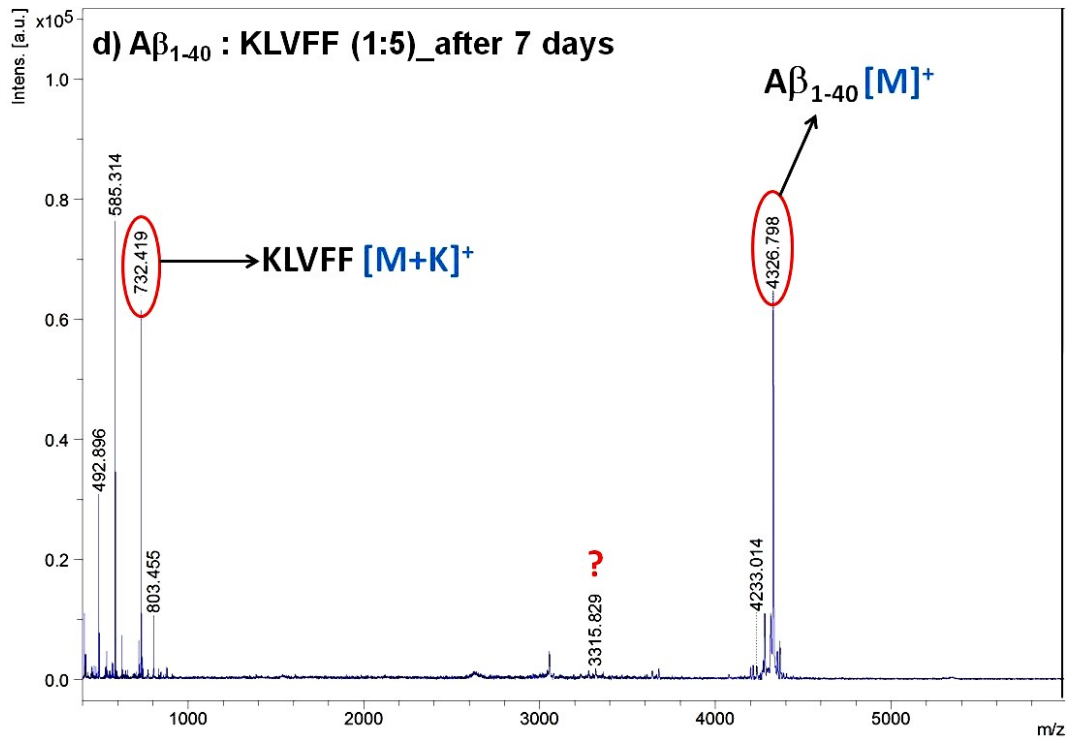


Fig. S66. MALDI-TOF mass spectrum of A $\beta$ <sub>1-40</sub> in the presence of KLVFF (1:5) after seven days of incubation in PBS.

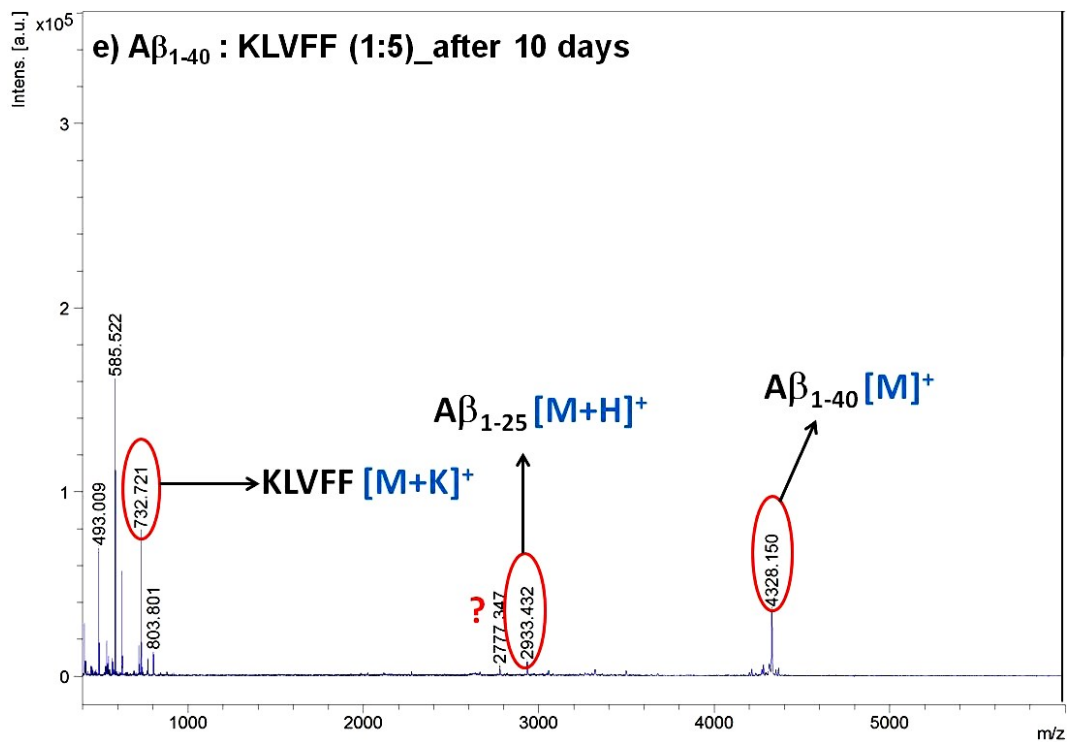
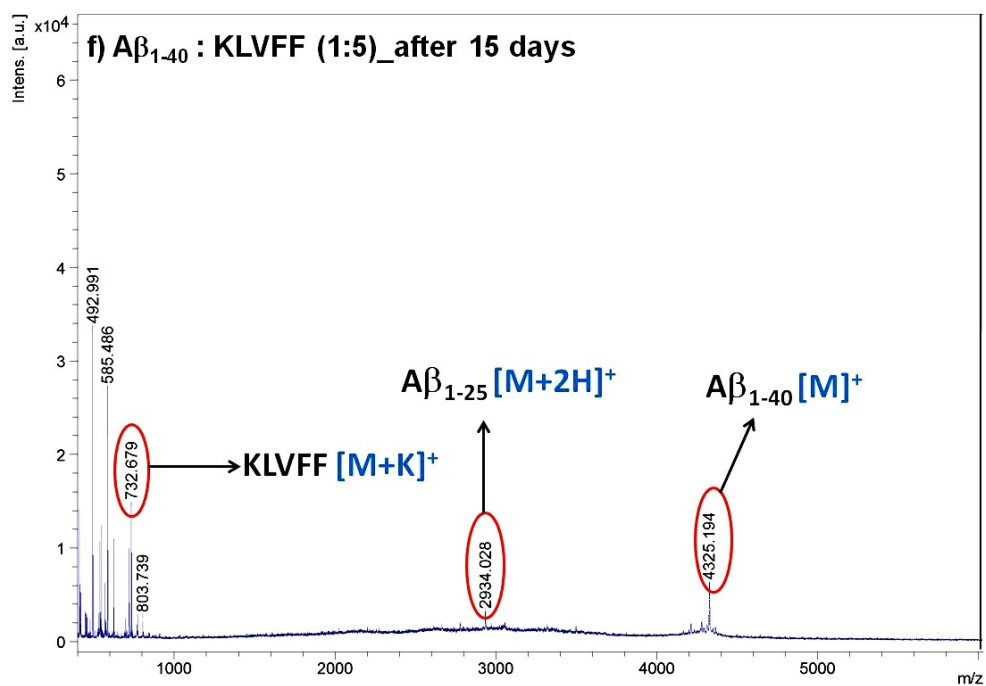


Fig. S67. MALDI-TOF mass spectrum of A $\beta$ <sub>1-40</sub> in the presence of KLVFF (1:5) after ten days of incubation in PBS due to Ser-mediated proteolysis.



**Fig. S68. MALDI-TOF mass spectrum of Aβ<sub>1-40</sub> in the presence of KLVFF (1:5) after fifteen days of incubation in PBS due to Ser-mediated proteolysis.**

#### **Inhibitory ability of EGCG on Aβ<sub>1-40</sub>:**

MALDI-TOF mass spectra of Aβ<sub>1-40</sub> in the presence of EGCG were analysed in a time-dependent manner (up to 15 days). However, mAPs mediated no such degradation product was observed in MALDI-TOF mass spectra, a few self-degraded peptide fragments were appeared due to the inhibition of Aβ<sub>1-40</sub> by EGCG.

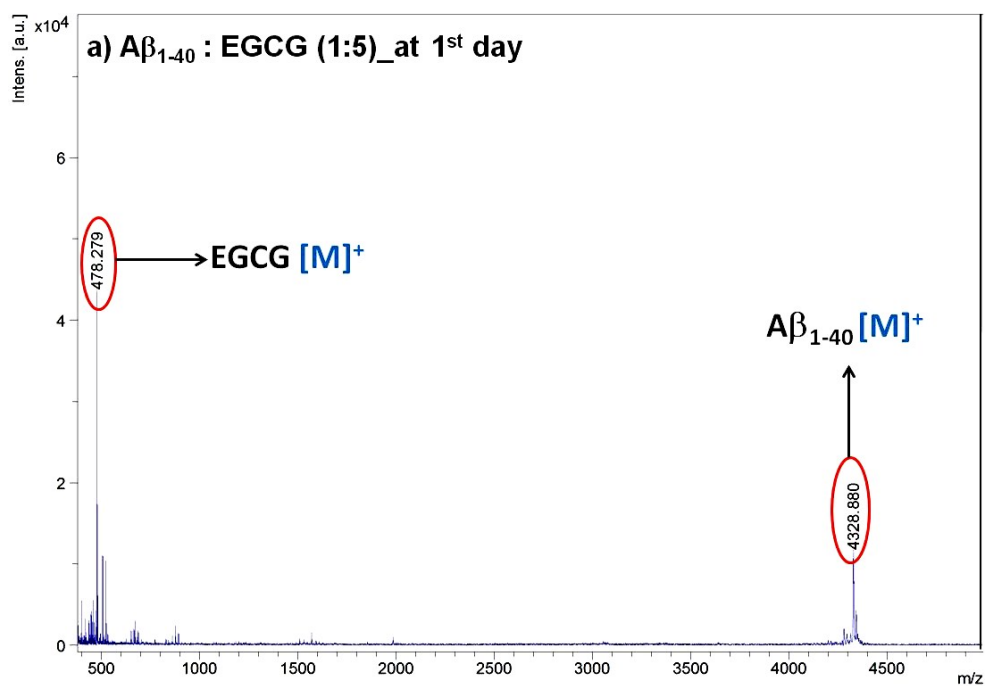


Fig. S69. MALDI-TOF mass spectrum of  $A\beta_{1-40}$  in the presence of EGCG (1:5) on the first day of incubation in PBS pH 7.4 at 37 °C.

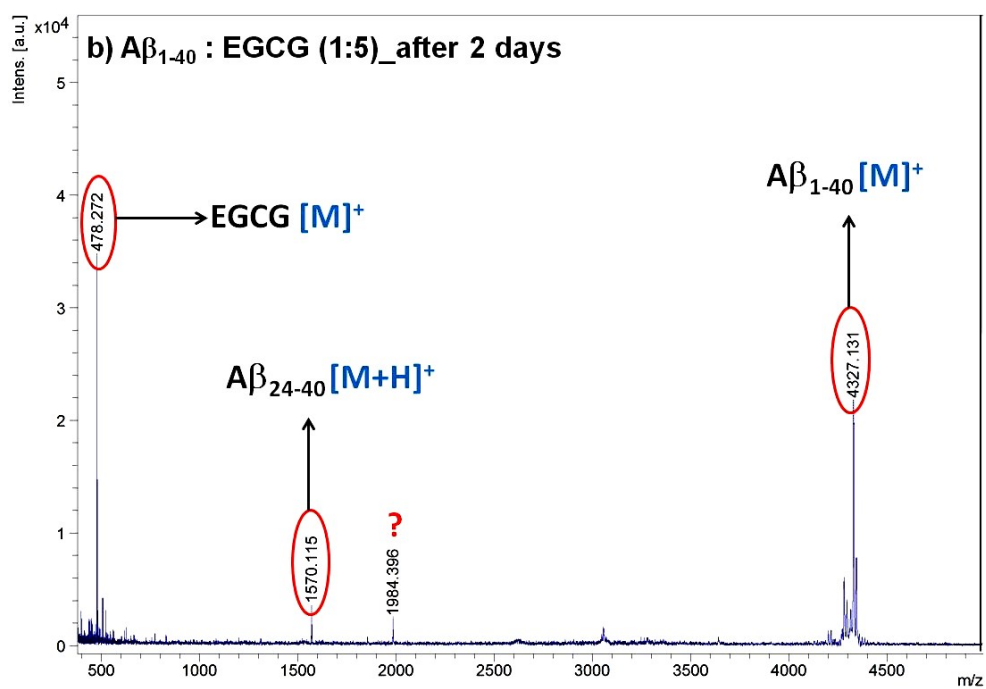
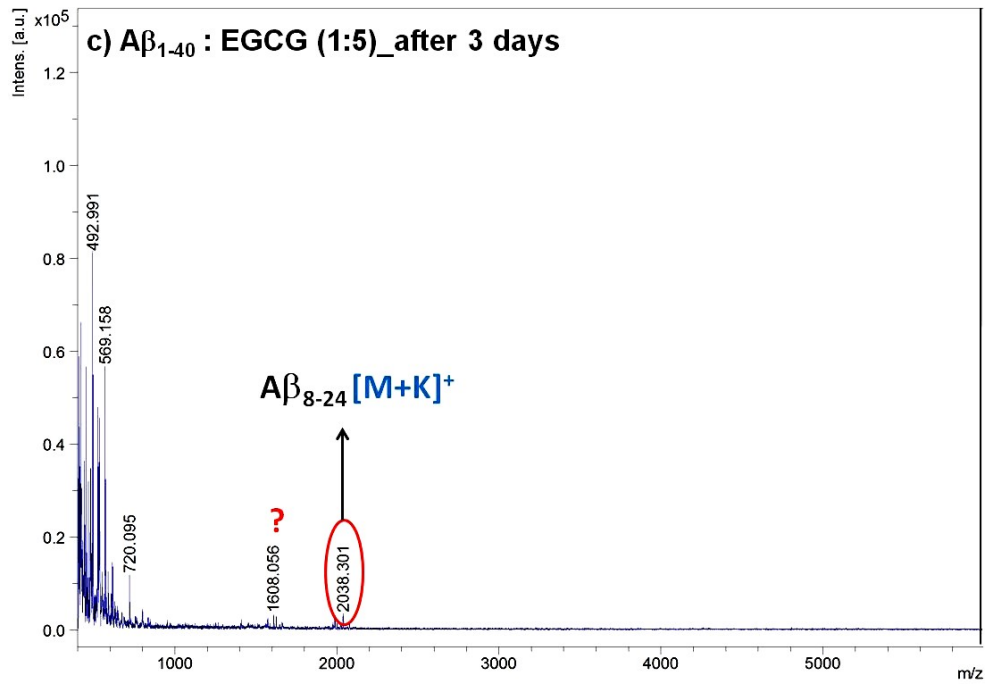
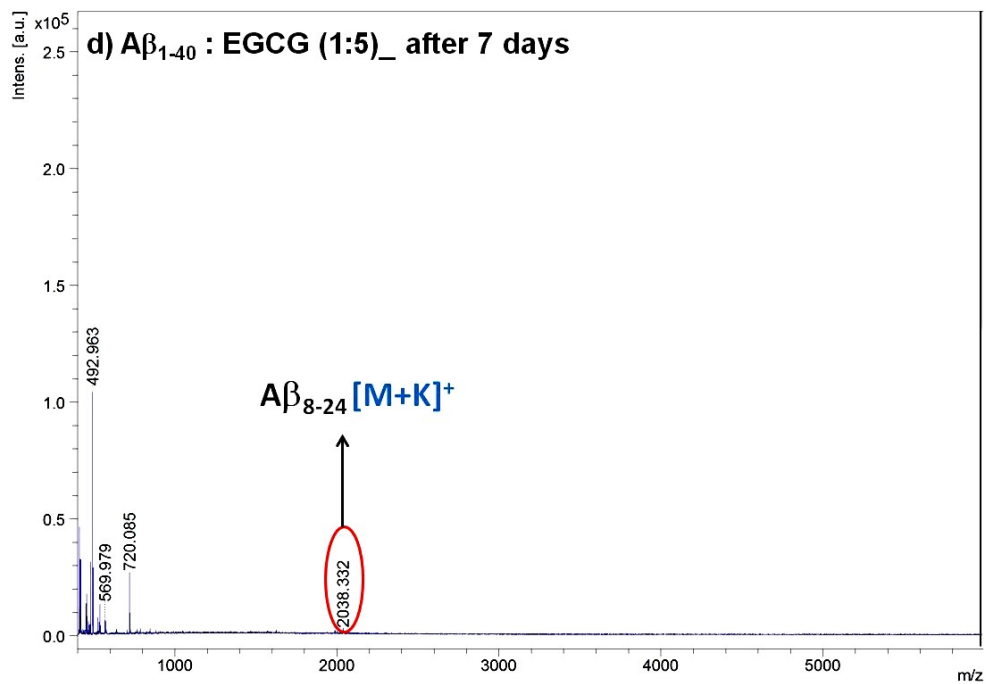


Fig. S70. MALDI-TOF mass spectrum of  $A\beta_{1-40}$  in the presence of EGCG (1:5) after two days of incubation in PBS due to Ser-mediated proteolysis.



**Fig. S71. MALDI-TOF mass spectrum of  $A\beta_{1-40}$  in the presence of EGCG (1:5) after three days of incubation in PBS due to Ser-mediated proteolysis.**



**Fig. S72. MALDI-TOF mass spectrum of  $A\beta_{1-40}$  in the presence of EGCG (1:5) after seven days of incubation in PBS due to Ser-mediated proteolysis.**

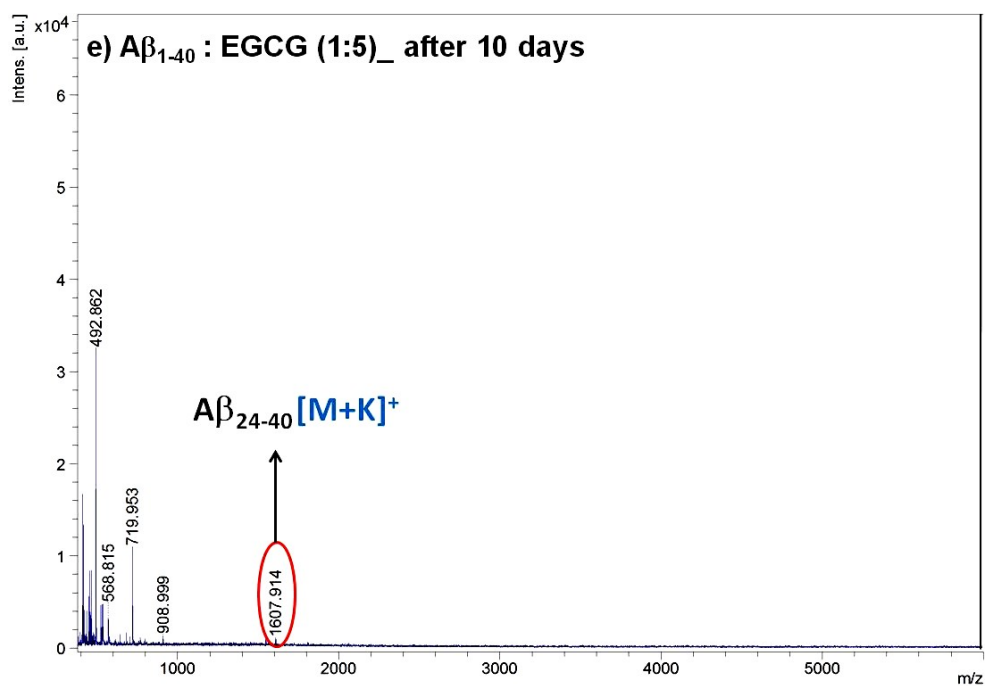


**Fig. S73. MALDI-TOF mass spectrum of  $A\beta_{1-40}$  in the presence of EGCG (1:5) after ten days of incubation in PBS due to Ser-mediated proteolysis.**

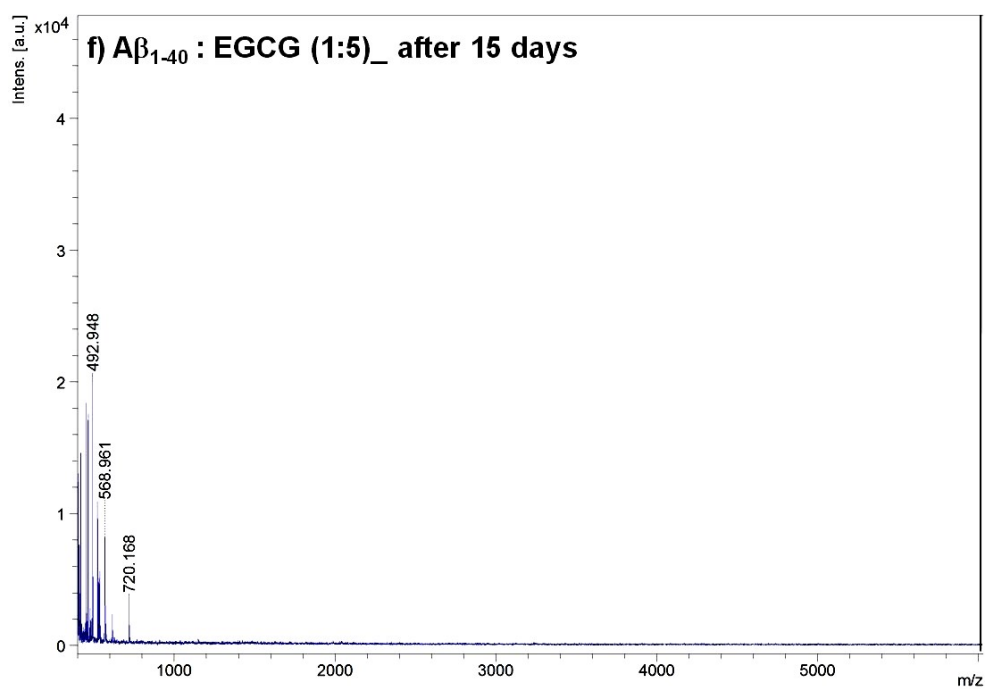


**Fig. S74. MALDI-TOF mass spectrum of  $A\beta_{1-40}$  in the presence of EGCG (1:5) after fifteen days of incubation in PBS.**

## Examination of the proteolytic activity of mAP3 on DTP28:

### Self-degradation of the negative control (NC) peptide, DTP28:

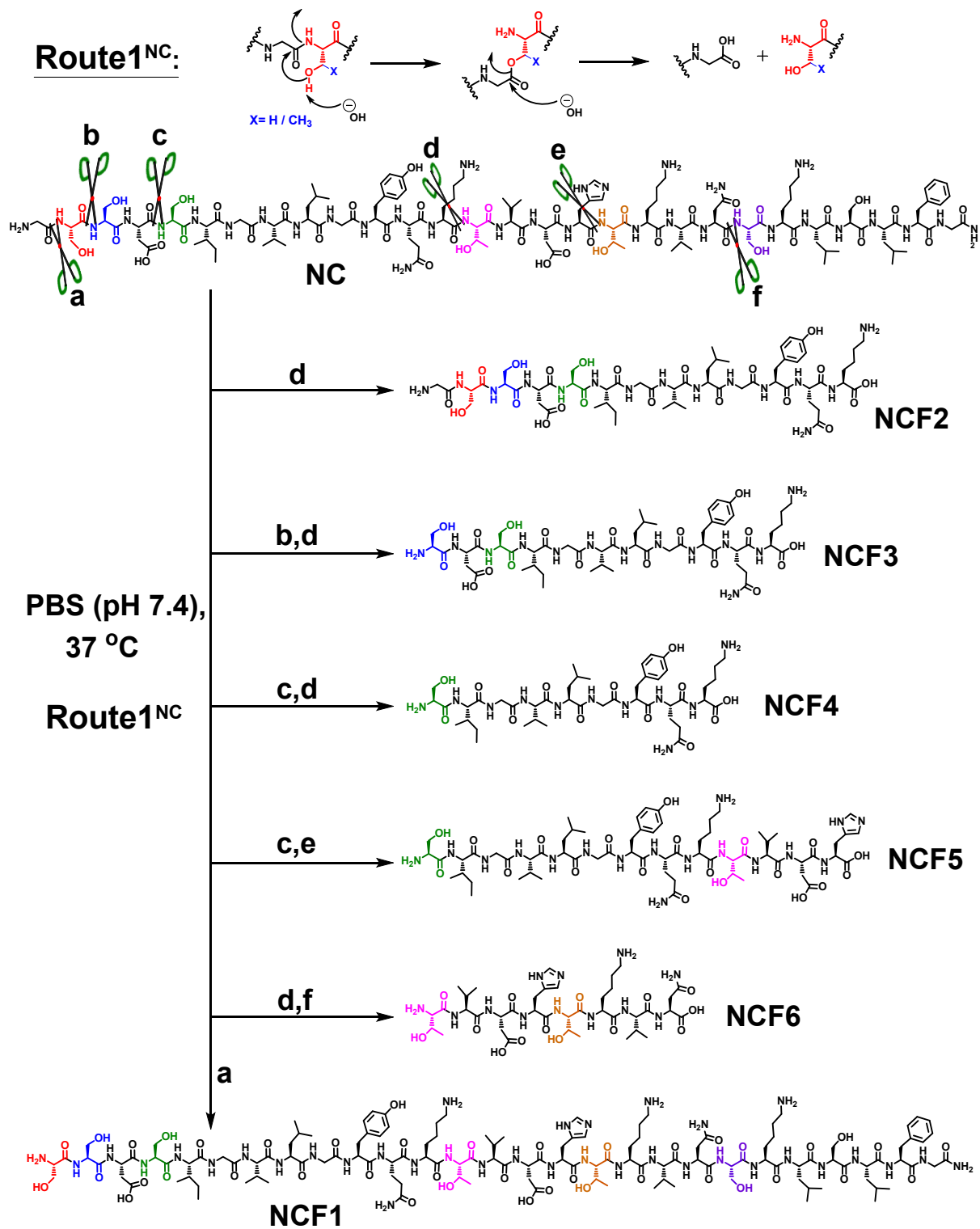
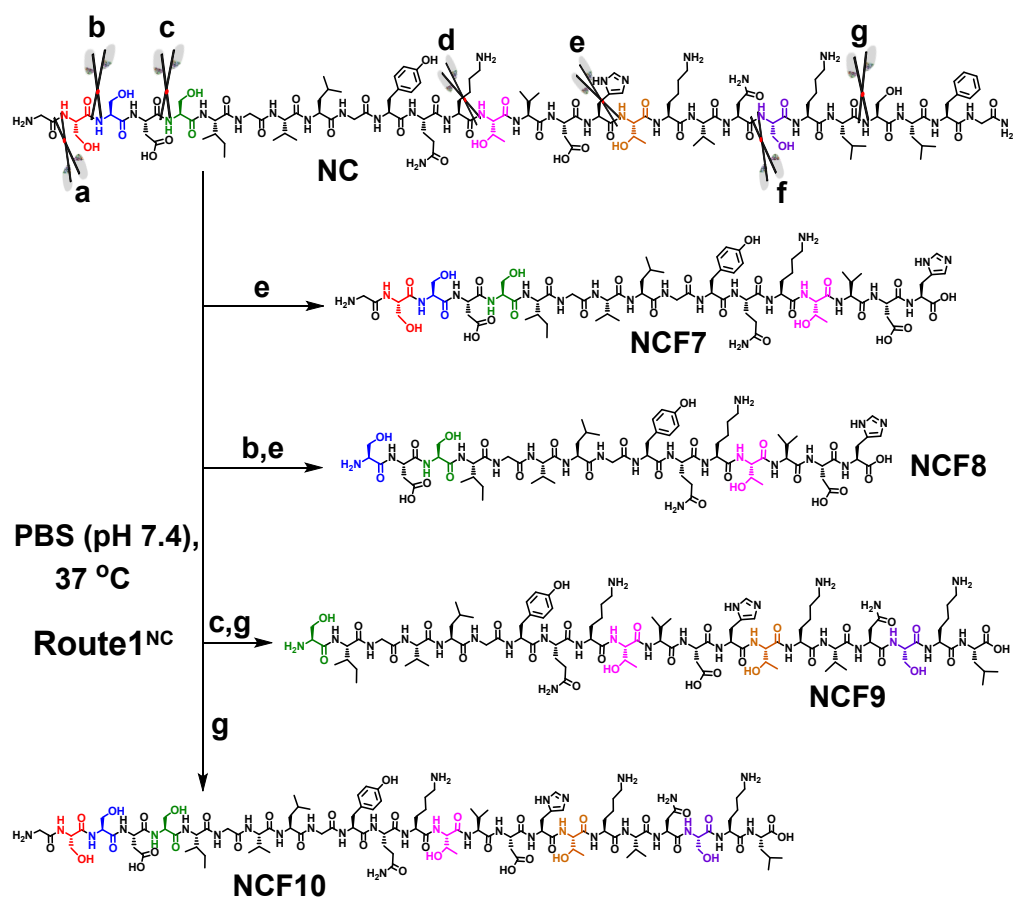
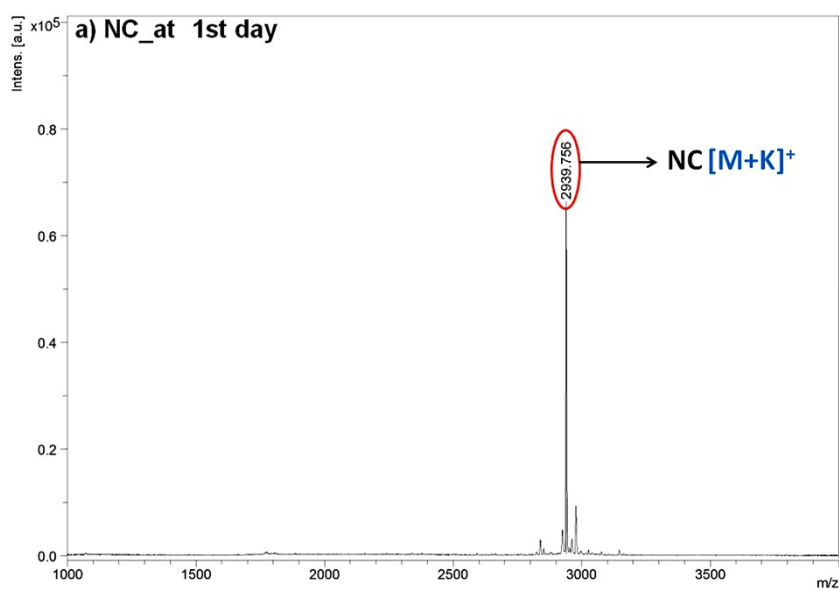


Fig. S75. Plausible route of the self-degradation of NC into various fragments (NCF1-NCF6).

**Route1<sup>NC</sup>** (continue):



**Fig. S76.** Plausible route of the self-degradation of NC into various fragments (NCF7-NCF10).



**Fig. S77.** MALDI-TOF mass spectrum of NC in the absence of mAP3 at the first day of incubation.

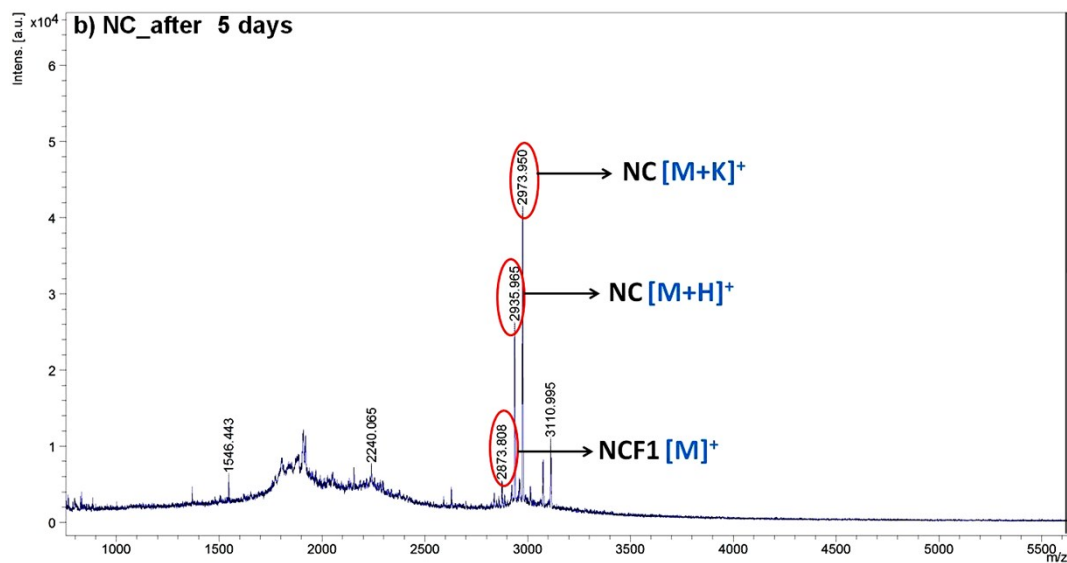


**Fig. S78.** MALDI-TOF mass spectrum of NC in the absence of mAP3 after five days of incubation. Here singly-charged NC and NCF1 ions were obtained.

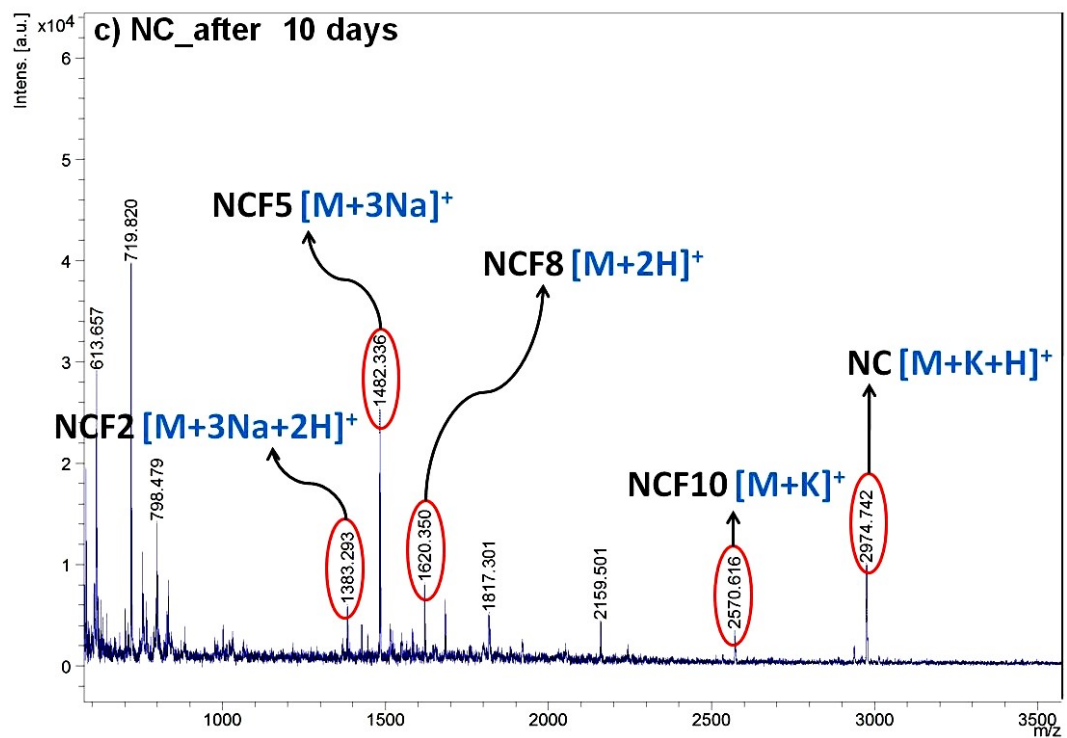


**Fig. S79.** MALDI-TOF mass spectrum of NC in the absence of mAP3 after ten days of incubation in PBS. Here multiply-charged ionized species of NC, NCF2, NCF5, and NCF8 were obtained along with singly-charged NCF10 ion.

Effect of mAP3 on the negative control (NC) peptide, DTP28:

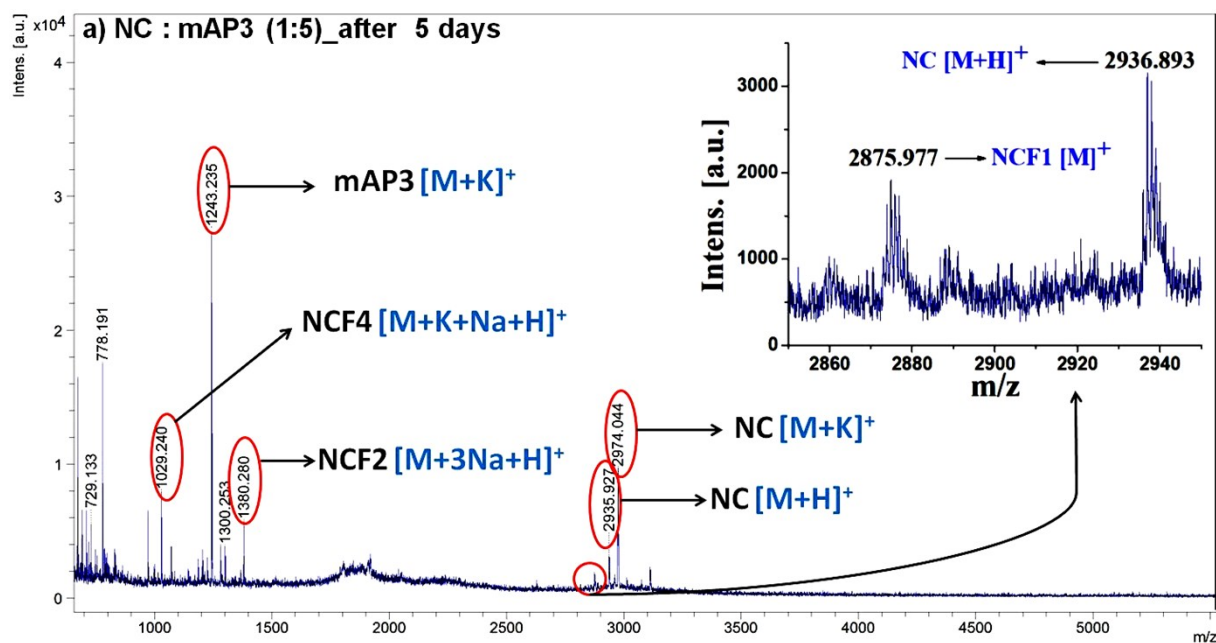


Fig. S80. MALDI-TOF mass spectrum of NC in the presence of mAP3 (1:5) after five days of incubation in PBS. Here multiply-charged ionized species of mAP3, NCF2 and NCF4 were obtained along with singly-charged NC and NCF1 ions.

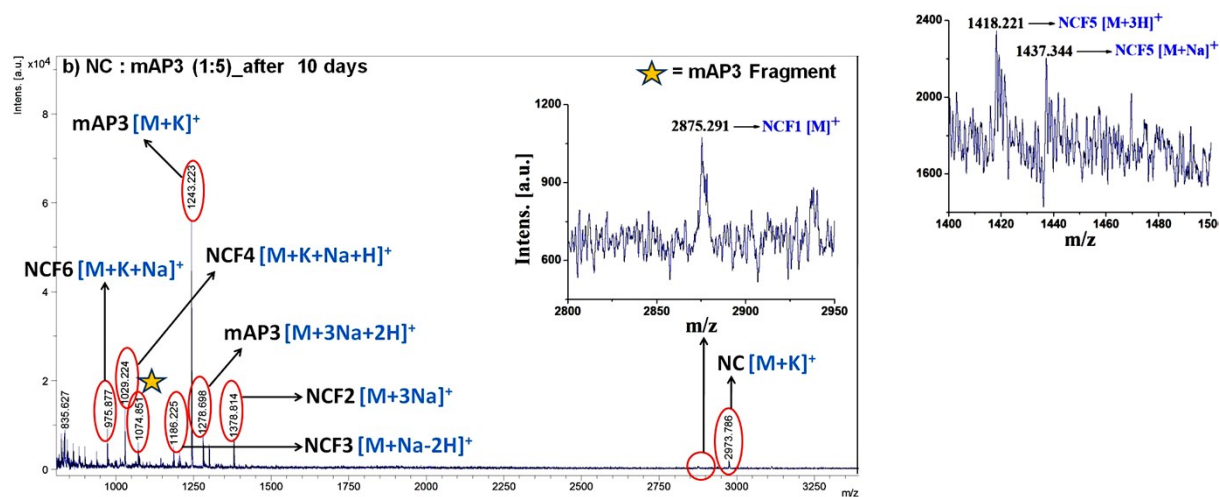
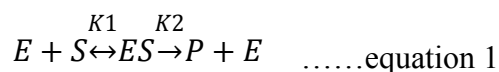


Fig. S81. MALDI-TOF mass spectrum of NC in the presence of mAP3 (1:5) after ten days of incubation in PBS. Here multiply-charged ionized species of mAP3, NCF2, NCF3, NCF4 and NCF6 were obtained along with singly-charged NC and NCF1 ions.

## Kinetics of the mAP3-catalyzed hydrolysis of p-Nitrophenyl Acetate (NPA):



$$\frac{1}{V} = \frac{1}{K_2[S_0]} + \frac{K_m}{K_2[S_0][E]} \quad \dots\dots\text{equation 2}$$

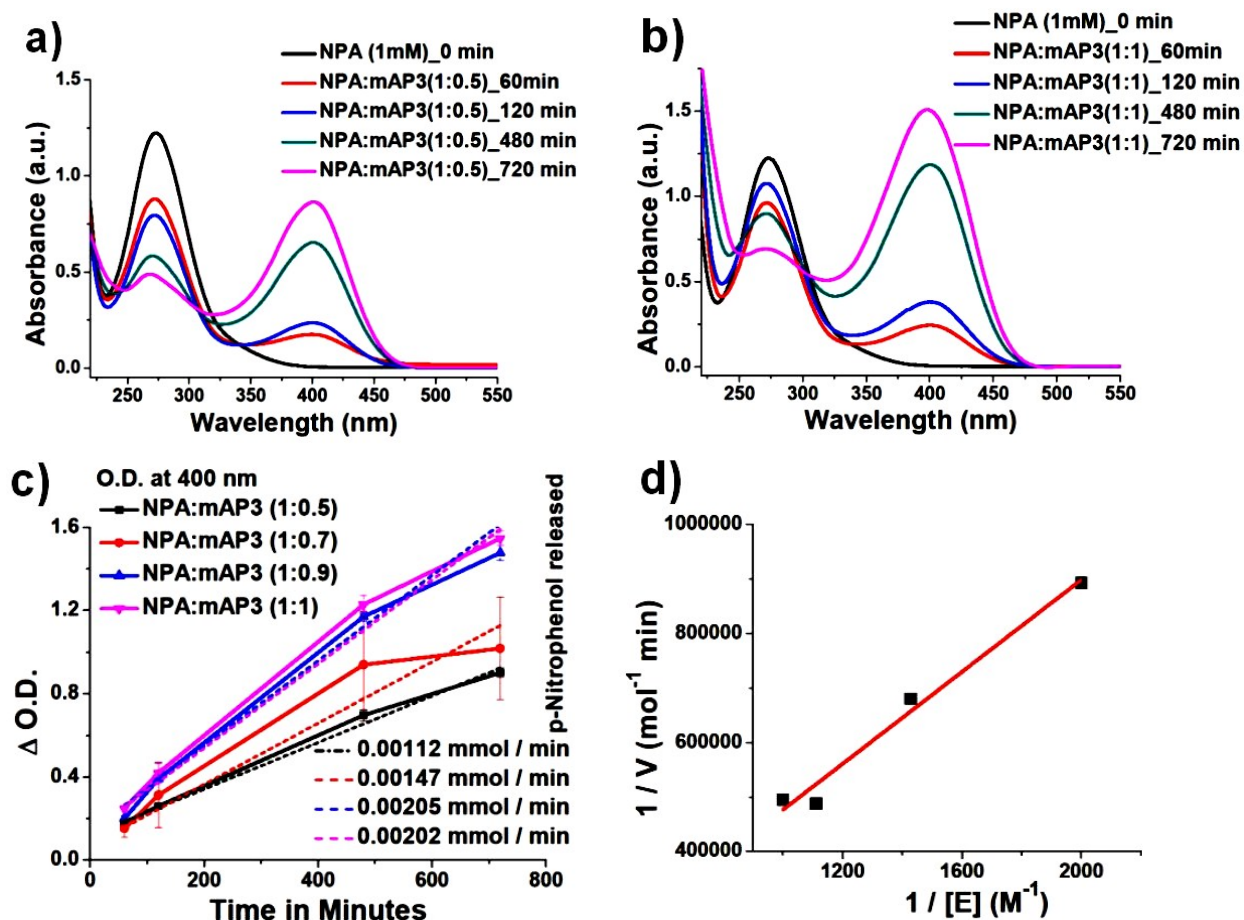


Fig. S82. UV-visible absorption of NPA in the presence of a) 0.5 eq. and b) 1 eq of mAP3 in PBS buffer (containing 2 vol% ethanol) of pH 7.0 at 25 °C. (c) The relationship between the increase in absorbance at 400 nm and time in the hydrolysis of NPA by mAP3. (d) The Lineweaver-Burk plot of mAP3-catalyzed hydrolysis of NPA. The Lineweaver-Burk plot shows excellent linearity; the slopes give Michaelis constant ( $K_m$ ) =  $4.22 \times 10^2$  M. The Turn Over Number (T.O.N.) was 1.01 moles hydrolyzed/min/moles of mAP3.

### Molecular Docking:

Molecular docking<sup>3</sup> study was performed by AutoDock Vina version 1.1.2 software following a reported article.<sup>4</sup> From the docking results, no pocket was found created by the DHS unit in the case of mAP1. Though Asp, His, and Ser are away from one another, a

pocket was found for mAP2. In the case of mAP3, a pocket with the close proximity of Asp, His, and Ser was found.

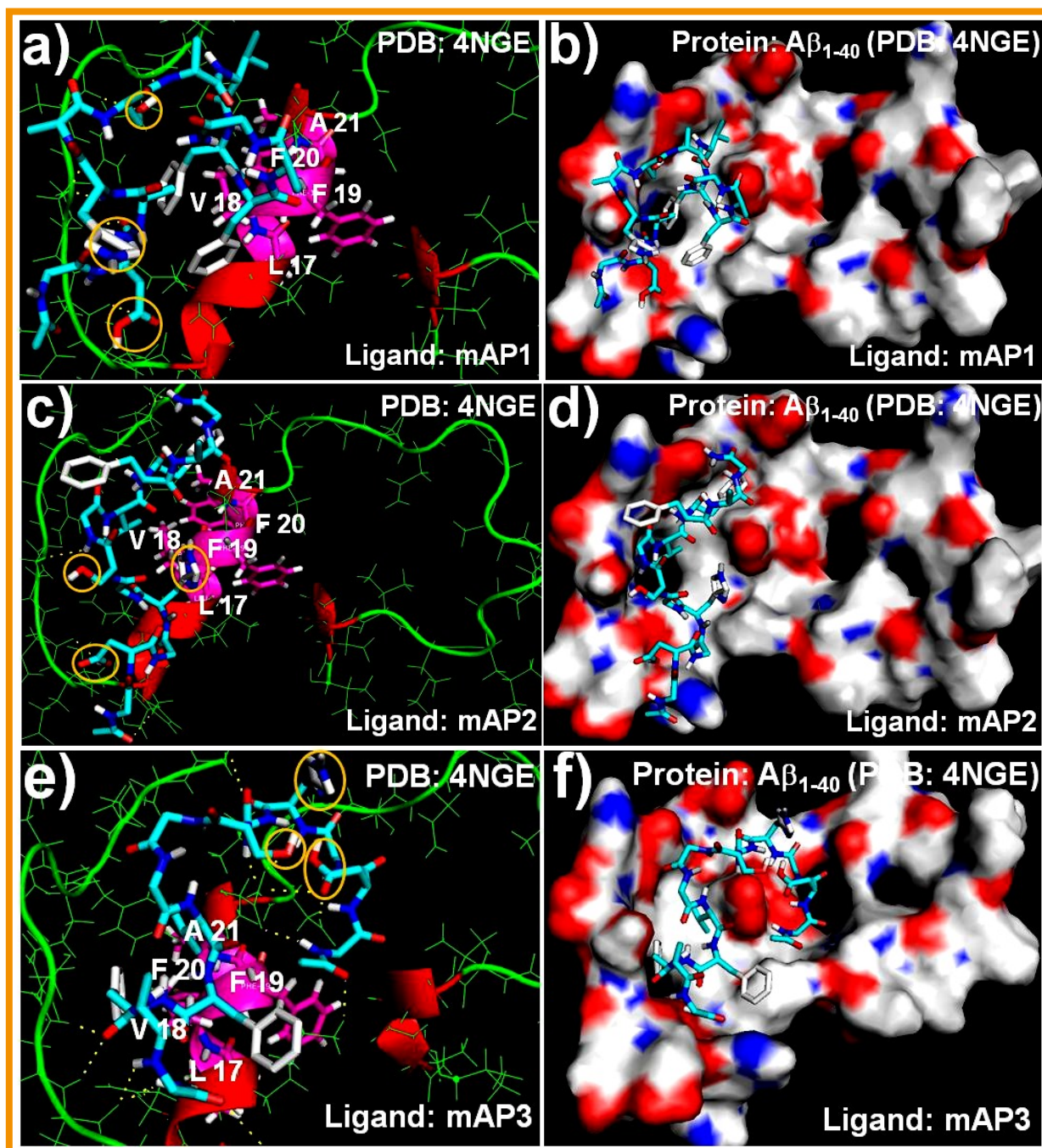


Fig. S83. Molecular docking images of mAP1 (a, b), mAP2 (c, d), and mAP3 (e, f) into helical  $A\beta_{1-40}$ <sup>5</sup> (PDB ID 4NGE) reveals that mAPs bind at the binding site (V<sub>18</sub>FFA<sub>21</sub>) with binding affinity -5.8 kcal/mol, -5.4 kcal/mol, and -6.6 kcal/mol, respectively. Structures are shown as line and cartoon representation (for a, c, e), and surface representation (for b, d, f). The surface of  $A\beta_{1-40}$  is coloured according to the charges of the atoms where negatively and positively charged zones are represented in red and blue, respectively.

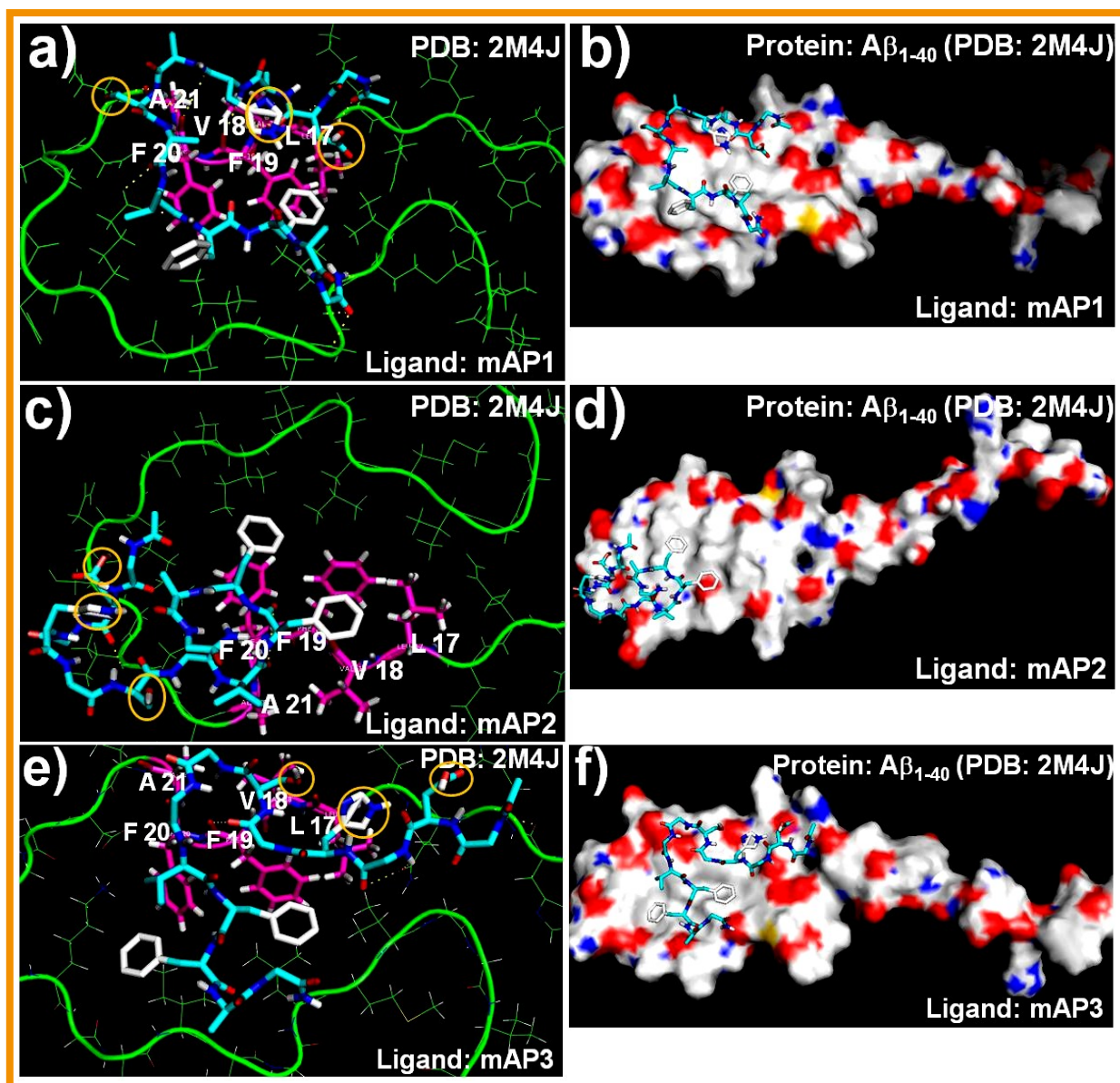


Fig. S84. Molecular docking images of mAP1 (a, b), mAP2 (c, d), and mAP3 (e, f) into fibril A $\beta_{1-40}$  (PDB ID 2M4J) reveals that mAPs bind at the binding site (V<sub>18</sub>FFA<sub>21</sub>) with binding affinity -6.3 kcal/mol, -4.7 kcal/mol, and -5.7 kcal/mol, respectively. Structures are shown as line and cartoon representation (for a, c, e), and surface representation (for b, d, f). The surface of A $\beta_{1-40}$  is coloured according to the charges of the atoms where negatively and positively charged zones are represented in red and blue, respectively.

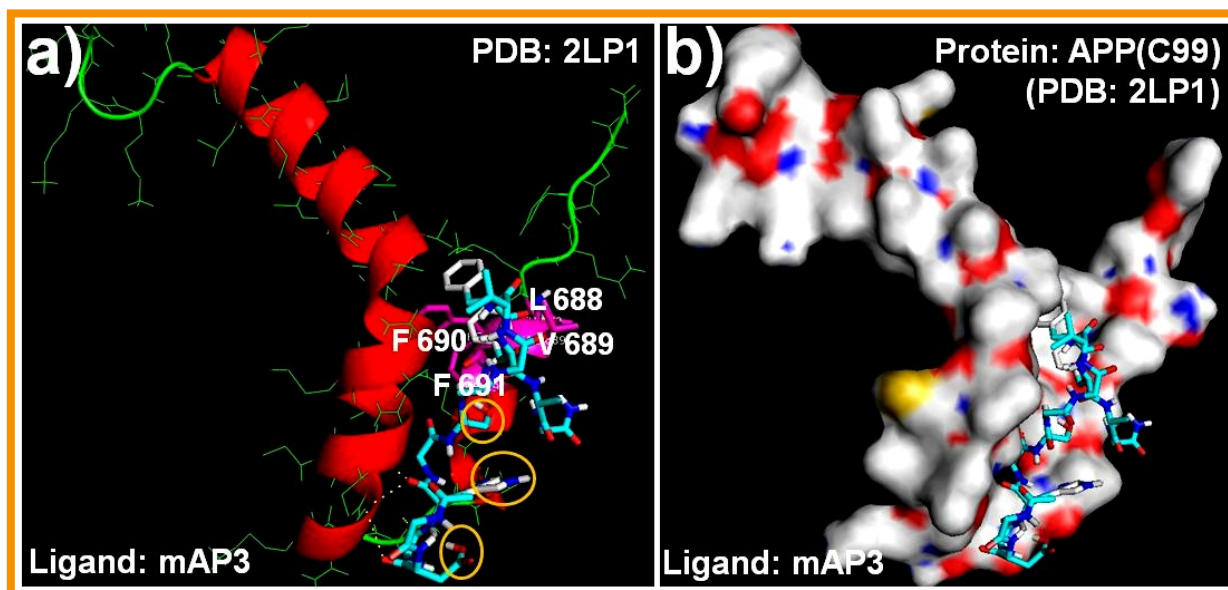


Fig. S85. Molecular docking images of mAP3 (a, b) into helical 99 residue C-terminal domain (PDB ID: 2LP1) of APP(C99) reveals that mAP3 binds at the binding site (L<sub>688</sub>VFF<sub>691</sub>) with binding affinity -5.2 kcal/mol. Structures are shown as line and cartoon representation (for a), and surface representation (for b). The surface of APP is coloured according to the charges of the atoms where negatively and positively charged zones are represented in red and blue, respectively.

#### DFT calculation of the mA $\beta$ \_mAP3 conjugate (A'')

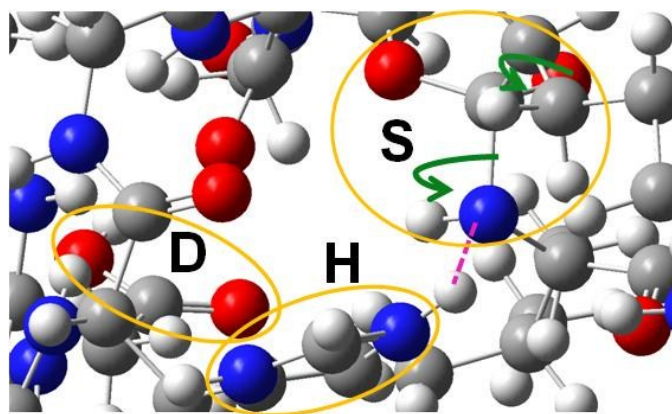


Fig. S86. The most stable conformation of the mA $\beta$ \_mAP3 conjugate A''. Image generated by Gaussian 09W obtained from DFT calculation [Calculation Method: B3LYP, Basis Set: 6-31G, Total Energy - 9336.72070930 a.u.]. Nitrogen & Oxygen atoms are represented in blue & red, respectively. The His proton (of mAP3) was close to the nitrogen of amide mA $\beta$  (marked by the pink colored dotted line) to be cleaved.

### The procedure of synthesis of the designed peptides:

All the designed peptides were synthesized by standard Fmoc/tBu solid phase peptide synthesis (SPPS) protocol.<sup>6</sup>

### Characterization of the peptides:

Crude peptides were purified and characterized (by HPLC and ESI-MS) as described in the article.<sup>2</sup>

### Characterization data of the peptides:

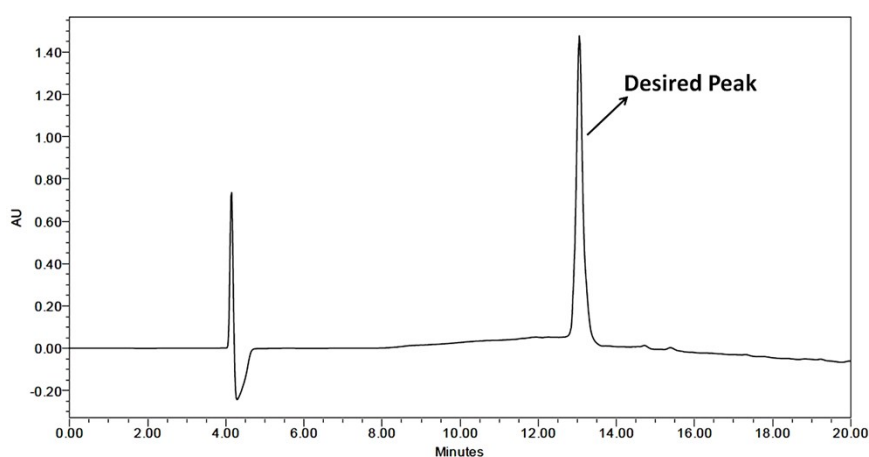


Fig. S87. HPLC profile picture of the pure mA $\beta$  peptide.

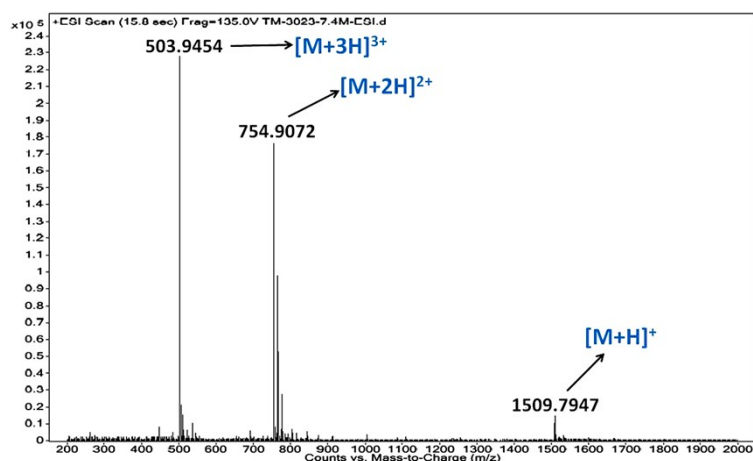
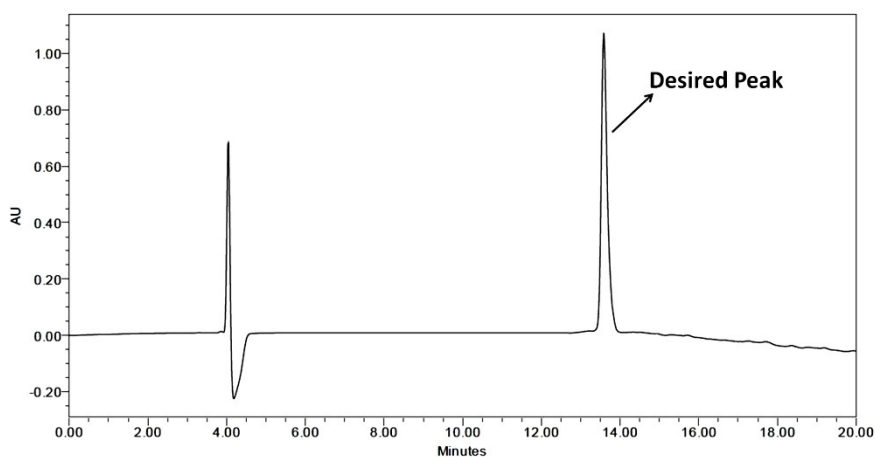
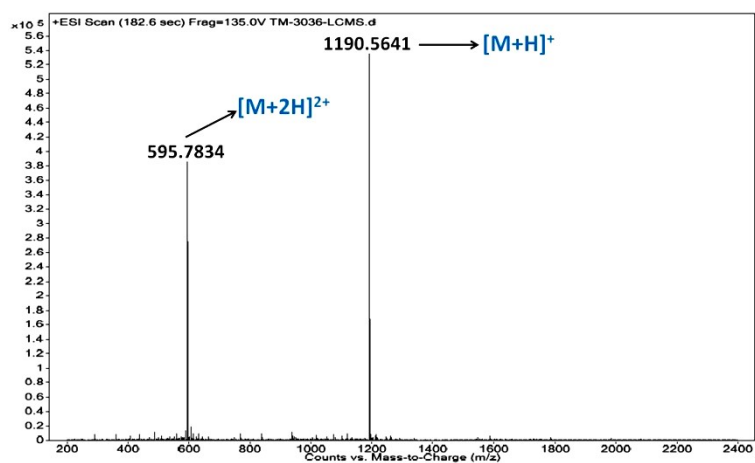


Fig. S88. ESI-MS profile picture of the pure mA $\beta$  peptide. Calculated m/z for C<sub>71</sub>H<sub>105</sub>N<sub>21</sub>O<sub>16</sub> [M+H]<sup>+</sup> is 1509.7323, observed 1509.7947, calculated m/z for C<sub>71</sub>H<sub>105</sub>N<sub>21</sub>O<sub>16</sub> [M+2H]<sup>2+</sup> is 755.4422, observed 754.9072 (Mass difference of 0.5 indicates a doubly charged peak), calculated m/z for C<sub>71</sub>H<sub>105</sub>N<sub>21</sub>O<sub>16</sub> [M+3H]<sup>3+</sup> is 503.9161, observed 503.9454.



**Fig. S89.** HPLC profile picture of the pure mAP1.



**Fig. S90.** ESI-MS profile picture of the pure mAP1. Calculated  $m/z$  for  $C_{54}H_{75}N_{15}O_{16}$   $[M+H]^+$  is 1190.5594, observed 1190.5641, calculated  $m/z$  for  $C_{54}H_{75}N_{15}O_{16}$   $[M+2H]^{2+}$  is 595.7836, observed 595.7834.

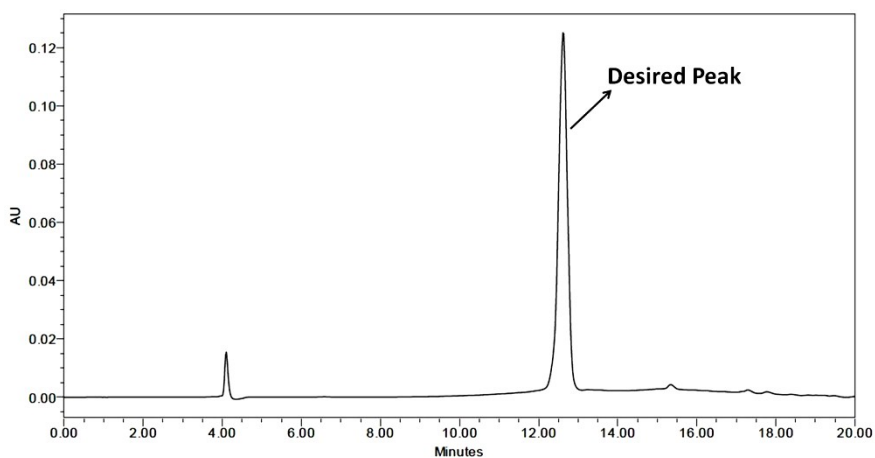


**Figure S91.** HPLC profile picture of the pure mAP2.

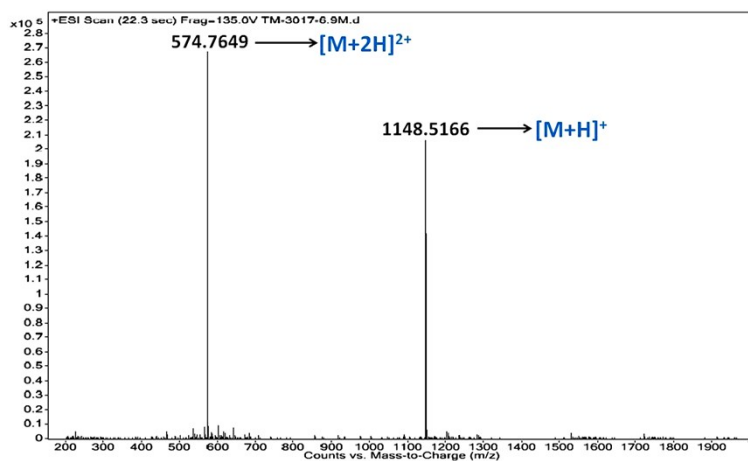


Fig. S92. ESI-MS profile picture of the pure mAP2. Calculated  $m/z$  for  $C_{51}H_{69}N_{15}O_{16}$   $[M+H]^+$  is 1148.5125, observed 1148.5166, calculated  $m/z$  for  $C_{51}H_{69}N_{15}O_{16}$   $[M+2H]^{2+}$  is 574.7601, observed 574.7649.

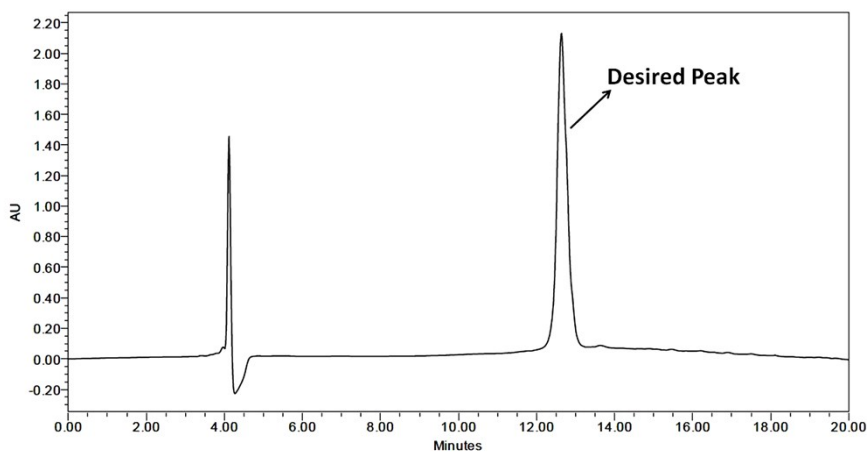


Fig. S93. HPLC profile picture of the pure mAP3.

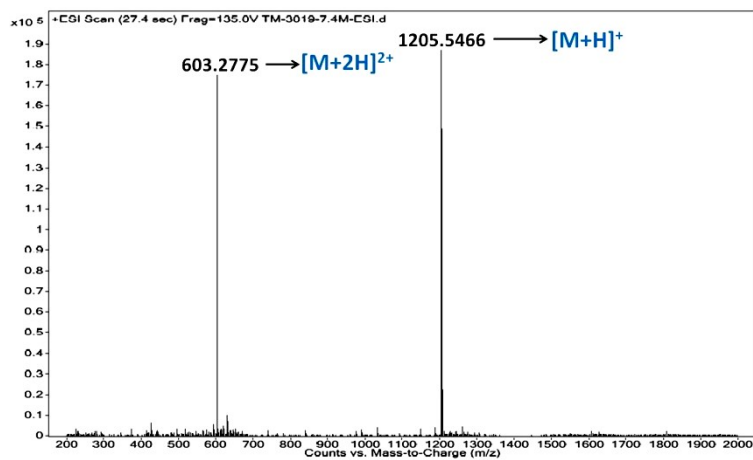


Fig. S94. ESI-MS profile picture of the pure mAP3. Calculated  $m/z$  for  $C_{53}H_{72}N_{16}O_{17}$   $[M+H]^+$  is 1205.5339, observed 1205.5466, calculated  $m/z$  for  $C_{53}H_{72}N_{16}O_{17}$   $[M+2H]^{2+}$  is 603.2708, observed 603.2775.

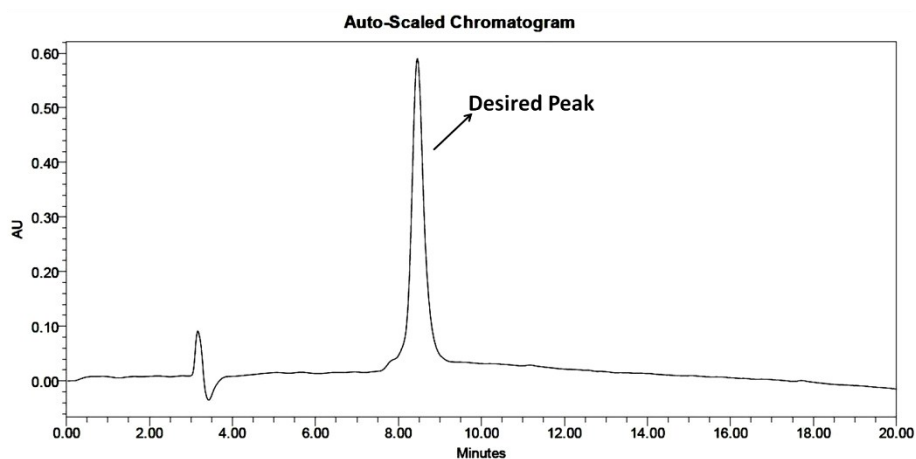


Fig. S95. HPLC profile picture of the pure DTP28.

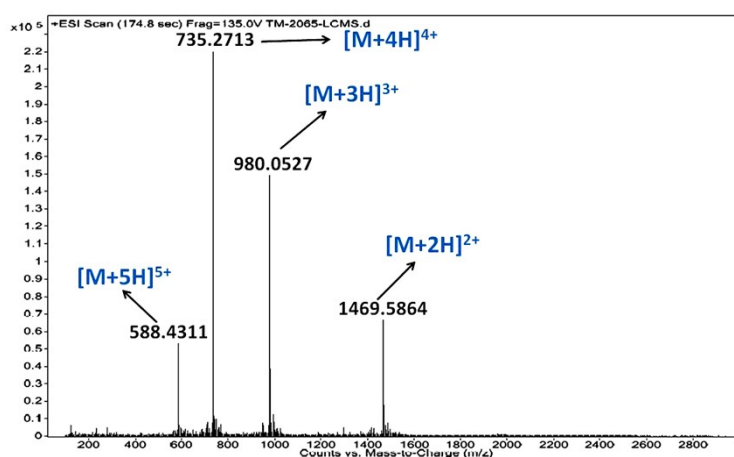


Fig. S96. ESI-MS profile picture of the pure DTP28. Calculated  $m/z$  for  $C_{129}H_{210}N_{36}O_{42}$   $[M+2H]^{2+}$  is 1469.6318 and observed 1469.5864, calculated  $m/z$  for  $C_{129}H_{210}N_{36}O_{42}$   $[M+3H]^{3+}$  is 980.0879 and observed 980.0527, calculated  $m/z$  for  $C_{129}H_{210}N_{36}O_{42}$   $[M+4H]^{4+}$  is 735.3159 and observed 735.2713, calculated  $m/z$  for  $C_{129}H_{210}N_{36}O_{42}$   $[M+5H]^{5+}$  is 588.4527 and observed 588.4311.

## References:

- <sup>1</sup> M. R. Nilsson, *Methods*, 2004, **34**, 151-160.
- <sup>2</sup> J. Peng, et al. *Sci. Rep.*, 2015, **5**, 10171.
- <sup>3</sup> O. Trott, A. J. Olson, *J. Comput Chem.*, 2010, **31**, 455-461.
- <sup>4</sup> T. Mondal, B. Mandal, *ChemComm*, 2019, **55**, 4933-4936.
- <sup>5</sup> S. Vivekanandan, J. R. Brender, S. Y. Lee, A. Ramamoorthy, *Biochem. Biophys. Res. Commun.*, 2011, **411**, 312-316.
- <sup>6</sup> I. Coin, M. Beyermann, M. Bienert, *Nat. Protoc.*, 2007, **2**, 3247-3256.